المجلد (8)
العدد (2)
نوفمبر
2023م
ربيع الثاني
1445هـ

مجلة الشمال
للعلوم
الأساسية والتطبيقية

دورية علمية محكمة

جامعة الحدود الشمالية
www.nbu.edu.sa

طباعة - ردمد: 1658-7022
إلكتروني - ردمد: 1658-7014

J
N
B
A
S

مجلة الشمال للعلوم الأساسية والتطبيقية (JNBAS)

هيئـة التحـــرير

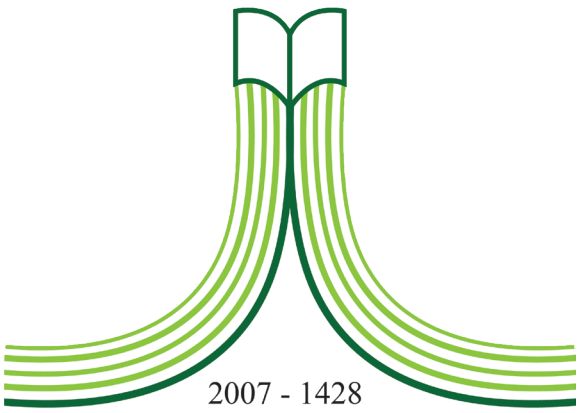

جامعة الحدود الشمالية

NORTHERN BORDER UNIVERSITY

المملكة العربية السعودية

مجلـة الشمــال
للعلوم الأساسية والتطبيقية
(JNBAS)

دورية علمية محكمة

تصدر عن

مركز النشر العلمي والتأليف والترجمة

جامعة الحدود الشمالية

المجلد الثامن ــ العدد الثاني

نوفمبر 2023م ــ ربيع الثَّاني 1445هـ

الموقع والبريد الإلكتروني

www.nbu.edu.sa

s.journal@nbu.edu.sa

طباعة - ردمد: 1658-7022 / إلكتروني - ردمد: 1658-7014

مجلة الشمال للعلوم الأساسية والتطبيقية (JNBAS)

التعريف بالمجلة

تعنى المجلة بنشر البحوث والدراسات العلمية الأصيلة في مجال العلوم الأساسية والتطبيقية، باللغتين العربية والإنجليزية، كما تهتم بنشر جميع ما له علاقة بعرض الكتب ومراجعتها أو ترجمتها، وملخصات الرسائل العلمية، وتقارير المؤتمرات والندوات العلمية، وتصدر مرتين في السنة (مايو ـ نوفمبر).

الرؤية

الريادة في نشر البحوث العلمية المحكمة، وتصنيف المجلة ضمن أشهر الدوريات العلمية العالمية.

الرسالة

نشر البحوث العلمية المحكمة في مجال العلوم الأساسية والتطبيقية وفق معايير عالمية متميزة.

أهداف المجلة

1) أن تكون المجلة مرجعًا علميًا للباحثين في العلوم الأساسية والتطبيقية.
2) تلبية حاجة الباحثين إلى نشر بحوثهم العلمية، وإبراز مجهوداتهم البحثية على المستويات المحلية والإقليمية والعالمية.
3) المشاركة في بناء مجتمع المعرفة بنشر البحوث الرصينة التي تؤدي إلى تنمية المجتمع.
4) تغطية أعمال المؤتمرات العلمية المحكمة.

شروط قبول البحث

1) الأصالة والابتكار وسلامة المنهج والاتجاه.
2) الالتزام بالمناهج والأدوات والوسائل العلمية المتبعة في مجاله.
3) الدقة في التوثيق والمصادر والمراجع والتخريج.
4) سلامة اللغة.
5) أن يكون البحث غير منشور أو مقدم للنشر في أي مكان آخر.
6) أن يكون البحث المستل من الرسائل العلمية غير منشور أو مقدم للنشر، وأن يشير الباحث إلى أنه مستلٌ.

للمراسلة

رئيس التحرير
مجلة الشمال للعلوم الأساسية والتطبيقية (JNBAS)
جامعة الحدود الشمالية
ص.ب 1321، عرعر 91431
المملكة العربية السعودية.
هاتف : +966146615499
فاكس: +966146614439

البريد الإلكتروني: *s.journal@nbu.edu.sa*
الموقع الإلكتروني: *www.nbu.edu.sa*

الاشتراك والتبادل

مركز النشر العلمي والتأليف والترجمة
جامعة الحدود الشمالية
ص.ب. 1321، عرعر، 91431
المملكة العربية السعودية.

شروط النشر

أولاً: ضوابط النص المقدم للنشر

1) ألا تزيد صفحاته عن (35) صفحة من القطع العادي (A4).
2) أن يحتوي على عنوان البحث وملخصه باللغتين العربية والإنجليزية في صفحة واحدة، بحيث لا يزيد عن (250) كلمة للملخص، وأن يتضمن البحث كلمات مفتاحية دالةٍ على التخصص الدقيق للبحث باللغتين، بحيث لا يتجاوز عددها (6) كلمات، توضع بعد نهاية كل ملخص.
3) أن يذكر اسم المؤلف وجهة عمله بعد عنوان البحث مباشرة باللغتين العربية والإنجليزية.
4) أن تقدم البحوث العربية مطبوعة بخط (Simplified Arabic)، بحجم (14) للنصوص في المتن، وبالخط نفسه بحجم (12) للهوامش.
5) أن تقدم البحوث الإنجليزية مطبوعة بخط (Times New Roman) بحجم (12) للنصوص في المتن، وبالخط نفسه بحجم (9) للهوامش.
6) كتابة البحث على وجه واحد من الصفحة، مع ترك مسافة سطر واحد بين السطور، وتكون الحواشي 2.5 سم على الجوانب الأربعة للصفحة، بما يعادل 1.00 إنش (بوصة).
7) التزام الترتيب الموضوعي الآتي:

المقدمة: تكون دالة على موضوع البحث، والهدف منه، ومنسجمة مع ما يَرِدُ في البحث من معلومات وأفكار وحقائق علمية، كما تشير باختصار إلى مشكلة البحث، وأهمية الدراسات السابقة.

العرض: يتضمن التفاصيل الأساسية لمنهجية البحث، والأدوات والطرق التي تخدم الهدف، وترتب المعلومات حسب أولويتها.

النتائج والمناقشة: يجب أن تكون واضحة موجزة، مع بيان دلالاتها دون تكرار.

الخاتمة: تتضمن تلخيصًا موجزًا للموضوع، وما توصل إليه الباحث من نتائج، مع ذكر التوصيات والمقترحات.

8) أن تدرج الرسوم البيانية والأشكال التوضيحية في النص، وترقم ترقيماً متسلسلاً، وتكتب أسماؤها والملاحظات التوضيحية أسفلها.
9) أن تدرج الجداول في النص، وترقم ترقيماً متسلسلاً، وتكتب أسماؤها أعلاها، وأما الملاحظات التوضيحية فتكتب أسفل الجدول.
10) ألا توضع الهوامش أسفل الصفحة إلا عند الضرورة فقط، ويشار إليها برقم أو نجمة، ويكون الخط فيها بحجم (12) للعربي و (9) للإنجليزي.
11) لا تنشر المجلة أدوات البحث والقياس، وتقوم بحذفها عند طباعة المجلة.
12) أن يُراعى في منهج توثيق المصادر والمراجع داخل النص نظام (APA)، وهو نظام يعتمد ذكر الاسم والتاريخ (name/year) داخل المتن، ولا يقبل نظام ترقيم المراجع داخل النص مع وضع الحاشية أسفل الصفحة، وتوضع المصادر والمراجع داخل المتن بين قوسين حسب الأمثلة الآتية: يذكر اسم عائلة المؤلف متبوعا بفاصلة، فسنة النشر، مثلا: (مجاهد، 1988م). وفي حالة الاقتباس المباشر يضاف رقم الصفحة مباشرة بعد تاريخ النشر مثلا: (خيري، 1985م، ص:33). أما إذا كان للمصدر مؤلفان فيذكران مع اتباع الخطوات السابقة مثلا: (الفالح وعياش، 1424هـ). وفي حالة وجود أكثر من مؤلفين فتذكر أسماء عوائلهم أول مرة، مثلا: (مجاهد والعودات والشيخ، 1408هـ)، وإذا تكرر الاقتباس من المصدر نفسه فيشار إلى اسم عائلة المؤلف الأول فقط، ويكتب بعده وآخرون مثل: (مجاهد وآخرون، 1408هـ)، على أن تكتب معلومات النشر كاملة في قائمة المصادر والمراجع.
13) تخرج الأحاديث والآثار على النحو الآتي:
(صحيح البخاري، ج:1، ص: 5، رقم الحديث 511).
14) توضع قائمة المصادر والمراجع في نهاية البحث مرتبة ترتيباً هجائياً حسب اسم العائلة، ووفق نظام جمعية علم النفس الأمريكية (APA) الإصدار السادس، وبحجم (12) للعربي و(9) للإنجليزي، وترتب البيانات الببليوغرافية على النحو الآتي:

- **الاقتباس من كتاب لمؤلف واحد:**

الخوجلي، أحمد. (2004م). ***مبادئ فيزياء الجوامد***. الخرطوم، السودان: عزة للنشر والتوزيع.

- **الاقتباس من كتاب لأكثر من مؤلف:**

نيوباي، تيموثي؛ ستيبتش، دونالد؛ راس، جيمس. (1434هـ/2013م). ***التقنية التعليمية للتعليم والتعلم***. الرياض، المملكة العربية السعودية: دار جامعة الملك سعود للنشر.

- **الاقتباس من دورية:**

النافع، عبداللطيف حمود. (1427هـ). أثر قيادة السيارات خارج الطرق المعبدة في الغطاء النباتي بالمنتزهات البرية: دارسة في حماية البيئة، في وسط المملكة العربية السعودية. ***المجلة السعودية في علوم الحياة***، *14*(1)، 53-72.

- **الاقتباس من رسالة ماجستير أو دكتوراه:**

القاضي، إيمان عبدالله. (1429هـ). ***النباتات الطبيعية للبيئة الساحلية بين رأسي تنورة والملوح بالمنطقة الشرقية: دراسة في الجغرافيا النباتية وحماية البيئة***. رسالة دكتوراه غير منشورة، كلية الآداب للبنات، الدمام، المملكة العربية السعودية: جامعة الملك فيصل.

- **الاقتباس من الشبكة العنكبوتية (الإنترنت):**

- الاقتباس من كتاب:

المزروعي، م.ر. و المدني، م.ف. (2010م). ***تقييم الأداء في مؤسسات التعليم العالي***. المعرِّف الرقمي (DOI:10.xxxx/xxxx-xxxxxxxx-x)، أو برتوكول نقل النصوص التشعبي (http://www...)، أو الرقم المعياري الدولي للكتاب (ISBN : 000-0- 00 - 000000-0)

– الاقتباس من مقالة في دورية:

المدني، م.ف. (2014). مفهوم الحوار في تقريب وجهات النظر. ***المجلة البريطانية لتكنولوجيا التعليم***، *11*(6)، 225-260. المعرِّف الرقمي (DOI:10.xxxx/xxxx-xxxxxxxx-x) أو برتوكول نقل النصوص التشعبي (http://onlinelibrary.wiley.com/journal/10.1111)، أو الرقم المعياري التسلسلي الدولي للمجلة - (ISSN: 1467 - 8535).

15) يلتزم الباحث بترجمة (أو رومنة) أسماء المصادر والمراجع العربية إلى اللغة الإنجليزية في قائمة المصادر والمراجع. وعلى سبيل المثال:

الجبر، سليمان. (1991م). تقويم طرق تدريس الجغرافيا ومدى اختلافها باختلاف خبرات المدرسين وجنسياتهم وتخصصاتهم في المرحلة المتوسطة بالمملكة العربية السعودية. ***مجلة جامعة الملك سعود- العلوم التربوية***، *3*(1)، 143-170.

Al-Gabr, S. (1991). The Evaluation of Geography Instruction and the Variety of its Teaching Concerning the Experience, Nationality, and the Field of Study in Intermediate Schools in Saudi Arabia *(in Arabic). Journal of King Saud University- Educational Sciences, 3*(1), 143-170.

16) تستخدم الأرقام العربية الأصلية (0، 1، 2، 3، ...) في البحث.

17) تؤول جميع حقوق النشر للمجلة في حال إرسال البحث للتحكيم وقبوله للنشر.

ثانياً: الأشياء المطلوب تسليمها

1) نسخة إلكترونية من البحث بصيغتي (WORD) و (PDF)، وترسلان على البريد الإلكتروني الآتي:

s.journal@nbu.edu.sa

2) السيرة الذاتية للباحث، متضمنة اسمه باللغتين العربية والإنجليزية، وعنوان البريد الإلكتروني الحالي، ورتبته العلمية.

3) تعبئة النماذج الآتية:

أ - نموذج طلب نشر بحث في المجلة.

ب - نموذج تعهد بأن البحث غير منشور أو مقدم للنشر في مكان آخر.

ثالثاً: تنبيهات عامة

1) أصول البحث التي تصل إلى المجلة لا تردّ سواء أُنشِرَتْ أم لم تنشر.

2) الآراء الواردة في البحوث المنشورة تعبر عن وجهة نظر أصحابها.

مجلة الشمال للعلوم الأساسية والتطبيقية (JNBAS)
طباعة - ردمد: 1658-7022 إلكتروني - ردمد: 1658-7014
المجلد الثامن - العدد الثَّاني نوفمبر 2023م - ربيع الثَّاني 1445هـ

المحتويات

الأبحاث العربية

الأبحاث الإنجليزية

الأبحاث باللغة العربية

المملكة العربية السعودية
جامعة الحدود الشمالية (NBU)
مجلة الشمال للعلوم الأساسية والتطبيقية (JNBAS)
طباعة ردمد: 1658-7022/ إلكتروني – ردمد: 1658-7014
www.nbu.edu.sa
http://jnbas.nbu.edu.sa

دراسة مقارنة لتقدير الخواص الفيزوكيميائية وبعض الفلزات الموجودة في مياه بعض آبار الشرب بوادي حضرموت

منير سعيد عُبّد[1](*) محمد صالح باشنيني[1] محمد برك القيسي[1]

(قدم للنشر في 1444/9/13هـ؛ وقبل للنشر في 1445/2/21هـ)

مستخلص البحث: هدفت هذه الدراسة إلى معرفة ومقارنة الخواص الفيزوكيميائية مثل الرقم الهيدروجيني، التوصيلية الكهربية، مجموع الأملاح الذائبة وعسر الماء الكلي إضافة إلى معرفة ومقارنة تركيزات الفلزات الرئيسية كالصوديوم، البوتاسيوم، الكالسيوم، المغنسيوم، الحديد، المنجنيز، النحاس، الخارصين، الكادميوم والرصاص الموجودة في بعض آبار مياه الشرب لأهم مديريات وادي حضرموت. واستخدمت في هذه الدراسة عدد من الأجهزة الحديثة كجهاز مقياس الرقم الهيدروجيني، جهاز الامتصاص الذري (AAS)، جهاز انبعاث اللهب وجهاز الامتصاص الجزيئي للطيف المرئي وفوق البنفسجي. وقورنت النتائج المتحصل عليها بالمعايير والمواصفات القياسية الدولية واليمنية. فبعد أن خضعت 80 عينة مأخوذة من 40 بئر لحوالي 1680تحليل، وجدنا أنه 15 % منها فقط غير متطابقة مع المعايير الدولية بما يتعلق بعسر الماء الكلي أو تراكيز بعض المعادن. أما بالنسبة للمعايير والمقاييس اليمنية فقد أظهرت النتائج أيضًا أن 85 % من هذه الآبار متطابقة نتائجها مع هذه المعايير. وخلصت النتائج أن نسبة عدم تطابق آبار مديرية سيئون العاصمة مع المعايير الدولية والمحلية بلغت حوالي 8.4 % فقط. في حين اختلف الأمر لمديرية شبام حيث أن 55.6 % من النتائج أظهرت عدم التطابق وتجاوزت الحد المسموح به دوليًا ومحليًا من حيث بعض الخواص المدروسة. كذلك لم يثبت من خلال هذه الدراسة أي تلوث عضوي بالنيترات في هذه الآبار رغم وجود بعض هذه الآبار بالقرب من مناطق سكنية. وحسب النتائج المتحصل عليها يمكن القول إن معظم مياه آبار حقل جوجة وبئر الحوطة في مديرية شبام وأيضًا بئر الغرفة في مديرية سيئون كانت ذات عسرة عالية. لذلك فأننا نوصي بعمل معالجة أولية مستمرة لمياه هذه الآبار أو استبدالها بآبار أخرى أقل ملوحة.

كلمات مفتاحية: الفلزات الرئيسية، جهاز الامتصاص الذري، جهاز انبعاث اللهب، المعايير والمواصفات القياسية الدولية واليمنية.

*** للمراسلة:**
أستاذ مساعد. قسم الكيمياء، كلية العلوم، جامعة حضرموت. ص ب: 50511 رمز بريدي: 00967 ، المكلا، الجمهورية اليمنية.

e-mail: m.obbed@hu.edu.ye

DOI:10.12816/0061646

Journal of the North for Basic and Applied Sciences, Vol. (8), Issue (2), (November 2023/ Rabi' II 1445 H) 63-78

KINGDOM OF SAUDI ARABIA
Northern Border University (NBU)
Journal of the North for Basic & Applied Sciences(JNBAS)
p - ISSN : 1658 -7022 / **e-ISSN: 1658 - 7014**
www.nbu.edu.sa
s.journal@nbu.edu.sa

Comparative study to estimate the physicochemical properties and some metals existent in the water of some drinking wells by Valley Hadhramout

Munir Saeed Obbed(*)[1] Mohammed Saleh Bashnaini[1] Mohammed Brek Al-qaisi[1]

(Received 4/4/2023 ; accepted 6/9/2023)

Abstract: Groundwater is one of the most important sources of drinking water; hence, this study aimed to know and compare between the physicochemical properties such as pH, conductivity, total Dissolved salts and total water hardness, in addition analyzing and studying some metals found in some drinking water wells in Hadhramout Valley, which are sodium, potassium, calcium, magnesium, iron, manganese, copper, zinc, cadmium and lead. With comparing it with international and Yemeni standards and specifications. In the analysis process, we used a number of modern devices such as the pH meter, the atomic absorption device (AAS), the flame photometer, and the visible - ultraviolet spectrum spectrophotometer. During this study, 80 samples from 40 wells were subjected to about 1680 analyzes. The results revealed that only15% of these wells do not conform with international and Yemeni standards and measurements. For example, in the wells of Seiyun directorate, we find that about 91.6% of which are consistent with international and Yemeni standards and measurements. As another example, for the Directorate of Shibam, the results showed that 44.4% of the wells studied matched the international and Yemeni standards and measurements. Also, this study did not prove any organic pollution with nitrates in these wells, despite the presence of some of these wells near residential areas. At the end of this study, we recommend a continuous primary treatment for the water of wells that suffer from high salinity and hardness or to stop work in these wells and replace them with other less saline wells.

Keywords: the main metals, flame photometer, atomic absorption device, international and Yemeni standards.

DOI: 10.12816/0061646

* **Corresponding Author:**
Assistant Professor, Dept., of Chemistry Faculty of Science, Hadhramout University, P.O. Box: 50511 Code: 00967, City of Mukalla, Yemen.

e-mail: m.obbed@hu.edu.ye

1- المقدمة:

يعتبر الماء المكون الأساس لمعظم الكائنات الحية، فثلثي وزن جسم الإنسان عبارة عن ماء، وليس الإنسان فقط فكل الكائنات الحية يشكل الماء نسبة عالية من وزنها (شحاته، 2014). ويعمل الماء على تنظيم درجة حرارة الجسم ويمنحه الرطوبة اللازمة ويساعد على تنشيط وظائف الكليتين ويخلص الجسم من السموم ويساعده على الاتزان الكيميائي حيث يقوم بدور الوسيط في كثير من العمليات الكيميائية داخل الجسم (سليمان، 2020). وتعتبر المياه الجوفية في حضرموت عمومًا ووادي حضرموت بشكل خاص أهم مصدر للمياه العذبة الصالحة للشرب أو للزراعة التي تعتمد على حوالي 27 % من المياه الجوفية في ريِّها، إضافة إلى الاستخدامات المنزلية والصناعية (عبدالجبار، 2020). إلا أن المياه الجوفية في اليمن شهدت تدهورًا كبيرًا في الفترة الأخيرة، وذلك بسبب قلة تغذية المخزون الجوفي مع الاستنزاف الجائر في استهلاك المياه المتوفرة به إضافة لما يحدث من تسرب لمياه الصرف الصحي والمبيدات الحشرية والأسمدة المستخدمة في الزراعة إليه (المنيفي، 2004).

وحيث إنه يشترط في مياه الشرب أن تكون نقية وصالحة للاستهلاك البشري مع خلوها من الملوثات الكيميائية، فلهذا فقد أصبحت الفحوصات المتعلقة بتحديد الخصائص النوعية لمياه الشرب في مقدمة الإجراءات المطلوبة والتي يجب أن تعمل بشكل دوري للتأكد من سلامة مياه الشرب من أي نوع من التلوث (الموسوي وحمزة، 2010 ؛ Gebresilasie, Berhe, Tesfay & Gebre 2021) وفي نفس الوقت فقد وُضِعت مواصفات قياسية للمياه متضمنة طريقة فحص هذه المياه والحد (المعيار) للملوثات المسموح بوجودها في مياه الشرب وذلك لحماية المستهلكين من نقص المعادن أو التسمم بها وكذلك من الأمراض التي تنتقل عبر المياه (الحديثي، 1986؛ Al-shaikh 2017). ومن الدراسات التي أجريت في هذا المجال، الدراسة التي أجريت في سنة 2016م من قبل الشيخ أبوبكر على بعض مدارس التعليم الأساسي والثانوي بمدينة المكلا لقياس بعض الخواص الفيزوكيميائية للمياه مثل درجة الحرارة والأملاح الذائبة الكلية وغيرها ومقارنتها بالمواصفات القياسية اليمنية والعالمية، وقد اتضح أنه كلما زادت قيم الأملاح الذائبة الكلية، الناقلية الكهربية، درجة الحرارة، تركيز أيون الهيدروجين، والعكارة زادت أعداد البكتيريا في المياه، مما يدل على عدم صلاحيتها للشرب (Bin Hameed & Bin Alshikh Bubkr, 2019) ودومًا تعتبر مشكلة تلوث مياه الشرب بكافة أنواعها سواءً كان هذا التلوث فيزيائي أو كيميائي أو حيوي أو إشعاعي من أوائل الموضوعات التي اهتم بها العلماء والمختصون بمجال التلوث لما للماء من أهمية وضرورة قصوى للحياة (محمد وأحمد، 2010)، وهو ما يعطي لهذا الموضوع أهمية كبيرة للباحثين مثل بن عباد الذي قام بتقدير تراكيز بعض المعادن الثقيلة والفحص الميكروبيولوجي لعينات مياه الشرب في بعض مناطق ساحل حضرموت (بن عباد، 2019)، وقد أظهرت نتائجه أن متوسط قياس الأس الهيدروجيني وتركيز أهم المعادن لمعظم العينات تقع ضمن الحدود المسموح بها لمياه الشرب حسب المواصفات القياسية اليمنية والدولية. ورغم أن هناك الكثير من الفوائد للمعادن المختلفة لجسم الإنسان مثل الصوديوم، الكالسيوم، البوتاسيوم، المغنيسيوم، الرصاص، الكادميوم، الحديد، النحاس وغيرها فهي تبني الخلايا والعظام وتساعد في التفاعلات الحيوية بالجسم وترسل الإشارات للأعصاب والعضلات وغيرها من المهام بجسم الإنسان، إلا أن استهلاكها بكميات كبيرة يكون ضارًا بل وسامًا (Kheiralla, Goja, Bakheet, Al-Gamdi & Sadath (2020، وتأتي خطورة المعادن الثقيلة من تراكمها الحيوي داخل جسم الإنسان بشكل أسرع من عملية التمثيل الغذائي (الأيض) أو إخراجها (زبار وشاكر، 2009؛ الهيئة العامة للموارد المائية، 1999). وعربيًا كان هناك الكثير من الاهتمام بجودة مياه الشرب، وقد عملت الكثير من الدراسات لذلك منها دراسة زاهد بسنة 2002م، لتقدير جودة مياه الشرب المعبأة المحلية والمستوردة في المملكة العربية السعودية، ومقارنتها بالمواصفات والمقاييس السعودية والعالمية، وتم من خلال هذه الدراسة تقييم المعايير الفيزيائية والكيميائية والميكروبيولوجية. وأظهرت النتائج أن الأصناف المحلية والمستوردة كانت مطابقة للمواصفات فيما عدا الرقم الهيدروجيني ال pH في صنف واحد والفلورايد في 15 صنفاً محلياً والمنجنيز في 12 صنفاً محلياً و6 أصناف مستوردة (زاهد، 2002).

ونظرًا لعزوف السكان المحليين بوادي حضرموت وقلة ثقتهم في مياه الشرب العامة واعتمادهم بشكل كبير على مياه التحلية ومياه الفلاتر المنزلية ومياه الشرب المعبأة المحلية والمستوردة ودفعهم مقابل الحصول عليها مبالغ مالية تثقل كاهلهم، إضافة لما يحدث من اختلاط لمياه الصرف الصحي بمصادر المياه الجوفية عن طريق حفر البيارات وكذلك استخدام شبكات لنقل المياه قديمة ومعرضة أنابيبها للتآكل والصدأ مما قد يؤدي إلى تلوثها بمخلفات الصداء. وهذا كله يترافق مع قلة الدراسات التي تثبت ملائمة هذه المياه للشرب، فقد استدعى كل ذلك لعمل هذه الدراسة والتي تتفق مع الدراسات التجريبية المختبرية في هذا الموضوع من حيث الطريقة في جمع العينات من مصادرها ثم إخضاع هذه العينات للتحليل والقياس في المختبر باستخدام الطرق المختلفة والأجهزة المتنوعة للتعرف على الخواص الفيزيائية والتي منها: الرقم الهيدروجيني، التوصيلية الكهربية، مجموع الأملاح الذائبة، مجموع المواد الصلبة العالقة، العسرة الكلية (علوان، 2017)، أو الخواص الكيميائية والتي منها: التعرف على تراكيز الصوديوم، البوتاسيوم، المغنسيوم، الكالسيوم، الحديد، الزئبق، الكبريتات، البيكربونات، وغيرها. وعند التعرف على النتائج، تتم مقارنتها بمعايير منظمة الصحة العالمية والمعايير والمواصفات اليمنية لمعرفة مدى تطابقها أو اختلافها للحكم على خصائص مياه الشرب ومدى صلاحيتها للشرب، ووضع الحلول للتغلب على المشكلات إما عن طريق المعالجة لهذه المياه أو غيرها من الحلول.

2- العرض:

2 – 1- موقع الدراسة وجمع العينات:

تعتبر محافظة حضرموت أكبر محافظات اليمن وأكثرها أهمية، وتنقسم إداريًا إلى 1- ساحل حضرموت 2- وادي وصحراء حضرموت. وتفصل بين حضرموت الساحل والوادي جبال تتفاوت في ارتفاعها. ويعتبر وادي حضرموت من أهم وأكبر وديان الجمهورية اليمنية حيث يمتد على مساحة تصل إلى أكثر من 1850 كيلومتر مربع (الصبان، 2000)، وهو من المناطق الجافة ويمتد من رملة السبعتين غربًا وينتهي بمصبه في سيحوت محافظة المهرة الواقعة على البحر العربي، ويقع بين خطي عرض 15 -17 درجة شمالاً وخطي طول 46-51 درجة شرقاً ويتراوح ارتفاعه عن سطح البحر بين 600-700 متر. وفي هذا الامتداد الجغرافي الكبير تعاقبت حضارات مازالت معالمها قائمة حتى الآن. وهناك كذلك مجموعة من الأودية الفرعية التي تصب في المجرى الرئيسي للوادي مثل وادي سر ووادي عمد ووادي دوعن وغيرها (بامومن، 2012). ومن أهم مديريات وادي حضرموت: 1- سيئون: وهي من أهم مديريات الوادي وبها أكبر مدنه وهي العاصمة سيئون. 2- تريم: والتي تشتهر بكثرة مساجدها وأشهرها مسجد المحضار وهي من أهم المدن التاريخية بحضرموت. 3- شبام: والتي تعتبر أيضًا من المدن التاريخية وتشتهر بمبانيها القديمة العالية. 4- القطن: وهي مديرية زراعية خصبة تشتهر بكثرة المزارع الصالحة للزراعة. 5- ساه: والتي تقع في موقع متميز على طريق السيول ومياه الأمطار وهي بساط أخضر يحتضن الكثير من المناطق السياحية والأثرية إضافة لمواقع التنقيب وإنتاج النفط (وزارة التخطيط والتعاون الدولي، 2015).

وفي هذه الدراسة تم جمع 80 عينة لمياه الشرب من 40 بئر من آبار وحقول تابعة للمؤسسة المحلية للمياه والصرف الصحي لمناطق الوادي والصحراء بمحافظة حضرموت، وبمعدل عينتين لكل بئر، وكانت الفترة الزمنية ما بين أخذ العينة الأولى والثانية ما بين الشهر والنصف إلى الشهرين، وهذه الآبار كانت موزعة على خمس مديريات من مديريات الوادي والصحراء بمحافظة حضرموت وهي سيئون – تريم – شبام – القطن – ساه. وتوزيع هذه الآبار على المديريات وأعماقها موضح في الجدول (1).

جدول (1):

عدد وتوزيع الآبار على المديريات وأعماقها.

المديرية	الحقل	عدد الآبار	متوسط عمق الآبار بالمتر
سيئون	جثمة، الغرفة	13	230
تريم	دمون	9	132-170
شبام	موشح، جوجه، الحوطة	9	245
القطن	شعب الحمضان	5	225
ساه	ساه	4	200- 100

(المؤسسة المحلية للمياه والصرف الصحي- مديريات الوادي والصحراء- محافظة حضرموت- اليمن)

وقد تم جمع العينات في الفترة من شهر ديسمبر 2021 م إلى شهر مارس2022م أي في فصلي الشتاء والربيع حيث كان الجو ما بين معتدل وبارد. فبعد فتح الحنفية بشكل كامل وترك الماء يسيل لمدة ثلاث إلى خمس دقائق يتم بعدها جمع عينة الماء المطلوبة في قناني بلاستيكية وزجاجية نظيفة سعة 500 مل ثم تغطى العلبة مباشرة مع وضع حماية لغطاء العلبة (الهيئة العامة للموارد المائية،1999؛ عبد الحافظ ومبارك، 1996). تم تحفظ هذه العينات في البراد إلى حين وصولها إلى المختبر للتحليل خلال فتره زمنية لا تتجاوز ال 48 ساعة.

2-2 - المواد والأجهزة:

لقد تم استخدام العديد من المواد الكيميائية ذات النقاوة العالية مصنوعة كلها من قبل شركة BDH الإنجليزية والتي شملت NaOH (99.5%), EBT, EDTA-Na_2 (99%), $CaCO_3$, NaOH (99%), Murrexide (98%), KCl (97%), $CuSO_4$ (98%), $CdCl_2$ (99.9%), $PbCl_2$ (100%), $ZnSO_4$ (99%). وتمت عملية تحليل العينات في كلًا من مختبر المؤسسة المحلية للمياه والصرف الصحي لمناطق الوادي والصحراء، وأيضًا في مختبر محطة البحوث الزراعية بسيئون. في هذه الدراسة تم استخدام جهاز قياس الرقم الهيدروجيني pH-meter ذو الموديل HQ40d والذي في نفس الوقت يقيس التوصيلية الكهربية، إضافة إلى جهاز الامتصاص الجزيئي للطيف المرئي وفوق البنفسجي Spectrophotometer والجهازان مصنوعان في الولايات المتحدة الأمريكية من قبل شركة HACH وموجودان بالمؤسسة المحلية للمياه والصرف الصحي بالوادي والصحراء. كذلك تم استخدام جهاز طيف الامتصاص الذري Atomic Absorption Spectrometer (AAS) من شركة Philips الإنجليزية مع جهاز الانبعاث الذري اللهبي Flame Photometer من شركة jeu way الإنجليزية، والجهازان موجودان في مختبر محطة البحوث الزراعية بسيئون.

2-3- تحليل عينات مياه الشرب بواسطة المعايرة (Titration):

استخدمت المعايرة في هذه الدراسة لتقدير الكالسيوم والمغنسيوم، وأيضًا عسر الماء الكلي وعسر المغنسيوم وعسر الكالسيوم.

2-3-1- إيجاد العسر الكلي (Total Hardness (TH:

تم وضع حجم مناسب حجم مناسب (50 مليليتر) من عينة المياه المدروسة في دورق مخروطي مناسب مضافًا لها 2 مليليتر من المحلول المنظم (pH 10)، وكمية بسيطة من دليل الـ EBT (Black T Eriochromo) والذي يحضر عن طريق خلط 0.5 جرام من صبغة الـ EBT مع 100 جرام من كلوريد الصوديوم ويخلطان خلطًا جيدًا، تتم بعدها المعايرة بواسطة بمحلول EDTA-Na_2 (Ethylene diamine tetra acetic acid disodium) ذو التركيز 0.01M والموضوع بالسحاحة لحين تحول اللون البنفسجي إلى اللون الأزرق ثم تسجل قراءة السحاحة. وبعدها نحسب تركيز العسر الكلي للعينات على هيئة كربونات الكالسيوم بتركيز المليجرام/ لتر باستخدام المعادلة 1.

$$\text{TH as } CaCO_3 = \frac{\text{M(EDTA) X 100 X 1000 X ml titration}}{\text{Sample volume (ml)}} \quad (1)$$

حيث أن M تمثل هنا التركيز المولاري (Ryan and Garabet, 1996).

2-3-2- تقدير الكالسيوم وعسره (Ca Hardness):

تم وضع 50 مليليتر من عينة المياه بالدورق المخروطي، ويضاف إليها 2 مليليتر من محلول هيدروكسيد الصوديوم ذو التركيز 1N وذلك لرفع الأس الهيدروجيني، مع كمية بسيطة من دليل الميروكسيد Murexide (والذي يحضر عن طريق خلط 0.2 جرام من صبغة الميروكسيد مع 100 جرام من كلوريد الصوديوم، ويخلطان خلطاً جيداً)، ثم قمنا بعدها بالمعايرة بواسطة محلول EDTA-Na_2 ذو التركيز 0.01M الموجود بالسحاحة لحين تحول اللون الوردي إلى اللون الأزرق وسجلت عندها القراءة، ثم تم حساب تركيز الكالسيوم بالمليجرام/ لتر عن طريق المعادلة 2. أما المعادلة 3 فاستخدمت لإيجاد عسر الكالسيوم.

$$\text{Ca} = \frac{\text{M(EDTA) X 40.08 X 1000 X ml titration}}{\text{Sample volume (ml)}} \quad (2)$$

$$\text{Ca Hardness} = \frac{\text{M(EDTA) X 100 X 1000 X ml titration}}{\text{Sample volume (ml)}} \quad (3)$$

حيث أن 100 هنا تمثل الوزن الجزيئي لكربونات الكالسيوم، وال 40.08 تمثل الوزن الذري للكالسيوم.

2-3-3- تقدير الماغنيسيوم وعسره:

وقد تم تقديره حسابياً من القيم المتحصل عليها للكالسيوم في الفقرة السابقة وذلك باستخدام المعادلتين 4 و5.

$$\text{Mg mg/L} = \frac{\text{TH} - (\text{Ca X } 2.5)}{4.11} \quad (4)$$

حيث أن TH هو عسر الماء الكلي، بينما المقصود بال 2.5 هي نسبة وجود المغنسيوم في القشرة الارضية. و4.11 تعبر عن وجود الكالسيوم في القشرة الأرضية (Rodger, Andrew and Eugene, 2017).

عسر المغنسيوم = عسر الماء الكلي – عسر الكالسيوم (5)

2-4- التحليل باستخدام جهاز الانبعاث الذري اللهبي (Flame Photometer):

تعتبر هذه التقنية من أقدم الوسائل لمعرفة وتقدير العناصر (أبو الكباش، 2012). وفي هذه الدراسة تم استخدام هذا الجهاز لتقدير كلًا من الصوديوم والبوتاسيوم في عينات مياه الشرب قيد الدراسة. ففي البداية تم ترشيح العينات للتخلص من أي مواد عالقة بها، ثم وضعت هذه العينات في عبوات بولي إيثيلين مع مراعاة أن الخزن الطويل في العبوات البلاستيكية يجب ألا يحدث بسبب فاقد التبخر من خلال الوعاء أو الغطاء. وتتم عملية التقدير من خلال تشغيل الجهاز بإشعال اللهب وتركه لمدة عشر دقائق أو أكثر لكي يسخن ثم ضبط شدة اللهب عن طريق تحريك صمام الغاز. بعد ذلك يتم وضع الجهاز في وضع قياس الصوديوم عند فلتر الصوديوم في حالة تقدير الصوديوم، وعند تقدير البوتاسيوم يتم وضع الجهاز في وضع قياس البوتاسيوم عند فلتر البوتاسيوم. بعدها يصفر الجهاز باستخدام الماء المقطر. وقد تم تحضير محاليل قياسية بتركيز10 جرام / لتر محضرة بشكل دقيق من مواد نقية مصنعة من شركة BDH الإنجليزية لكل عنصر (كلوريد الصوديوم وكلوريد البوتاسيوم). يتم بعدها قياس امتصاص هذه المحاليل القياسية على الجهاز لكل عنصر بحسب متطلباته ثم يعاد تصفير الجهاز بالماء المقطر. بعدها تمت عملية إيجاد تراكيز الصوديوم والبوتاسيوم في كل عينات مياه الشرب بوحدة المليجرام/ لتر وعند الطول الموجي المناسب لكل عنصر. ونستخدم بعدها القانون التالي لإيجاد تركيز عنصري الصوديوم والبوتاسيوم في عينات مياه الشرب:

تركيز العنصر بوحدة ppm = قراءة العينة X $\frac{\text{تركيز المحلول القياسي}}{\text{قراءته}}$ (6)

2-5- التحليل باستخدام جهاز الامتصاص الجزيئي للطيف المرئي والفوق البنفسجي Spectrophotometer:

استخدم هذا الجهاز في هذه الدراسة لتقدير عنصري الحديد والمنجنيز في عينات مياه الشرب قيد الدراسة. وعند التحليل يجب هنا أولًا مراعاة أنه عند أخذ العينات وخزنها فإن الحديد المذاب يمكن

أن يتأكسد بعوامل الأكسدة ومن الممكن أن يترسب أيضًا على سطح وعاء العينة، ولذا يمكن منع هذا بإضافة 1.5 ملليلتر من حامض النتريك المركز لكل لتر من العينة مباشرةً بعد جمعها. ولعملية التحليل على الجهاز، نقوم أولًا بتشغيل الجهاز والانتظار قليلًا ثم نضبط الجهاز على الطول الموجي المناسب لقياس الحديد عند 265 nm ولقياس المنجنيز عند 552 nm. نملأ بعدها خليتين من خلايا القياس الخاصة بالجهاز والمصنوعة من الكوارتز لكل عينة من العينات المراد قياسها ونضيف الكاشف الخاص بالحديد إلى إحدى الخليتين مع تغطية الخلية التي بها الكاشف في حالة تقدير الحديد واستعمال الكاشف الخاص بالمنجنيز في حالة تقدير المنجنيز، ونترك العينة بعدها لمدة 3 دقائق وهو الوقت اللازم للتفاعل، وبعد انتهاء وقت التفاعل ندخل الخلية غير المحتوية على الكاشف (Blank) أولًا ونضغط على الزر Zero ثم بعدها ندخل العينة المحتوية على الكاشف ونضغط على الزر Read ونقرأ تركيز الفلز المطلوب بوحدة المليجرام/ لتر.

2-6- التحليل باستخدام جهاز الامتصاص الذري (AAS):

تم هنا استخدام جهاز الامتصاص الذري مع جميع توابعه (الشفاط، اسطوانة الغاز، وخلايا القياس والتوابع الأخرى ذات العلاقة). وذلك لتقدير كلًا من فلزات النحاس Copper والخارصين (الزنك) Zinc وكذلك لتقدير الرصاص Lead والكادميوم Cadmium. ولتحقيق ذلك، تم في البداية تشغيل الجهاز وإشعال اللهب مع ضبط شدة اللهب عن طريق تحريك صمام الغاز، ويترك لمدة عشر دقائق تقريبًا لكي يسخن ثم بعدها يتم وضع الجهاز عند قياس العنصر المطلوب في كل مرة وبتحديد الطول الموجي المناسب لكل عنصر (النحاس 324.8 nm، الخارصين 213.9 nm، الرصاص 217 nm والكادميوم 228.8 nm). وبعدها يصفر الجهاز باستخدام الماء المقطر. وقد حضرت محاليل قياسية بتركز 1 مليجرام/ لتر (1 ppm) للفلزات المدروسة، ومحضرة بدقة من مواد نقية لكل عنصر من العناصر المدروسة (كبريتات النحاس $CuSO_4$، كبريتات الخارصين $ZnSO_4$، كلوريد الرصاص $PbCl_2$ وكلوريد الكادميوم $CdCl_2$). وبعد كل قياس للمحلول القياسي بالجهاز يعاد تصفير الجهاز بالماء المقطر ثم يتم بعدها قياس تركيز الفلز المطلوب في عينات ماء الشرب المدروسة وتؤخذ القيمة من الجهاز بوحدة مليجرام/ لتر. وإذا كانت قيمة القراءة على الجهاز للعينة أعلى من 1 مليجرام/لتر يتم تخفيفها بالماء المقطر وتضرب القراءة بعد ذلك في معامل التخفيف. ونستخدم المعادلة الآتية لإيجاد تركيز العنصر.

تركيز العنصر بوحدة ppm = (7)

$$\text{قراءة العينة} \times \frac{\text{تركيز المحلول القياسي}}{\text{قراءته}}$$

(8)

2-7- قياس الأس الهيدروجيني (pH) والتوصيلية الكهربية ومجموع الأملاح الذائبة لعينات مياه الشرب المدروسة:

لقياس الأس الهيدروجيني والتوصيلية الكهربية ومجموع الأملاح الذائبة لعينات الماء قيد الدراسة، فهي تتم كلها على نفس الجهاز وهو pH meter، حيث تُغسل أولاً أقطاب الجهاز جيدًا بالماء المقطر ثم تجفف الأقطاب برفق بواسطة مناديل الورق الناعم قبل استخدام الجهاز. وبعد ذلك تتم معايرة الجهاز بالمحاليل المنظمة الخاصة بالجهاز وذلك للتحقق من صلاحيته للاستخدام وضبطه. وقد تم أخذ كل عينة على انفراد ووضعها في دورق زجاجي نظيف وترج جيدًا لمجانستها، وبعد ذلك تمت عملية قياس الخواص المطلوبة لعينات المياه المأخوذة وذلك بوضع قطبي الجهاز في العينة وتدوين النتيجة على أن يتم غسل قطبي الجهاز بالماء المقطر بين كل قياس وآخر. وقد تم أخذ ثلاث قراءات لكل عينة، وأخذ متوسط القراءات بعد ذلك. مع العلم أن قراءة مجموع الأملاح الذائبة يتم أخذها عن طريق ضرب قيمة التوصيلية الكهربية للعينة في المعامل الخاص باليمن وهو 0.65.

جدول(2):

يوضح العناصر التي تم قياسها وطريقة تحليلها أو قياسها

الرقم	العنصر	طريقة التحليل
1	الكالسيوم	المعايرة
2	المغنسيوم	المعايرة
3	الصوديوم	الانبعاث الذري اللهبي
4	البوتاسيوم	الانبعاث الذري اللهبي
5	الخارصين	الامتصاص الذري
6	المنجنيز	الامتصاص الجزيئي للطيف المرئي والفوق البنفسجي

7	النحاس	الامتصاص الذري
8	الحديد	الامتصاص الجزيئي للطيف المرئي والفوق البنفسجي
9	الرصاص	الامتصاص الذري
10	الكادميوم	الامتصاص الذري

3- النتائج والمناقشة:

بعد إخضاع 80 عينة مجموعة من 40 بئر والتي تشمل الخمس المديريات المستهدفة للتحليل والقياس في مختبر المؤسسة المحلية للمياه والصرف الصحي ومختبر البحوث الزراعية بسيئون، وباستخدام الأجهزة المختلفة المذكورة سابقًا، والتي تم من خلالها إيجاد الخواص الفيزوكيميائية لعينات مياه الشرب مثل التوصيلية الكهربية، مجموع الأملاح الذائبة الكلية والرقم الهيدروجيني وغيرها، هذا إضافة إلى تقدير تراكيز فلزات الصوديوم والبوتاسيوم والكالسيوم والمغنسيوم والحديد والرصاص والمنجنيز والنحاس والزنك والكادميوم. وبعد أن تم أخذ متوسط القراءتين لكل هذه الخواص والتقديرات تم بعد ذلك مقارنة هذه النتائج المتحصل عليها مع المعايير والمقاييس الدولية واليمنية لكل من الخواص الفيزوكيميائية وتراكيز الفلزات قيد الدراسة. وكانت النتائج المتحصل عليها كالآتي:

3-1- قيم الرقم الهيدروجيني والتوصيلية الكهربية لعينات مياه الشرب المدروسة:

أن متوسط قراءات جميع الآبار قيد الدراسة لقيم الرقم الهيدروجيني كانت بين (7.29 – 8.04) حيث كانت أدنى قيمة له لبئر سيئون رقم (9) بينما أعلى قيمة له هي لبئر جوجة القبلية فهي تميل نوعًا ما إلى القلوية. وبالنسبة للحد الأدنى والحد الأعلى لقيم الرقم الهيدروجيني لمياه آبار المديريات الخمس التابعة لمؤسسة المياه بوادي حضرموت فجميعها تقريبًا تقع في إطار الحد المسموح به، ففي مديرية سيئون تراوحت هذه القيم ما بين 7.29 – 7.74 لبئري سيئون رقم (9) وسيئون رقم (2) على التوالي. أما مديرية شبام، فأن أدنى قيمة للرقم الهيدروجيني هي لبئر موشح رقم (3) وكانت 7.45، بينما أعلى قيمة كانت لبئر جوجة القبلية ومقدارها 8.04 والتي تعتبر أيضًا أعلى قيمة لجميع الآبار ككل. وفي مديرية تريم، فأن القيم تتأرجح في المتوسط ما بين 7.55 – 7.90 لبئري تريم رقم (7) وتريم رقم (2) على التوالي. وعند أخذ متوسط قيم الرقم الهيدروجيني لآبار مديرية القطن، فأدنى قيمة كانت لبئر الحمضان رقم (6) وأعلى قيمة لبئر الحمضان رقم (2) وسجلت هذان البئران القيم 7.52 – 7.84 على التوالي. وأخيرًا بمديرية ساه يكون متوسط القيم المسجل لدينا هو ما بين 7.68 – 7.86 في أدنى قيمة له لبئر ساه رقم (3) وأعلى قيمة لبئر ساه رقم (1) وجدول (3) يوضح هذه القيم. وعمومًا فأن هذه النتائج تتفق مع ما توصلت إليه دراسات سابقة لبعض آبار الشرب باليمن من حيث قيم الرقم الهيدروجيني للآبار المدروسة لديهم، مثل دراسات بامتيرف وحسن وبن يحيى (بامتيرف،2007؛ Bin yahia, 2005؛ Hassan, Mugbil and Alballem 2008). أما متوسط قيم التوصيلية الكهربية (EC) لجميع الآبار قيد الدراسة فقد تراوحت ما بين (753 - 2220) ميكرو سيمنس/ سم، حيث سجلت أدنى قيمة لبئر سيئون رقم (13) تليها بئر ساه رقم 4 بمقدار 767 ميكرو سيمنس/ سم. أما أعلى قيمة فهي من نصيب بئر جوجة الوسطى بشبام ويليها بئر الغرفة بمقدار 2168، وهذه القيمة المرتفعة تجاوزت الحد المسموح به عالميًا. وبالنظر إلى نتائج قيم الرقم الهيدروجيني والتوصيلية الكهربية المتحصل عليها بشكل عام، نرى أن معظم مياه آبار الشرب بوادي حضرموت التابعة للمؤسسة المحلية للمياه والصرف الصحي متطابقة تقريبًا مع المواصفات القياسية لمنظمة الصحة العالمية والمواصفات اليمنية ماعدا بئر الغرفة بمديرية سيئون وبئر جوجة الوسطى بمديرية شبام حيث كانت قيم التوصيلية الكهربية لهاتين البئرين قد تجاوزت الحد المسموح به حسب معايير منظمة الصحة العالمية بنسبة زيادة وصلت إلى 49 % لتلك البئرين مما يدل دلالة واضحة إلى ارتفاع نسبة الملوحة بهما، لكنهما لا يزالان في إطار الحد المسموح به حسب المواصفات اليمنية. ومن الجدول (3) نلاحظ أن مديرية شبام سجلت أعلى متوسط للموصلية الكهربية بالنسبة لجميع الآبار قيد الدراسة بها. وحيث إن هناك تناسب طردي بين التوصيلية الكهربية ومجموع الأملاح الذائبة، فأي زيادة بالموصلية يقابلها دائمًا زيادة لمجموع الأملاح الذائبة، وهذا يتوافق مع ما توصلت اليه دراسات سابقة (Gharan, Bharti, Giri and Kumar 2023).

جدول (3):
يوضح النتائج النهائية لقيم الرقم الهيدروجيني pH والتوصيلية الكهربية EC بالميكرو موز/ سم لعينات الشرب المدروسة.

مديرية سيئون			مديرية شبام			مديرية تريم			مديرية ساه			مديرية القطن		
البئر	EC	pH	البئر	EC	pH	البئر	EC	pH	البئر	EC	pH	البئر	EC	pH
سيئون 1	1098	7.68	جوجة الشرقية	1449	8	تريم 1	1067	7.79	ساه 1	886	7.86	الحمض ان 2	1246	7.84
سيئون 2	922	7.74	جوجة القبلية	1518	8.04	تريم 2	1023	7.90	ساه 2	832	7.85	الحمض ان 3	1203	7.62
سيئون 3	849	7.68	جوجة الوسطى	2220	7.58	تريم 3	959	7.68	ساه 3	862	7.68	الحمض ان 4	1277	7.62
سيئون 4	828	7.68	الحوطة	1950	7.59	تريم 4	905	7.82	ساه 4	767	7.69	الحمض ان 5	1214	7.54
سيئون 5	836	7.58	موشح 1	1383	7.82	تريم 5	895	7.74				الحمض ان 6	1250	7.52
سيئون 6	917	7.57	موشح 2	1175	7.63	تريم 6	932	7.70						
سيئون 7	847	7.58	موشح 3	1210	7.45	تريم 7	945	7.55						
سيئون 8	1167	7.53	موشح 4	1262	7.51	تريم 8	934	7.66						
سيئون 9	1034	7.29	موشح 5	1210	7.49	تريم 9	934	7.59						
سيئون 10	946	7.58												
سيئون 11	817	7.69												
سيئون 13	753	7.57												
الغرفة	2168	7.58												

2-3- مجموع الاملاح الذائبة (TDS) والعسرة الكلية لعينات مياه الشرب المدروسة:

تقع قيم الاملاح الذائبة الكلية المتحصل عليها ما بين (489 – 1444) ppm. وكانت أدنى قيمة هي لبئر سيئون رقم (13) وأعلى قيمة هي لبئر جوجة الوسطى، تليها بئر الغرفة بسيئون بقيمة 1409ppm، وهي قيمة تجاوزت الحد المسموح به عالميًا، لكنها لاتزال في إطار الحد المسموح به حسب المعيار اليمني. أما العسرة الكلية لهذه العينات المدروسة والتي هي عبارة عن عسرة الكالسيوم والمغنسيوم (فائق،2020)، فقد تراوحت قيمها بين (266 – 608) ppm حيث إن أدنى قيمة كانت لبئر سيئون رقم (13) وأعلى قيمة هي لبئر جوجة الوسطى بشبام، وكما نلاحظ فإن أعلى قيمة قد تجاوزت الحد المسموح به حسب المعيار اليمني ومعيار منظمة الصحة العالمية. وعليه فإننا نعتبر بئر سيئون رقم (13) هي من أفضل الآبار من ناحية نسبة الأملاح، بينما أكثر هذه الآبار ارتفاعًا لنسبة الأملاح هي بئر الغرفة بمديرية سيئون وبئر جوجة الوسطى بمديرية شبام. ويوضح الجدولان (4 و7) قيم هذه النتائج لكل بئر وكذلك متوسط القيم لكل مديرية والذي يمكن أن نلاحظه كذلك بالشكل (1) وهذه النتائج اتفقت كذلك مع دراسات سابقة مشابهة لمدن ساحل حضرموت (بارجاء، 2006; بامتيرف، 2007).

أما بالنسبة للكربونات فقد تراوحت قيمها في المتوسط ما بين 230 – 320 ppm. فأدنى قيمة تشترك فيها آبار سيئون 3, 4, 13. وأعلى قيمة تظهرها بئر سيئون رقم 9 كما هو واضح بالجدول 4 والذي يوضح كذلك قيم عسرة الكالسيوم والمغنيسيوم لجميع الآبار المدروسة.

شكل (1): مخطط لمتوسط قيم آبار كل مديرية بالنسبة لمجموع الاملاح الذائبة (TDS) والعسرة الكلية لعينات مياه الشرب المدروسة.

جدول (4):

عسر الماء الكلي و عسرة الكالسيوم والمغنيسيوم بوحدة mg / L لعينات مياه الشرب المدروسة.

مديرية القطن					مديرية ساه					
البئر	TDS	العسر الكلي لـ $CaCO_3$	عسر الكالسيوم	عسر المغنيسيوم	عسر الكربونات	البئر	TDS	العسر الكلي لـ $CaCO_3$	عسر الكالسيوم	عسر المغنيسيوم	عسر الكربونات
الحمضان 2	810	381	215	166	280	ساه 1	576	321	192	130	260
الحمضان 3	782	398	210	189	290	ساه 2	541	289	163	127	250
الحمضان 4	821	432	237	195	300	ساه 3	560	312	182	130	250
الحمضان 5	789	397	218	177	300	ساه 4	499	290	156	134	290
الحمضان 6	813	397	220	178	300	مديرية شبام					
مديرية سيئون						البئر	TDS	العسر الكلي	عسر الكالسيوم	عسر المغنيسيوم	عسر الكربونات

البئر	TDS	العسر الكلي لـ $CaCO_3$	عسر الكالسيوم	عسر المغنيسيوم	عسر الكربونات			لـ $CaCO_3$		
سيئون 1	713	377	218	160	280	جوجة الشرقية	942	404	233	171	270
سيئون 2	599	309	204	128	250	جوجة القبلية	987	523	264	260	260
سيئون 3	552	302	173	124	230	جوجة الوسطى	1444	608	319	289	306
سيئون 4	539	290	182	108	230	الحوطة	1267	560	303	257	290
سيئون 5	544	308	181	127	240	موشح 1	899	419	261	158	310
سيئون 6	616	303	172	131	240	موشح 2	764	384	236	148	260
سيئون 7	550	287	185	102	250	موشح 3	787	401	246	160	270
سيئون 8	759	375	211	164	280	موشح 4	820	416	253	163	270
سيئون 9	672	378	204	174	320	موشح 5	787	391	230	158	270
سيئون 10	615	336	212	124	240	مديرية تريم					
سيئون 11	531	314	201	113	250	البئر	TDS	العسر الكلي لـ $CaCO_3$	عسر الكالسيوم	عسر المغنيسيوم	عسر الكربونات
سيئون 13	489	266	190	76	230	تريم 1	694	365	211	154	260
الغرفة	1409	624	325	275	300	تريم 2	665	351	200	152	280
						تريم 3	624	323	195	128	260
						تريم 4	588	311	180	131	240
						تريم 5	582	318	175	143	250
						تريم 6	606	325	185	140	260
						تريم 7	615	317	182	135	270
						تريم 8	672	364	200	164	290
						تريم 9	608	360	206	154	270

3-3- إيجاد تراكيز الفلزات الرئيسية (الصوديوم، البوتاسيوم، مغنيسيوم والكالسيوم) لعينات مياه الشرب المدروسة:

من النتائج لدينا، فقد تراوحت قيم الصوديوم ما بين (44 – 273) ppm فأدنى قيمة له كانت لبئر ساه رقم (4) وأعلى قيمة هي لبئر جوجة الوسطى بشبام والتي تجاوزت الحد المسموح به عالميًا لكنها في إطار الحد المسموح به وفق المعيار اليمني. ونلاحظ أن هناك ارتباط وتناسب طردي بين كلًا من الملوحة والتوصيلية الكهربية وبين تركيز الصوديوم والبوتاسيوم والكلوريد فالآبار المرتفعة فيها قيم التوصيلية الكهربية ومجموع الأملاح الذائبة نجد أن قيم الصوديوم والبوتاسيوم والكلوريد فيها ايضاً مرتفعة. ومن خلال النتائج يتضح لنا أن معظم مياه آبار حقل جوجه وبئر الحوطة والغرفة مرتفعة الملوحة وذلك لتجاوز التوصيلية الكهربية لها 2000 ميكروموز/ سم ومجموع الأملاح الذائبة لها تجاوز 1000 مليجرام/ لتر ويعود السبب في ذلك إلى الطبيعة الجيولوجية والمحتوى الملحي للأراضي التي تحتضن مصدر المياه، وهذا بدوره أدى إلى ارتفاع الملوحة، وهذا يتوافق مع ما توصل إليه علوان في دراسته (علوان، 2017). أما بالنسبة لبئر الحوطة وهي بئر حديثة الإنشاء أو الحفر فقد أظهرت النتائج السابقة أن هذه البئر منذ حفرها كانت منخفضة الملوحة وشهدت في الأشهر الأخيرة ارتفاعاً في الملوحة، أي أن الملوحة هنا مؤقتة وسببها هو الضخ الجائر والمستمر الذي أدى إلى فقدان التوازن في الطبقات الحاملة للماء وهذا أدى بدوره إلى ارتفاع الملوحة وهو ما يتوافق مع ما توصل إليه الزرقة في دراسته (الزرقة، 2010). كما إن عدم تجديد وتغذية الخزان الجوفي بمياه الأمطار على مدار السنة أو لعدة سنوات له دور في ذلك (Komex,1996)

أما قيم البوتاسيوم فكانت ما بين أدناها 5 ppm لبئر ساه رقم (4) وأعلاها 13 ppm لبئري الغرفة بسيئون وجوجة الوسطى بشيام، وهي قيمة مرتفعة تجاوزت الحد المسموح به يمنيًا، ويعود السبب في ذلك لارتفاع نسبة الملوحة فيهما حيث سجلت نسبة الملوحة لهما أعلى قيمة بالنسبة للآبار بشكل عام.

وبالنسبة لقيم الكالسيوم فقد تراوحت في جميع آبار هذه الدراسة ما بين (63 – 130) ppm، فأدنى قيمة لها لبئر ساه رقم (4) وأعلى قيمة هي لبئر الغرفة، وجميع القيم المسجلة لاتزال في إطار الحد المسموح به كما يوضح جدول (5). ونلاحظ من النتائج أن ارتفاع قيم الكالسيوم يكون مصحوبًا بارتفاع قيمة العسرة الكلية للعينة مما يشير إلى ارتباط وتناسب طردي بينهما، وهذا يتوافق مع ما توصلت إليه دراسة للرزوقي وآخرون (رزوقي والراوي، 2010). وتتراوح قيم تراكيز المغنسيوم في العينات ما بين (19 – 70) ppm، وقد سجلت أدنى قيمة له ببئر سيئون رقم (13) وأعلى قيمة كانت لبئر جوجة الوسطى بشبام تليها بئر الغرفة حيث كان تركيز المغنسيوم بها 66 ppm لكنهما لا يزالان في إطار الحد المسموح به. كما نلاحظ أن ارتفاع قيم المغنسيوم لكل من بئر الغرفة وبئر جوجة الوسطى صاحبه ارتفاع لقيم العسرة الكلية لكل منهما (الجدولان 4،5)، مما يدل على الارتباط بين العسرة وتركيز المغنسيوم ويتوافق هذا مع ما توصل إليه طه وزملاءه في دراستهم (طه و أسري وعبيد 2005).

3-4- إيجاد تراكيز العناصر الانتقالية (الحديد، المنجنيز، الرصاص، الكادميوم، النحاس والخارصين) لعينات مياه الشرب المدروسة:

بينت النتائج الموضحة في الجدولين (5،6) أن قيم الحديد تراوحت ما بين (0.03 – 2.61) ppm، فأدنى قيمة هي للآبار ساه (3) و (4) و تريم رقم (2) و(3) و (8) و بئر سيئون رقم (2)، حيث أخذت نفس النتيجة، وأعلى قيمة هي لبئر موشح رقم (4) تليها بئر موشح رقم (2) بشبام، وقد تجاوزت قيم هذين البئرين الحد المسموح به عالميًا ومحليًا فقط عند أخذ القراءة الأولى ولكن عند أخذ القراءة الثانية انخفضت قيم الحديد وأصبحت طبيعية ولعل السبب في ارتفاع قيم الحديد هو تعرض أنابيب الحديد للصدأ بسبب توقف بعض هذه الآبار عن العمل لفترة من الزمن بسبب أعمال الصيانة، أما سبب انخفاض نسب الحديد في القراءة الثانية هو بسبب المعالجة الأولية من قبل الجهات المعنية في المؤسسة حسب إفادتهم بذلك، كما أن الماء يتم ضخه أولاً إلى خزان قبل ضخه إلى المنازل. وهذا يتوافق مع ما توصلت إليه دراسة قام بها حسين واخرون (حسين وعبد وكاظم، 2010).

ولم يظهر جهاز الامتصاص الذري (AAS) أي تراكيز لعناصر النحاس والرصاص والكادميوم في جميع آبار الشرب التابعة للمؤسسة بوادي وصحراء حضرموت، ويعود السبب في ذلك إما لعدم وجود هذه العناصر في ماء الشرب لكون معظم آبار الشرب محكمة الإغلاق وبالقرب من مناطق جبلية بعيدة عن المناطق السكنية ومصادر التلوث الأخرى وبالتالي استبعاد تلوث مياه الشرب بهذه العناصر، أو أن تراكيز هذه العناصر منخفضة جدًا وتقع في خارج نطاق الجهاز. ويتوافق هذا مع ما توصل إليه بن عباد عندما قام بدراسة تركيز هذه العناصر بساحل حضرموت (بن عباد، 2019) حيث وجد أن معظم تركيز هذه العناصر لم يظهرها جهاز الامتصاص الذري (AAS) وأعطى القيمة صفرًا كذلك. وفي هذه الدراسة كانت كذلك قيم تركيز الخارصين بشكل عام منخفضة كما في الجدولين (5،6) وجاءت ما بين (0.01 – 0.49) ppm فأدنى قيمة هي لبئر جوجة الشرقية بشبام وأعلى قيمة هي لبئر الحمضان رقم (2) بالقطن. وجميع القيم لم تتجاوز الحد المسموح به. مع العلم أن تركيز الخارصين لم يظهره الجهاز لبعض آبار الشرب وأعطى القراءة صفر، والسبب في ذلك كما ذكرنا آنفًا وهو عدم وجود العنصر في ماء الشرب لكون هذه الآبار محكمة الإغلاق ولبعدها عن مصادر التلوث أو أن تركيزه منخفض جداً أقل من مدى الجهاز.

ونجد هنا كذلك، أن معظم الآبار قيد الدراسة لم يتجاوز فيها المنجنيز الحد المسموح به عالميًا ويمنيًا، وتراوحت قيمه ما بين (0.3 – 0.7) ppm. فأدنى قيمة هي لبئر سيئون رقم (13) وتريم (6). وأعلى قيمة هي لبئر موشح (2) وساه (4) وتريم (1).

جدول (5):

قيم االعناصر في مياه آبار سيئون شبام وتريم*.

	رقم البير	1	2	3	4	5	6	7	8	9	10	11	13	الغرفة
سيئون	الصوديوم	108	77	67	74	64	75	104	114	110	79	67	76	223
	البوتاسيوم	9	8	7	7	6	7	8	9	8	8	8	8	13
	مغنيسيوم	39	31	30	26	31	28	33	38	42	29	28	19	66
	كالسيوم	87	82	69	73	66	69	77	83	82	85	81	76	130
	منجنيز	0.5	0.5	0.4	0.6	0.4	0.4	0.6	0.6	0.5	0.6	0.3	0.4	0.5
	حديد	0.04	0.03	0.44	0.44	0.25	0.26	0.44	0.08	0.26	0.39	0.35	0.31	0.04
	خارصين						0.28	0.40	0.03					0.03
شبام	رقم البير	جوجة الشرقية	جوجة القبلية	جوجة الوسطة	الحوطة	موشح 1	موشح 2	موشح 3	موشح 4	موشح 5				
	الصوديوم	160	136	273	191	149	109	112	111	104				

	البوتاسيوم	9	10	11	12	13	10	10	10	9			
	مغنيسيوم	41	63	38	62	70	36	39	39	38			
	كالسيوم	93	106	105	122	127	94	99	102	68			
	منجنيز	0. 5	0. 6	0. 5	0. 5	0. 4	0. 7	0. 5	0. 5	0. 4			
	حديد	0. 24	0. 08	0. 20	0. 04	0. 15	1. 43	0. 16	2. 61	0. 31			
	خارصين	0. 01		0. 04	0. 02		0. 12	0. 01					
تربع	رقم البير	1	2	5	4	3	6	7	8	9			
	الصوديوم	110	92	80	82	91	90	104	104	104			
	البوتاسيوم	8	8	7	7	8	8	7	8	9			
	مغنيسيوم	37	36	35	32	32	34	32	40	37			
	كالسيوم	84	80	70	72	78	74	73	80	83			
	منجنيز	0.7	0.6	0.5	0.5	0.4	0.3	0.6	0.4	0.5			
	حديد	0.04	0.03	0.06	0.08	0.03	0.11	0.04	0.03	0.05			
	خارصين		0.03	0.04	0.03	0.05	0.07	0.04					

*عناصر النحاس والرصاص والكادميوم كانت قيمها صفرًا

جدول (6):
قيم االعناصر في مياه آبار ساه والقطن.*

	رقم البير	الصوديوم	البوتاسيوم	مغنيسيوم	كالسيوم	منجنيز	حديد	خارصين
ساه	1	54	10	31	77	0. 6	0. 04	
	2	48	9	30	65	0. 6	0. 38	
	3	46	6	31	73	0. 6	0. 03	0. 03
	4	44	5	32	63	0. 7	0. 03	0. 05
القطن	الحمضان 2	112	9	40	86	0. 4	0. 16	0. 49
	الحمضان 3	116	8	45	84	0. 4	0. 04	0. 11
	الحمضان 4	121	10	47	95	0. 4	0. 17	0. 04
	الحمضان 5	109	9	43	88	0.5	0. 20	0. 02
	الحمضان 6	118	9	43	88	0. 4	0. 04	0. 03

*عناصر النحاس والرصاص والكادميوم كانت قيمها صفرًا

4- الخاتمة:

من النتائج المتحصل عليها يمكن القول، أن بئر الغرفة في حقل الغرفة التابع لمديرية سيئون تظهر ارتفاعًا في قيم التوصيلية الكهربية تصل إلى 2168 ميكرو/ سيمنس كحد متوسط، لذلك تصنف حسب تصنيف منظمة الصحة العالمية بأن ماءها شديد الملوحة غير أنها لاتزال في إطار حدود المياه العذبة حسب ما هو موضح في الجداول أعلاه، ولكن لا ننسى أننا حصلنا على قيم مجموع الأملاح الذائبة بضربها في المعامل الخاص باليمن (منطقة الدراسة) وهو 0.65 وهو معامل منخفض القيمة مقارنة بالمعاملات الخاصة بالدول الأخرى. كما نلاحظ أيضًا ارتفاع لقيم العسرة والصوديوم والبوتاسيوم لبئر الغرفة التي يمكن وصف مياها بأنها شديدة العسرة بسبب أن الصخور التي حفرت فيها هذه البئر حاوية لكميات كبيرة من ملح كلوريد الصوديوم والبوتاسيوم، غير أنه لم يلاحظ أي تلوث عضوي بالنيترات رغم أن هذه البئر قريبة من منطقة سكنية. وتعتبر

بئر سيئون رقم (13) في حقل جثمة من أفضل وأعذب مياه الآبار التابعة للمؤسسة في صحراء ووادي حضرموت وذلك لوصول قيم التوصيلية الكهربية والأملاح الذائبة إلى أدنى قيمة. وفي مديرية شبام أظهرت قيم التوصيلية الكهربية سواء في حقل موشح بوادي بن علي أو حقل جوجة أو حقل الحوطة أن معظم الآبار تصنف حسب تصنيف منظمة الصحة العالمية بأنها مياه متوسطة الملوحة. إلا أن هذه الملوحة قد تكون موقتة كما في حقل الحوطة وناتجة عن الضخ الجائر للمياه الذي أدى إلى فقدان التوازن في الطبقات الحاملة للماء مما أعطى فرصة لاندفاع الملوحة إلى أعلى، أو تكون دائمة ومستمرة كما في آبار حقل جوجة نتيجة لتكوين التربة أو الصخور التي حفرت فيها هذه الآبار. ويصاحب ارتفاع العسرة ارتفاع في قيم أملاح الكالسيوم والمغنسيوم لكون العسرة تتوزع على هذه الأملاح ولكونها السبب في تكون العسرة، كما أظهرت النتائج ارتفاعًا ملحوظًا في قيم الحديد لكل من بئر موشح رقم (1) و (2) عند أخذ العينة الأولى في شهر يناير مع العلم أن هاتين البئرين كانتا مغلقتين قبل ذلك لإجراء صيانة بها وعند تشغيلهما وأخذ العينة الأولى كانت قيم الحديد فيها مرتفعة ولكن عند أخذ العينة الثانية في شهر فبراير كان هناك انخفاضًا ملحوظًا في قيم الحديد مع العلم أن مؤسسة المياه بالمديرية تجري معالجة أولية في حالة ارتفاع قيم الحديد عن الحد المسموح به. وفي مديرية تريم وحسب الجداول أعلاه، كانت مياه آبارها تقع حسب التصنيف ضمن المياه الجيدة والمتوسطة الملوحة، أي في إطار حدود المياه العذبة. بينما لم تشهد آبار مياه هذه المديرية أي تلوث عضوي أو ارتفاع في قيم بقية الخواص أو الفلزات قيد الدراسة. ونفس النتائج كانت لآبار مديريتي القطن وساه فهما تقع ضمن حدود المياه العذبة المتوسطة الملوحة.

جدول (7):
متوسط آبار كل مديرية

	سيئون	شبام	تريم	ساه	القطن	المعايير اليمنية*	المعايير الدولية*
EC	1014	1486.3	954.9	836.75	1238	2500 – 450	1500
pH	7.6	7.68	7.7	7.77	7.63	9 – 6.5	8.5 – 6.5
TDS	660.6	966.3	628.2	544	803	1500 – 650	1000
العسر الكلي لـ $CaCO_3$	341.9	456.2	337.1	303	401	500 – 100	500
عسر الكالسيوم	204.46	260.56	192.67	173.25	220		
عسر المغنيسيوم	138.9	196	144.56	130.25	181		
عسر الكربونات	256.9	278.4	264.4	262.5	294		
الصوديوم	95.23	155.12	95.22	48	116	400 – 200	200
البوتاسيوم	8.15	10.62	7.78	7.5	9	12 – 8	
مغنيسيوم	33.85	48.5	35	31	44.5	150 – 30	
كالسيوم	81.54	106	77.11	69.5	88.75	200 – 75	200
منجنيز	0.48	0.51	0.5	0.625	0.42	0.1 – 0.2	0.1
حديد	0.26	0.58	0.052	0.12	0.122	1 – 0.3	0.3
خارصين	0.185	0.04	0.043	0.04	0.138	5 – 1.5	1.5
النحاس	0	0	0	0	0	1 – 0.5	1
الرصاص	0	0	0	0	0	0.05	0.05
الكادميوم	0	0	0	0	0	0.005	0.005

*(المصدر: منظمة الصحة العالمية (WHO) والمواصفات القياسية اليمنية لمياه الشرب العامة)

التوصيات:

- إجراء دراسات تهتم بالفحص الميكروبيولوجي لجميع آبار الشرب بوادي حضرموت.
- عدم خلط مياه الآبار مرتفعة الملوحة مع مياه الآبار منخفضة الملوحة في خزان واحد قبل إجراء المعالجة الأولية لها وذلك للتقليل من كمية الأملاح الزائدة فيها قبل وصولها إلى المنازل.
- استبدال الآبار مرتفعة الأملاح في حالة توفر الإمكانيات بآبار أخرى نقية لتحسين جودة المياه ولرفع الإنتاجية للمياه بشكل عام بحيث تغطي مساحات أكبر من المحافظة.
- عند حفر الآبار وتكون هذه الآبار على مرتفع أو تلة يجب أن يؤخذ بعين الاعتبار ارتفاع هذا التل أو المرتفع أو الجبل عن سطح الأرض بحيث لا يقل من عمق البئر وبالتالي يزيد من احتمالية وصول الملوثات إليها خصوصًا في المناطق السكنية.

- فرض رقابة صارمة على حفر آبار مياه الصرف الصحي (الحفر الامتصاصية) وعدم إيصال هذه الحفر إلى منابع المياه الجوفية حتى لا تلوثها مياه الصرف الصحي.
- إعادة النظر من قبل الجهات المختصة في المعايير أو المواصفات القياسية اليمنية التي وضعت لمياه الشرب العامة حيث إنها تعتبر أعلى المعايير في الدول الأخرى.

شكر وعرفان:
يعرب الباحثون عن جزيل شكرهم وتقديرهم لكل من المؤسسة المحلية للمياه والصرف الصحي لمناطق وادي وصحراء حضرموت- اليمن ومختبر محطة البحوث الزراعية بسيئون على ماقدموه من تعاون سواء بتوفير البيانات أو السماح باستخدام مختبراتهم لأجراء الكثير من تجارب هذا البحث.

المراجع:

أبو الكباش، عبد الله محمد. (2012). **الكيمياء التحليلية المفاهيم الأساسية في التحليل التقليدي**. الطبعة الأولى، العبيكان للنشر.

الحديثي، هديل توفيق (1986). **الأحياء المجهرية المائية**. مجلة جامعة الموصل، مديرية دار الكتب للطباعة، (ط1).

الصبان، عبد القادر محمد (2000). **تعريفات تاريخية عن وادي حضرموت**. الطبعة الخامسة. إصدار مكتب وزارة الثقافة بالمكلا محافظة حضرموت.

الزرقة، محمد عبد الناصر (2010). **تلوث المياه في محافظتي الشمال والوسطى وتأثيراتها على صحة الانسان**. رسالة ماجستير، الجامعة الإسلامية-غزة-كلية الآداب-قسم الجغرافيا.

المؤسسة المحلية للمياه والصرف الصحي- مديريات الوادي والصحراء- محافظة حضرموت.

المنيفي، عبد اللطيف أحمد (2004). نوعية مياه الشرب في مدينة صنعاء. **مجلة جامعة حضرموت**، 7 (3)،161 – 178.

الموسوي، بهاء نظام عيسى؛ حمزة عصام شاكر (2010). التحري عن الملوثات الميكروبية والكيميائية لمياه الشرب المعبأة بالقناني البلاستيكية. **المجلة العراقية لبحوث الأسواق وحماية المستهلك**، 2 (3)،168-184.

الهيئة العامة للموارد المائية (1999). **المواصفات القياسية لمياه الشرب العامة في الجمهورية اليمنية**. صنعاء.

بارجاء، هود أحمد (2006). **التحليل الكيميائي والفيزيائي والبكتيري لمياه الشرب في مدينة القطن في وادي حضرموت**. رسالة ماجستير، كلية التربية، جامعة عدن.

بامتيرف، سالم خميس (2007). دراسة تقويمية لمياه الشرب في مدينة المكلا. **مجلة جامعة حضرموت**، 6 (12)، 12 -19.

باومن، سالم صالح (2012). **الموارد الطبيعية بوادي حضرموت**. الطبعة الأولى، دار حضرموت للنشر.

بن عباد، خيران برك (2019). **تقدير تركيز بعض المعادن الثقيلة والفحص الميكروبولوجي لعينات مياه الشرب في بعض مناطق ساحل حضرموت**. رسالة ماجستير غير منشورة، كلية العلوم، جامعة حضرموت.

حسين، طالب خماس؛ عبد مجيد محمود؛ زبون ، كاظم جبر (2010). تقويم مياه الشرب الشبكة العامة لبعض مناطق بغداد والمياه المعبأة المحلية والمستوردة. **مجلة جامعة كربلاء العلمية**، 9 (2).

رزوقي، سراب محمد محمود؛ الراوي محمد عمار (2010). دراسة بعض الخصائص الفيزوكيميائية والميكروبية للمياه المعبأة المنتجة محليًا والمستوردة في مدينة بغداد. **المجلة العراقية لبحوث السوق وحماية المستهلك**، 3 (2) 75-103.

زاهد، وليد محمد كامل. (2002). جودة مياه الشرب المعبأة المحلية والمستوردة في المملكة العربية السعودية. **مجلة جامعة الملك عبد العزيز، العلوم الهندسية**، 14 (2).

زبار، سامي شاكر محمود (2009). تلوث مياه الشرب بالعناصر الثقيلة في مدينة بيجي. **مجلة كلية دار العلم الجامعة**، 1 (1)، 27-36.

سليمان، صبحي (2020). **كيف تربح معركتك ضد طعامك**. الطبعة الأولى، وكالة الصحافة العربية.

شحاتة، حسن أحمد (2014). **معجزات السماء من آيات الله في الكون**. الأكاديمية الحديثة للكتاب الجامعي.

طه، داخل ناصر؛ أسري، سعدي عبد الأمير؛ عبيد فوزي مراد (2005). **الماء الخام وماء الشرب في محافظة بابل دراسة وتحليل**. رسالة ماجستير، جامعة بابل كلية العلوم.

عبد الجبار، حسن عبد الله. (2002). **أزمة المياه في اليمن**. مركز الدراسات والنشر، الطبعة الأولى، صنعاء-اليمن.

علوان، محمد دياب محمود. (2017). **خصائص مياه الشرب في محافظة خان يونس**. رسالة ماجستير، كلية الآداب – قسم الجغرافيا، الجامعة الاسلامية بغزة.

عبد الحافظ، عبد الوهاب محمد؛ مبارك محمد الصاوي. (1996). **الميكروبيولوجيا التطبيقية**. المكتبة الأكاديمية – القاهرة، الطبعة الأولى.

فائق، أفنان جنكيز. (2020). **دراسة تحليلية حياتيه لمدى تلوث مياه الآبار بالعناصر الثقيلة بواسطة الامتصاص الذري في القرى المحيطة بمحافظة كركوك**. رسالة ماجستير، قسم علوم الكيمياء بجامعة كركوك.

محمد، أنصاف حميد؛ أحمد هبة ياسين. (2010). دراسة واقع مياه الشرب في بعض مناطق مدينة بغداد. **المجلة العراقية لبحوث السوق وحماية المستهلك**، 2 (3) 228-243.

وزارة التخطيط والتعاون الدولي (2015). **النشرة الإحصائية لعام 2015 الجهاز المركزي للإحصاء**، مكتب سيئون، محافظة حضرموت، اليمن.

المراجع العربية مترجمة:

Abdel Hafez, A. M.; Al-Sawy M. M. (1996). Applied Microbiology. Academic Library - Cairo, 1st ed.

Abdul-Jabbar H. A. (2002). Water crisis in Yemen. Center for Studies and Publishing, 1st ed, Sanaa-Yemen.

Abu Al-Kabash, A. M. (2012). Analytical Chemistry Basic concepts in conventional analysis. 1st ed, Obeikan Publishing.

Al-Hadithi H. T. (1986). Aquatic microorganisms. Mosul University Journal, Directorate of Dar Al-Kutub for Printing, 1st ed.

Al-Moussawi B. N. I.; Hamza E. S. (2010). Investigating microbial and chemical contaminants in drinking water bottled in plastic bottles. Iraqi Journal of Market Research and Consumer Protection, 2 (3), .184-168.

Al-Munifi, A. A. (2004). Drinking water quality in Sana'a city. Hadramout University Journal, 7 (3), 178-161.

Al-Sabban A. M. (2000). Historical definitions about Wadi Hadhramaut. 5th ed. Issued by the Office of the Ministry of Culture in Mukalla, Hadramaut Governorate.

Alwan, M. D. M. (2017). Characteristics of drinking water in Khan Yunis Governorate. Dissertation, Faculty of Arts - Department of Geography, Islamic University of Gaza.

Al-Zarqa M. A. (2010). Water pollution in the northern and central governorates and its effects on human health. Dissertation, Islamic University - Gaza - Faculty of Arts - Department of Geography.

Bamoumn, S. S. (2012). Natural resources in Valley Hadhramaut. 1st ed, Hadhramaut Publishing House.

Bamterv S. K. (2007). An evaluation study of drinking water in the city of Mukalla. Hadhramaut University Journal, 6 (12), 12-19.

Baraja, H. A. (2006). Chemical, physical and bacterial analysis of drinking water in the city of Cotton in Valley Hadhramaut. Dissertation, College of Education, University of Aden.

Ben Abbad K. B. (2019). Estimation of the concentration of some heavy metals and microbiological examination of drinking water samples in some areas of Hadramout coast. Unpublished, Dissertation, College of Science, Hadramout University.

Faiq A. C. (2020). A real-life analytical study of the extent of well water contamination with heavy metals by atomic absorption in the villages surrounding Kirkuk Governorate. Dissertation, Department of Chemistry, University of Kirkuk.

Hussein, T. K.; Abdul Majeed M.; Zaboun, K. J. (2010). Evaluation of drinking water, the public network for some areas of Baghdad, and bottled water, local and imported. Karbala University Scientific Journal, 9 (2).

Ministry of Planning and International Cooperation (2015). Statistical Bulletin for the year 2015, Central Bureau of Statistics, Sayun Office, Hadhramaut Governorate, Yemen.

Muhammad, A. H.; Ahmed H. Y. (2010). Study of the reality of drinking water in some areas of the city of Baghdad. Iraqi Journal of Market Research and Consumer Protection, 2 (3) 228-243.

Public Authority for Water Resources (1999). Standard specifications for public drinking water in the Republic of Yemen. Sana'a.

Razouki, S. M. M.; Narrator M. A. (2010). Study of some physicochemical and microbial characteristics of locally produced and imported bottled water in the city of Baghdad. Iraqi Journal of Market Research and Consumer Protection, 3(2).103-75.

Shehata, H. A. (2014). Heaven's miracles are God's signs in the universe. Modern Academy for University Books.

Suleiman S. (2020). How to win your battle against your food. 1st ed, Arab Press Agency.

Taha, D. N.; Asry S. A.; Obaid F. M. (2005). Raw water and drinking water in Babil Governorate, study and analysis. Dissertation, University of Babylon, College of Science.

The Local Corporation for Water and Sanitation - Valley and Desert Directorates - Hadramout Governorate.

Zabbar, S. S. M. (2009). Contamination of drinking water with heavy elements in the city of Baiji. Dar Al-Ilm University College Journal, 1 (1), 36-27.

Zahid, W. M. K. (2002). Quality of domestic and imported bottled drinking water in the Kingdom of Saudi Arabia. King Abdulaziz University Journal, Engineering Sciences, 14 (2).

المراجع الإجنبية:

Al-shaikh T. M. (2017). Study of microbial characteristics of well groundwater in the city of Arar, Kingdom of Saudi Arabia. **Journal of the North for basic and Applied Sciences**, 2 (2), 41-50.

Bin Hameed E. A., Bin Alshikh Bubkr, K. S. (2019). Assessment of Bacteriological Quality of Drinking Water in Some Primary and Secondary Schools in Mukalla City-Hadhramout/ Yemen. **Hadhramout University Journal of natural and applied sciences**, 16 (2), 185- 191.

Bin yahia A. (2005). The qulity of drinking water in Al-Ghaydah city- Al-Mahraa governorate. **Journal of Nutural and applied Sciences**, 9 (2), 259- 268.

mass index, age, and gender with bone mineral density in patients referred to king Fahad university hospital. **Journal of the North for basic and Applied Sciences**, 5 (2), 132-141.

Komex I. (1996). **Ground water assessment, project in the Masila**-Hadramout – Yemen. fourth, Quarter report.

Rodger, B. B., Andrew, D. E. and Eugene, W. R. (2017). **Standard methods for the examination of water and wastewater**. American Public Health Association, Washington.

Ryan J., Garabet S., Harmsen K., Abdul Rashid. (1996). **A soil and Plant Analysis Manual Adapted for the West Asia and North Africa Region**. Beirut, Lebanon: International Center for Agricultural Research in the Dry Areas (ICARDA).

Charan G., Bharti V. K., Giri A., Kumar P. (2023). Evaluation of physico-chemical and heavy metals status in irrigation, stagnant, and Indus River water at the trans-Himalayan region. **Discover Water**, 3 (3), https://doi.org/10.1007/s43832-023-00027-z

Gebresilasie K. G., Berhe G. G., Tesfay a. H., Gebre S. E. (2021). Assessment of Some Physicochemical Parameters and Heavy Metals in Hand-Dug Well Water Samples of Kafta Humera Woreda, Tigray, Ethiopia. **International Journal of Analytical Chemistry**, https://doi.org/10.1155/2021/8867507

Hassan N.A., Mugbil N.A. and Alballem F.A. (2008). Biological Analysis of Drinking Water in Aden Governorate. **Aden University Journal of Natural and Applied Sciences**, 3 (12), 509- 516.

Kheiralla O. A. M., Goja A.M., Bakheet A. O., Al-Ghamdi. A., Sadath S. M. (2020). Association of body

Natesan, K. S. Vora & K. Sharun (2021) Immunological aspects and gender bias during respiratory viral infections including novel Coronavirus disease-19 (COVID-19): A scoping review. *Journal of Medical Virology,* 93**,** 5295-5309.

Van Doremalen, N., T. Bushmaker, D. H. Morris, M. G. Holbrook, A. Gamble, B. N. Williamson, A. Tamin, J. L. Harcourt, N. J. Thornburg & S. I. Gerber (2020) Aerosol and surface stability of SARS-CoV-2 as compared with SARS-CoV-1. *New England journal of medicine,* 382**,** 1564-1567.

Velazquez-Salinas, L., A. Verdugo-Rodriguez, L. L. Rodriguez & M. V. Borca (2019) The role of interleukin 6 during viral infections. *Frontiers in microbiology,* 10**,** 1057.

Verma, M. & S. Shakya (2021) Genetic variation in the chemokine receptor 5 gene and course of HIV infection; review on genetics and immunological aspect. *Genes & Diseases,* 8**,** 475-483.

Wang, B., R. Li, Z. Lu & Y. Huang (2020a) Does comorbidity increase the risk of patients with COVID-19: evidence from meta-analysis. *Aging (albany NY),* 12**,** 6049.

Wang, C., P. W. Horby, F. G. Hayden & G. F. Gao (2020b) A novel coronavirus outbreak of global health concern. *The lancet,* 395**,** 470-473.

Wang, W., J. Tang & F. Wei (2020c) Updated understanding of the outbreak of 2019 novel coronavirus (2019-nCoV) in Wuhan, China. *Journal of medical virology,* 92**,** 441-447.

Wang, X., T. Wang, T. Pan, M. Huang, W. Ren, G. Xu, H. K. Amin, R. B. Kassab & A. E. Abdel Moneim (2020d) Senna alexandrina extract supplementation reverses hepatic oxidative, inflammatory, and apoptotic effects of cadmium chloride administration in rats. *Environmental Science and Pollution Research,* 27**,** 5981-5992.

Xiao, F., M. Tang, X. Zheng, Y. Liu, X. Li & H. Shan (2020) Evidence for gastrointestinal infection of SARS-CoV-2. *Gastroenterology,* 158**,** 1831-1833. e3.

Xu, X., P. Chen, J. Wang, J. Feng, H. Zhou, X. Li, W. Zhong & P. Hao (2020) Evolution of the novel coronavirus from the ongoing Wuhan outbreak and modeling of its spike protein for risk of human transmission. *Science China Life Sciences,* 63**,** 457-460.

Yuan, J., M. Li, G. Lv & Z. K. Lu (2020) Monitoring transmissibility and mortality of COVID-19 in Europe. *International Journal of Infectious Diseases,* 95**,** 311-315.

Zhang, C., L. Shi & F.-S. Wang (2020) Liver injury in COVID-19: management and challenges. *The lancet Gastroenterology & hepatology,* 5**,** 428-430.

Zhou, F., T. Yu, R. Du, G. Fan, Y. Liu, Z. Liu, J. Xiang, Y. Wang, B. Song & X. Gu (2020) Clinical course and risk factors for mortality of adult inpatients with COVID-19 in Wuhan, China: a retrospective cohort study. *The lancet,* 395**,** 1054-1062.

diseases. *The lancet Gastroenterology & hepatology,* 5**,** 425-427.

Mason, R. J. 2020. Pathogenesis of COVID-19 from a cell biology perspective. Eur Respiratory Soc.

Mehta, S., S. Kulkarni, A. N. Nikam, B. S. Padya, A. Pandey & S. Mutalik (2021) Liposomes as Versatile Platform for Cancer Theranostics: Therapy, Bio-imaging, and Toxicological Aspects. *Current Pharmaceutical Design,* 27**,** 1977-1991.

Middeldorp, S., M. Coppens, T. F. van Haaps, M. Foppen, A. P. Vlaar, M. C. Müller, C. C. Bouman, L. F. Beenen, R. S. Kootte & J. Heijmans (2020) Incidence of venous thromboembolism in hospitalized patients with COVID-19. *Journal of Thrombosis and Haemostasis,* 18**,** 1995-2002.

Mohapatra, R. K., P. K. Das, L. Pintilie & K. Dhama (2021) Infection capability of SARS-CoV-2 on different surfaces. *Egyptian Journal of Basic and Applied Sciences,* 8**,** 75-80.

Pan, F., T. Ye, P. Sun, S. Gui, B. Liang, L. Li, D. Zheng, J. Wang, R. L. Hesketh & L. Yang (2020) Time course of lung changes on chest CT during recovery from 2019 novel coronavirus (COVID-19) pneumonia. *Radiology*.

Patel, K. P., P. A. Patel, R. R. Vunnam, A. T. Hewlett, R. Jain, R. Jing & S. R. Vunnam (2020) Gastrointestinal, hepatobiliary, and pancreatic manifestations of COVID-19. *Journal of Clinical Virology,* 128**,** 104386.

Polonikov, A. (2020) Endogenous deficiency of glutathione as the most likely cause of serious manifestations and death in COVID-19 patients. *ACS infectious diseases,* 6**,** 1558-1562.

Rabaan, A. A., S. H. Al-Ahmed, M. A. Garout, A. M. Al-Qaaneh, A. A. Sule, R. Tirupathi, A. A. Mutair, S. Alhumaid, A. Hasan & M. Dhawan (2021a) Diverse immunological factors influencing pathogenesis in patients with COVID-19: a review on viral dissemination, immunotherapeutic options to counter cytokine storm and inflammatory responses. *Pathogens,* 10**,** 565.

Rabaan, A. A., S. H. Al-Ahmed, J. Muhammad, A. Khan, A. A. Sule, R. Tirupathi, A. A. Mutair, S. Alhumaid, A. Al-Omari & M. Dhawan (2021b) Role of inflammatory cytokines in COVID-19 patients: a review on molecular mechanisms, immune functions, immunopathology and immunomodulatory drugs to counter cytokine storm. *Vaccines,* 9**,** 436.

Ragab, D., H. Salah Eldin, M. Taeimah, R. Khattab & R. Salem (2020) The COVID-19 cytokine storm; what we know so far. *Frontiers in immunology***,** 1446.

Rothan, H. A. & S. N. Byrareddy (2020) The epidemiology and pathogenesis of coronavirus disease (COVID-19) outbreak. *Journal of autoimmunity,* 109**,** 102433.

Sah, R., A. P. Khatiwada, S. Shrestha, K. Bhuvan, R. Tiwari, R. K. Mohapatra, K. Dhama & A. J. Rodriguez-Morales (2021) COVID-19 vaccination campaign in Nepal, emerging UK variant and futuristic vaccination strategies to combat the ongoing pandemic. *Travel medicine and infectious disease,* 41**,** 102037.

Samavati, L. & B. D. Uhal (2020) ACE2, much more than just a receptor for SARS-COV-2. *Frontiers in cellular and infection microbiology***,** 317.

Shekhar, S., Y. Yadav, A. P. Singh, R. Pradhan, G. R. Desai, A. Dey & S. Dey (2018) Neuroprotection by ethanolic extract of Syzygium aromaticum in Alzheimer's disease like pathology via maintaining oxidative balance through SIRT1 pathway. *Experimental gerontology,* 110**,** 277-283.

Sinha, R., I. Sinha, A. Calcagnotto, N. Trushin, J. S. Haley, T. D. Schell & J. Richie (2018) Oral supplementation with liposomal glutathione elevates body stores of glutathione and markers of immune function. *European journal of clinical nutrition,* 72**,** 105-111.

Smith, E. C. (2017) The not-so-infinite malleability of RNA viruses: Viral and cellular determinants of RNA virus mutation rates. *PLoS pathogens,* 13**,** e1006254.

Sungnak, W., N. Huang, C. Bécavin, M. Berg, R. Queen, M. Litvinukova, C. Talavera-López, H. Maatz, D. Reichart & F. Sampaziotis (2020) SARS-CoV-2 entry factors are highly expressed in nasal epithelial cells together with innate immune genes. *Nature medicine,* 26**,** 681-687.

Syed, A., A. Khan, F. Gosai, A. Asif & S. Dhillon (2020) Gastrointestinal pathophysiology of SARS-CoV2–a literature review. *Journal of Community Hospital Internal Medicine Perspectives,* 10**,** 523-528.

Tang, T., M. Bidon, J. A. Jaimes, G. R. Whittaker & S. Daniel (2020a) Coronavirus membrane fusion mechanism offers a potential target for antiviral development. *Antiviral research,* 178**,** 104792.

Tang, X., C. Wu, X. Li, Y. Song, X. Yao, X. Wu, Y. Duan, H. Zhang, Y. Wang & Z. Qian (2020b) On the origin and continuing evolution of SARS-CoV-2. *National science review,* 7**,** 1012-1023.

Tang, X., Z. Zhang, M. Fang, Y. Han, G. Wang, S. Wang, M. Xue, Y. Li, L. Zhang & J. Wu (2020c) Transferrin plays a central role in coagulation balance by interacting with clotting factors. *Cell research,* 30**,** 119-132.

Tian, Y., L. Rong, W. Nian & Y. He (2020) gastrointestinal features in COVID-19 and the possibility of faecal transmission. *Alimentary pharmacology & therapeutics,* 51**,** 843-851.

Uddin, M., F. Mustafa, T. A. Rizvi, T. Loney, H. Al Suwaidi, A. H. H. Al-Marzouqi, A. Kamal Eldin, N. Alsabeeha, T. E. Adrian & C. Stefanini (2020) SARS-CoV-2/COVID-19: viral genomics, epidemiology, vaccines, and therapeutic interventions. *Viruses,* 12**,** 526.

Vadakedath, S., V. Kandi, R. K. Mohapatra, V. B. Pinnelli, R. R. Yegurla, P. R. Shahapur, V. Godishala, S.

Galanopoulos, M., F. Gkeros, A. Doukatas, G. Karianakis, C. Pontas, N. Tsoukalas, N. Viazis, C. Liatsos & G. J. Mantzaris (2020) COVID-19 pandemic: Pathophysiology and manifestations from the gastrointestinal tract. *World journal of gastroenterology,* 26**,** 4579.

Gao, M., P. Monian, Q. Pan, W. Zhang, J. Xiang & X. Jiang (2016) Ferroptosis is an autophagic cell death process. *Cell research,* 26**,** 1021-1032.

García, L. F. (2020) Immune response, inflammation, and the clinical spectrum of COVID-19. *Frontiers in immunology,* 11**,** 1441.

Gómez-Pastora, J., M. Weigand, J. Kim, X. Wu, J. Strayer, A. F. Palmer, M. Zborowski, M. Yazer & J. J. Chalmers (2020) Hyperferritinemia in critically ill COVID-19 patients–is ferritin the product of inflammation or a pathogenic mediator? *Clinica Chimica Acta; International Journal of Clinical Chemistry,* 509**,** 249.

Gordon, D. E., G. M. Jang, M. Bouhaddou, J. Xu, K. Obernier, K. M. White, M. J. O'Meara, V. V. Rezelj, J. Z. Guo & D. L. Swaney (2020) A SARS-CoV-2 protein interaction map reveals targets for drug repurposing. *Nature,* 583**,** 459-468.

Goyal, P., J. J. Choi, L. C. Pinheiro, E. J. Schenck, R. Chen, A. Jabri, M. J. Satlin, T. R. Campion Jr, M. Nahid & J. B. Ringel (2020) Clinical characteristics of Covid-19 in New York city. *New England Journal of Medicine,* 382**,** 2372-2374.

Griffin, D. O., A. Jensen, M. Khan, J. Chin, K. Chin, J. Saad, R. Parnell, C. Awwad & D. Patel (2020) Pulmonary embolism and increased levels of d-dimer in patients with coronavirus disease. *Emerging infectious diseases,* 26**,** 1941.

Gu, J., B. Han & J. Wang (2020) COVID-19: gastrointestinal manifestations and potential fecal–oral transmission. *Gastroenterology,* 158**,** 1518-1519.

Guan, W.-j., Z.-y. Ni, Y. Hu, W.-h. Liang, C.-q. Ou, J.-x. He, L. Liu, H. Shan, C.-l. Lei & D. S. Hui (2020) Clinical characteristics of coronavirus disease 2019 in China. *New England journal of medicine,* 382**,** 1708-1720.

Guloyan, V., B. Oganesian, N. Baghdasaryan, C. Yeh, M. Singh, F. Guilford, Y. Ting & V. Venketaraman (2020). Glutathione supplementation as an adjunctive therapy in COVID-19. Antioxidants (Basel) 9: E914.

Hoffmann, M., H. Kleine-Weber, S. Schroeder, N. Krüger, T. Herrler, S. Erichsen, T. S. Schiergens, G. Herrler, N.-H. Wu & A. Nitsche (2020) SARS-CoV-2 cell entry depends on ACE2 and TMPRSS2 and is blocked by a clinically proven protease inhibitor. *cell,* 181**,** 271-280. e8.

Horowitz, R. I., P. R. Freeman & J. Bruzzese (2020) Efficacy of glutathione therapy in relieving dyspnea associated with COVID-19 pneumonia: A report of 2 cases. *Respiratory medicine case reports,* 30**,** 101063.

Jiang, Y., M. Yang, X. Sun, X. Chen, M. Ma, X. Yin, S. Qian, Z. Zhang, Y. Fu & J. Liu (2018) IL-10+ NK and TGF-β+ NK cells play negative regulatory roles in HIV infection. *BMC Infectious Diseases,* 18**,** 1-10.

Kautz, T. F. & N. L. Forrester (2018) RNA virus fidelity mutants: a useful tool for evolutionary biology or a complex challenge? *Viruses,* 10**,** 600.

Kim, D., J.-Y. Lee, J.-S. Yang, J. W. Kim, V. N. Kim & H. Chang (2020) The architecture of SARS-CoV-2 transcriptome. *Cell,* 181**,** 914-921. e10.

Lang, F. M., K. M.-C. Lee, J. R. Teijaro, B. Becher & J. A. Hamilton (2020) GM-CSF-based treatments in COVID-19: reconciling opposing therapeutic approaches. *Nature Reviews Immunology,* 20**,** 507-514.

Lee, I.-C., T.-I. Huo & Y.-H. Huang (2020) Gastrointestinal and liver manifestations in patients with COVID-19. *Journal of the Chinese Medical Association*.

Li, J.-Y., C.-H. Liao, Q. Wang, Y.-J. Tan, R. Luo, Y. Qiu & X.-Y. Ge (2020a) The ORF6, ORF8 and nucleocapsid proteins of SARS-CoV-2 inhibit type I interferon signaling pathway. *Virus research,* 286**,** 198074.

Li, Y., K. Zhao, H. Wei, W. Chen, W. Wang, L. Jia, Q. Liu, J. Zhang, T. Shan & Z. Peng (2020b) Dynamic relationship between D-dimer and COVID-19 severity. *British journal of haematology*.

Lippi, G., J. Wong & B. M. Henry (2020) Hypertension and its severity or mortality in Coronavirus Disease 2019 (COVID-19): a pooled analysis. *Pol Arch Intern Med,* 130**,** 304-309.

Liu, T., J. Zhang, Y. Yang, H. Ma, Z. Li, J. Zhang, J. Cheng, X. Zhang, Y. Zhao & Z. Xia (2020) The role of interleukin-6 in monitoring severe case of coronavirus disease 2019. *EMBO molecular medicine,* 12**,** e12421.

Luan, J., Y. Lu, X. Jin & L. Zhang (2020) Spike protein recognition of mammalian ACE2 predicts the host range and an optimized ACE2 for SARS-CoV-2 infection. *Biochemical and biophysical research communications,* 526**,** 165-169.

Lutchmansingh, F. K., J. W. Hsu, F. I. Bennett, A. V. Badaloo, N. McFarlane-Anderson, G. M. Gordon-Strachan, R. A. Wright-Pascoe, F. Jahoor & M. S. Boyne (2018) Glutathione metabolism in type 2 diabetes and its relationship with microvascular complications and glycemia. *PloS one,* 13**,** e0198626.

Mann, R., S. Sekhon & S. Sekhon (2021) Drug-induced liver injury after COVID-19 vaccine. *Cureus,* 13.

Mantlo, E., N. Bukreyeva, J. Maruyama, S. Paessler & C. Huang (2020) Antiviral activities of type I interferons to SARS-CoV-2 infection. *Antiviral research,* 179**,** 104811.

Mao, R., J. Liang, J. Shen, S. Ghosh, L.-R. Zhu, H. Yang, K.-C. Wu & M.-H. Chen (2020) Implications of COVID-19 for patients with pre-existing digestive

ulcer in rats. *Oxidative medicine and cellular longevity,* 2016.

Andersen, K. G., A. Rambaut, W. I. Lipkin, E. C. Holmes & R. F. Garry (2020) The proximal origin of SARS-CoV-2. *Nature medicine,* 26**,** 450-452.

Arias-Carrasco, R., J. Giddaluru, L. E. Cardozo, F. Martins, V. Maracaja-Coutinho & H. I. Nakaya (2021) OUTBREAK: a user-friendly georeferencing online tool for disease surveillance. *Biological Research,* 54**,** 1-6.

Astuti, I. (2020) Severe Acute Respiratory Syndrome Coronavirus 2 (SARS-CoV-2): An overview of viral structure and host response. *Diabetes & Metabolic Syndrome: Clinical Research & Reviews,* 14**,** 407-412.

Baud, D., X. Qi & K. Nielsen-Saines (2020) Real estimates of mortality following COVID-19 infection. Lancet Infect Dis.

Boyette, L. B., C. Macedo, K. Hadi, B. D. Elinoff, J. T. Walters, B. Ramaswami, G. Chalasani, J. M. Taboas, F. G. Lakkis & D. M. Metes (2017) Phenotype, function, and differentiation potential of human monocyte subsets. *PloS one,* 12**,** e0176460.

Bray, M. A., S. E. Sartain, J. Gollamudi & R. E. Rumbaut (2020) Microvascular thrombosis: experimental and clinical implications. *Translational Research,* 225**,** 105-130.

Brodin, P. (2021) Immune determinants of COVID-19 disease presentation and severity. *Nature medicine,* 27**,** 28-33.

Cao, W. & T. Li (2020) COVID-19: towards understanding of pathogenesis. *Cell research,* 30**,** 367-369.

Cao, Y., L. Li, Z. Feng, S. Wan, P. Huang, X. Sun, F. Wen, X. Huang, G. Ning & W. Wang (2020) Comparative genetic analysis of the novel coronavirus (2019-nCoV/SARS-CoV-2) receptor ACE2 in different populations. *Cell discovery,* 6**,** 1-4.

Ceriello, A. (2020) Hyperglycemia and the worse prognosis of COVID-19. Why a fast blood glucose control should be mandatory. *Diabetes research and clinical practice,* 163**,** 108186.

Chen, Y., Q. Liu & D. Guo (2020) Emerging coronaviruses: genome structure, replication, and pathogenesis. *Journal of medical virology,* 92**,** 418-423.

Cheung, K. S., I. F. Hung, P. P. Chan, K. Lung, E. Tso, R. Liu, Y. Ng, M. Y. Chu, T. W. Chung & A. R. Tam (2020) Gastrointestinal manifestations of SARS-CoV-2 infection and virus load in fecal samples from a Hong Kong cohort: systematic review and meta-analysis. *Gastroenterology,* 159**,** 81-95.

Coelho, É. M. P., M. C. Barbosa, M. S. Mito, G. C. Mantovanelli, R. S. Oliveira & E. L. Ishii-Iwamoto (2017) The activity of the antioxidant defense system of the weed species Senna obtusifolia L. and its resistance to allelochemical stress. *Journal of chemical ecology,* 43**,** 725-738.

Corman, V. M., O. Landt, M. Kaiser, R. Molenkamp, A. Meijer, D. K. Chu, T. Bleicker, S. Brünink, J. Schneider & M. L. Schmidt (2020) Detection of 2019 novel coronavirus (2019-nCoV) by real-time RT-PCR. *Eurosurveillance,* 25**,** 2000045.

Cortese-Krott, M. M., A. Koning, G. G. Kuhnle, P. Nagy, C. L. Bianco, A. Pasch, D. A. Wink, J. M. Fukuto, A. A. Jackson & H. van Goor (2017) The reactive species interactome: evolutionary emergence, biological significance, and opportunities for redox metabolomics and personalized medicine. *Antioxidants & redox signaling,* 27**,** 684-712.

Costela-Ruiz, V. J., R. Illescas-Montes, J. M. Puerta-Puerta, C. Ruiz & L. Melguizo-Rodríguez (2020) SARS-CoV-2 infection: The role of cytokines in COVID-19 disease. *Cytokine & growth factor reviews,* 54**,** 62-75.

Ebada, M. E. (2018) Essential oils of green cumin and chamomile partially protect against acute acetaminophen hepatotoxicity in rats. *Anais da Academia Brasileira de Ciências,* 90**,** 2347-2358.

El Sayed, S. M., M. S. Aboonq, Y. T. Aljehani, M. A. Hassan, R. M. Abou El-Magd, A. I. Abdelrahman, R. El-Tahlawi, M. M. H. Nabo, R. S. Yousef & A. A. Mahmoud (2020a) TaibUVID nutritional supplements help rapid cure of COVID-19 infection and rapid reversion to negative nasopharyngeal swab PCR: for better public prophylaxis and treatment of COVID-19 pandemic. *American journal of blood research,* 10**,** 397.

El Sayed, S. M., M. S. Aboonq, A. G. El Rashedy, Y. T. Aljehani, R. M. Abou El-Magd, A. M. Okashah, M. E. El-Anzi, M. B. Alharbi, R. El-Tahlawi & M. M. H. Nabo (2020b) Promising preventive and therapeutic effects of TaibUVID nutritional supplements for COVID-19 pandemic: towards better public prophylaxis and treatment (A retrospective study). *American Journal of Blood Research,* 10**,** 266.

El Sayed, S. M., H. H. Almaramhy, Y. T. Aljehani, A. M. Okashah, M. E. El-Anzi, M. B. AlHarbi, R. El-Tahlawi, M. M. H. Nabo, M. S. Aboonq & O. Hamouda (2020c) The evidence-based TaibUVID nutritional treatment for minimizing COVID-19 fatalities and morbidity and eradicating COVID-19 pandemic: a novel Approach for Better Outcomes (A Treatment Protocol). *American Journal of Public Health Research,* 8**,** 54-60.

El Sayed, S. M., S. Bahashwan, M. Aboonq, H. Baghdadi, M. Elshazley, A. Okashah, A. El Rashedy, R. El-Magd, Y. Aljehani & R. El-Tahlawi (2020d) Adjuvant TaibUVID nutritional supplements proved promising for novel safe COVID-19 public prophylaxis and treatment: enhancing immunity and decreasing morbidity period for better outcomes (A retrospective study). *Int J Med Develop Countries,* 4**,** 1375-1389.

TaibUVID inhalation therapies were quite effective in the management of the COVID-19 pandemic in addition to minimizing the morbidity period without causing any side effects (El Sayed et al. 2020d, El Sayed et al. 2020c, El Sayed et al. 2020b, El Sayed et al. 2020a).

Interestingly, all components of TaibUVID nutritional supplements cause increased glutathione. *Nigella sativa* fixed seeds and essential oil increase levels of reduced glutathione and related antioxidant enzymes (Abd-Elkareem, El-Rahman, Mokhless, Khalil & Amer 2021). Natural honey also increases reduced glutathione, antioxidant power, anti-inflammatory effects, and antiulcer potential against gastric ulcers in rats (Almasaudi, El-Shitany, Abbas, Abdel-Dayem, Ali, Al Jaouni et al., 2016). Senna results in increased activity of the antioxidant defense systems, including reduced glutathione (Coelho, Barbosa, Mito, Mantovanelli, Oliveira & Ishii-Iwamoto 2017). Fennel also increases the antioxidant power, the whole content of reduced glutathione and anticarcinogenic effects (Wang, Wang, Pan, Huang, Ren, Xu, et al., 2020d). Likewise, clove also increases the antioxidant power and reduces glutathione (Shekhar, Yadav, Singh, Pradhan, Desai, Dey et al., 2018). Moreover, chamomile (*Anthemis hyaline*) oil moderately ameliorated glutathione depletion (via increasing the reduced glutathione content) and the decrease in superoxide dismutase activity in the liver of acetaminophen-administered rats (Ebada 2018). Current therapeutics for COVID-19 may carry a lot of side effects due to free radicals generation that may deteriorate patients' condition and hence the bad need for adjuvant antioxidant therapies. Unfortunately, corticosteroids given to COVID-19 patients are known to decrease lymphocyte count which may aggravate the health status of the patients. Fortunately, this can be corrected by giving nigella sativa and natural honey that is contained in TaibUVID nutritional supplements. Natural antioxidants such as nigella sativa, honey, senna, fennel, and costus are recommended prophetic medicine remedies. Prophetic medicine is the medical knowledge gained from the sayings, deeds, and teachings of Prophet Muhammad peace be upon him.

Conclusion

COVID-19 is a devastating pandemic. Oxidant/antioxidant status is impaired in COVID-19 patients prone to depleted total antioxidant capacity. Decreased serum antioxidants can be regarded as a predictive marker of COVID-19 severity. COVID-19 patients had elevated levels of oxidative stress and reduction of antioxidant indices that aggravated the severity of COVID-19 in hospitalized patients. Gastrointestinal symptoms usually worsen with disease progression and include anorexia, diarrhea, liver injury, nausea, and abdominal pain. Cytokine storm-induced acute respiratory distress syndrome occurs in severe COVID-19 cases due to overwhelming proinflammatory hypercytokinemia and multisystem tissue damage. Antioxidant (e.g. glutathione) deficiency exaggerates SARS-CoV-2 infection. High serum-reduced glutathione causes decreased ROS and a shorter course of illness. Antioxidants are strongly suggested as adjuvant therapeutics to combat the pandemic. COVID-19 patients presenting with pneumonia, dysgeusia, and hyposmia scored immediate improvements upon treatment with the reduced glutathione precursor N-acetyl cysteine. In previous publications, we introduced TaibUVID antioxidant nutritional supplements that were found to be effective in helping COVID-19 patients recover.

Conflict of interest

The author declares that there is no conflict of interest.

References

Abd-Elkareem, M., A. El-Rahman, A. Mokhless, N. S. A. Khalil & A. S. Amer (2021) Antioxidant and cytoprotective effects of Nigella sativa L. seeds on the testis of monosodium glutamate challenged rats. *Scientific reports,* 11**,** 1-16.

Almasaudi, S. B., N. A. El-Shitany, A. T. Abbas, U. A. Abdel-Dayem, S. S. Ali, S. K. Al Jaouni & S. Harakeh (2016) Antioxidant, anti-inflammatory, and antiulcer potential of manuka honey against gastric

manifestation of the COVID-19 pandemic. Likewise, high serum reduced glutathione caused decreased ROS and a shorter course of COVID-19 infection (Polonikov 2020).

Moreover, SARS-CoV-2 significantly suppresses the content of intracellular reduced glutathione levels by decreasing the activity of intracellular erythroid 2-related factor that stimulates reduced glutathione production. Interestingly, exogenous supplementation of reduced glutathione enhances immunity against different bacterial and viral infections. Liposomes containing reduced glutathione caused an improvement in cytokine response of Th1 lymphocytes in patients having human immunodeficiency virus and *Mycobacterium tuberculosis* infections (Guloyan, Oganesian, Baghdasaryan, Yeh, Singh, Guilford, et al., 2020). Interestingly, the intracellular reduced glutathione concentration in erythrocytes is suppressed in type II diabetic patients (Lutchmansingh, Hsu, Bennett, Badaloo, McFarlane-Anderson, Gordon-Strachan, et al., 2018). Thus, these high-risk or immunocompromised populations may strongly benefit from receiving liposomal reduced glutathione supplementation.

In addition, common COVID-19 presentations such as pneumonia, dysgeusia, and hyposmia scored immediate improvements upon treatment with N-acetyl cysteine (a precursor of reduced glutathione), oral or intravenous reduced glutathione intake, and α-lipoic acid (Pan, Ye, Sun, Gui, Liang, Li, et al., 2020). Dyspnea in some COVID-19 patients improved one hour after intake of reduced glutathione and continued to improve with subsequent doses. Patients' sense of well-being and improvements started to increase rapidly (Horowitz, Freeman & Bruzzese 2020). Liposomal drug formulations improve the delivery of hydrophilic and lipophilic substances to prevent drug load degradation (in acidic environments such as gastric luminal pH), drug inactivation, and drug dilution in the circulation (Mehta, Kulkarni, Nikam, Padya, Pandey & Mutalik 2021). Interestingly, supplementation of oral liposomal reduced glutathione to healthy adults caused increased levels of reduced glutathione (by 100%) in peripheral blood mononuclear cells with a concomitant decrease in the biomarkers used to track oxidative stress, e.g. 8-isoprostane and the oxidized glutathione/reduced glutathione ratio. Likewise, liposomes containing reduced glutathione and given orally caused increased cytotoxicity in natural killer cells (by 400%) within a relatively short period (2 weeks). This confirms that increasing the antioxidant power conferred decreased oxidative stress and increased immunity (Sinha, Sinha, Calcagnotto, Trushin, Haley, Schell, et al., 2018). Liposomes containing reduced glutathione supplementation is a highly advisable supplement for treating COVID-19 patients.

In COVID-19 patients, oxidative stress increases in the presence of associated comorbidities such as diabetes mellitus and rheumatoid arthritis. Liposomal glutathione intake may be more beneficial than N-acetyl L-cysteine supplementation, as the enzymes essential for the synthesis of glutathione from L-cysteine may be deficient in such comorbidities.

TaibUVID nutritional supplements enhance antioxidants and combat COVID-19

Adjuvant nutritional treatment is a commonly missed health factor when treating fatal viral diseases such as COVID-19. We recently introduced TaibUVID nutritional supplements, composed of six medicinal plants and natural products. TaibUVID components include *Nigella sativa*, chamomile, and natural honey. Adding clove was optional (El Sayed, Almaramhy, Aljehani, Okashah, El-Anzi, AlHarbi, et al., 2020c; El Sayed, Bahashwan, Aboonq, Baghdadi, Elshazley, Okashah, et al., 2020d; El Sayed, Aboonq, El Rashedy, Aljehani, Abou El-Magd, Okashah, El-Anzi, Alharbi, El-Tahlawi & Nabo 2020b &El Sayed, Aboonq, Aljehani, Hassan, Abou El-Magd, Abdelrahman, et al., 2020a). This is suggested for both treatment and prophylaxis of COVID-19. TaibUVID Forte adds Costus, senna, and fennel to TaibUVID. Many meta-analyses and systematic reviews have confirmed the therapeutic benefits of TaibUVID components in the management of many co-morbidities and human diseases, e.g. diabetes mellitus and hypertension that are commonly encountered in COVID-19 patients. TaibUVID, TaibUVID Forte and

fecal-oral transmission. More attention should be given to monitoring liver function tests during COVID-19, particularly in patients with more disease severity (Gu et al. 2020, Lee, Huo and Huang 2020). Liver biopsies confirm the presence of RNA of SARS-COV-2 in hepatic cells. In addition, evidence of liver damage may take place e.g. apoptosis, lobular inflammation, acidophilic bodies, and cellular ballooning (Gu et al. 2020). Unfortunately, liver injury may be due to drugs given to COVID-19 patients such as NSAIDs, antibiotics, and antiretroviral medications. Moreover, the cytokine storm aggravates the production of pro-inflammatory cytokines, causing extensive cardio-pulmonary tissue damage, hypoxemia, hypoxia, and vascular thrombosis. All these complications may aggravate any underlying liver injury (Zhang et al. 2020).

ACE2 has a renin-angiotensin system-independent function that regulates intestinal neutral amino acid transporters facilitating decreased expression of antimicrobial peptides and gut microbiota. That facilitates intestinal inflammation and diarrhea (Syed, Khan, Gosai, Asif & Dhillon (2020).

COVID-19 and its impact on chronic liver diseases

Hepatitis B infection aggravates clinical outcomes in SARS-CoV-2 patients, causing extensive hepatic damage. Likewise, immunosuppressive medications given to cancer patients and people with autoimmune conditions may enhance COVID-19 infection, related tissue damage, and mortality. In the same context, it is quite advisable to screen liver donors and recipients for SARS-CoV-2 before a liver transplant to avoid transmitting the virus in the graft. Cancer patients and those with liver cirrhosis are more vulnerable to SARS-CoV-2 infection owing to their suppressed immunity (Zhang et al. 2020; Mao, Liang, Shen, Ghosh, Zhu, Yang, et al., 2020).

Pancreatic injury in COVID-19 infection

ACE2 receptors are highly expressed in pancreatic islet cells. SARS-CoV-2 may cause direct cytopathic effects, indirect systemic inflammation, or immune-mediated cellular effects. These collectively cause pancreatic damage and related enzyme abnormalities. NSAIDs and antipyretics may aggravate such tissue damage. 17% of COVID-19 patients got pancreatic injury (evidenced by increased serum amylase or lipase) that might result in the occurrence of acute diabetes (or abnormal blood glucose levels), but not reaching severe pancreatitis (Patel et al. 2020).

Antioxidant (e.g. glutathione) deficiency exaggerates SARS-CoV-2 infection (Figure 2)

The pathogenesis of COVID-19 and previous coronavirus infections (SARS-CoV-1 and MERS-CoV) involves the production of many proinflammatory cytokines, e.g. TNF-α, IL-8, IL-6, IL-7, IL-10, and others (Goyal, Choi, Pinheiro, Schenck, Chen, Jabri, et al., 2020). Angiotensin II is a potent activator of nicotinamide adenine dinucleotide phosphate (NADPH) oxidase and hence an inducer of reactive oxygen species (ROS) production. ACE2 receptors are common receptors for NADPH oxidase-4 (causing the generation of reactive oxygen species) (Samavati and Uhal 2020) and both SARS-CoV-1 and the novel SARS-CoV-2. Glycosylation of serum and tissue proteins occurs via a non-enzymatic reaction that commonly happens in diabetic subjects. ACE2 glycosylation is accelerated under hyperglycemic conditions and facilitates the attachment of the SARS-CoV-2 virus to target cells (Ceriello 2020). The cytokine storm during SARS-CoV-2 infection includes increased formation of proinflammatory cytokines such as IL-6, IL-2, IL-7, IL-10, and TNF-α levels, which are all associated with severe respiratory failure. This picture carries significant similarity to SARS-CoV-1 and MERS-CoV (Goyal et al. 2020).

The clinical deterioration of COVID-19 to acute respiratory distress syndrome is a product of cytokine storm. This is closely associated with increased serum IL-6 levels, extensive inflammatory reaction (increased pro-inflammatory vs. decreased anti-inflammatory cytokines), prolonged admission to the intensive care unit, progression to acute respiratory distress, and subsequent mortality. Reduced glutathione deficiency caused increased ROS levels and aggravated the severity of the clinical

increased viral transmission (Galanopoulos, Gkeros, Doukatas, Karianakis, Pontas, Tsoukalas, et al., 2020).

Digestive symptoms e.g. diarrhea, are strongly related to a higher incidence of positive stool PCR swabs (about 48.1% of patients) for viral RNA. Affected patients may have a high viral load for SARS-CoV-2 RNA. The presence of viral RNA in stool was confirmed with a relatively long duration (33-47 days after the first onset of the disease). Unfortunately, stool samples remained positive even after viral clearance of nasal RT-PCR swabs (Galanopoulos et al. 2020; Cheung, Hung, Chan, Lung, Tso, Liu, et al., 2020).

Table 2. :Symptomatology of COVID-19

***Mild COVID-19 presentation**:

- Fever, cough, somnolence; drowsiness, diarrhea, nausea, vomiting, and abdominal pain.
- Anorexia, malaise, muscle pain, sore throat, dyspnea, nasal congestion, and headache.
- Upper respiratory symptoms (loss of taste, loss of smell, dry cough, nasal congestion and pharyngitis)

*** Moderate COVID-19 presentation:** high fever, lymphopenia, (leukopenia or leukocytosis), and high serum transaminases, **pneumonia, and bronchopneumonia (**requiring oxygen support).

***Severe COVID-19 presentation: Acute respiratory distress syndrome (ARDS):**

Bilateral lung opacities, lobar congestion, consolidation, collapse with massive lung collapse, or nodular lesions in chest radiographs or CT scans.

*** Gastrointestinal symptoms (17.6%):** usually deteriorate upon COVID-19 progression, indicating disease severity.

- Anorexia
- Diarrhea
- Liver impairment causing acute hepatitis or mild to moderate elevation of serum transaminases (ALT and AST).
- Nausea
- Abdominal pain

Pathophysiology of gastrointestinal and hepatic COVID-19

The mucus membranes and adjacent tissues in the esophagus, stomach, duodenum, and rectum exhibit edema with patchy infiltrations. Such infiltrations may be plasmacytic and lymphocytic. SARS-CoV-2-induced gastrointestinal symptoms may take place via direct virus invasion of digestive cells, immunological-mediated tissue damage, or end-organ tissue injury (Tian, Rong, Nian & He 2020). Attachment of SARS-CoV-2 to ACE2 receptors takes place using the viral spike proteins (Luan, Lu, Jin & Zhang 2020). This occurs 10-20-fold more than with the virus SARS-CoV-1. Such high infectivity may denote massive human-to-human transmission of SARS-CoV-2 (Gordon, Jang, Bouhaddou, Xu, Obernier, White, et al., 2020). The viral spike protein mediates SARS-CoV-2 attachment to the ACE2 receptor with secondary entry into the target digestive and hepatic cells. Such entry is facilitated by the patient's transmembrane serine protease 2. Serine protease 2 causes the viral spike protein to divide into two functional monomers: S1 and S2. The S1 monomer attaches the virus to the ACE2 receptor, while the S2 monomer mediates viral fusion with the target cell membrane with subsequent viral entry into the target cells (Hoffmann et al. 2020). This may support the use of protease inhibitors for future COVID-19 treatment.

ACE2 receptors are also present in gall bladder cells (cholangiocytes). This may lead to hepatobiliary infection and damage that may occur in an opposite direction to bile flow upon viral entry into the biliary tree (Zhang, Shi &Wang 2020). SARS-CoV-2 is still present in the stools of infected patients, implicating the possibility of

use of drugs (Wang, Li, Lu & Huang 2020a). Immunological barriers preventing SARS-COV-2 infection and related damage include antiviral immune barriers such as antibody production by activated B cells (plasma cells), regulatory T cells, and the immunological effects conferred by IFN-α and IFN-β. In addition to the cell-mediated immunity conferred by NK cells and T cytotoxic cells, this response may eradicate SARS-CoV-2 virus infection (Bray, Sartain, Gollamudi & Rumbaut 2020).

Step 4. Cytokine storm-induced acute respiratory distress syndrome in COVID-19

Progression to acute respiratory distress syndrome then respiratory failure in COVID-19 patients may be due to massive host cytokine production (cytokines storm). This causes inflammation-induced tissue damage, increased capillary membrane permeability, pulmonary edema, and acute respiratory distress syndrome. Ultimately, the patients necessitate mechanical ventilation. Increased serum IL-6 (with an optimal predictive threshold at 80 pg/ml) is correlated with respiratory failure and the need for mechanical ventilation. Presence of associated comorbidities (diabetes mellitus, cancer, immunosuppressive therapy, and others), radiological findings, and rapid subsequent organ failure (Jiang, Yang, Sun, Chen, Ma, Yin, et al., 2018).

Step 5. Severe progression with shock

COVID-19 may present a variable clinical course. Respiratory impairment may be sudden due to overwhelming proinflammatory hypercytokinemia, multisystem tissue failure, respiratory failure (necessitating mechanical ventilation), and shock (Ragab, Salah Eldin, Taeimah, Khattab & Salem 2020).

Step 6. Septicemia and hypercoagulability

Severe cases of SARS-CoV-2 may involve hypercoagulable complications e.g. venous thromboembolism (e.g. cavernous sinus thrombosis) and pulmonary embolism. In addition, associated coagulation abnormalities may occur (Ragab et al., 2020). Thrombotic complications including increased D-dimer, manifest pulmonary embolism and venous thromboembolism may increase patient mortality in intensive care units (Middeldorp, Coppens, van Haaps, Foppen, Vlaar, Müller, et al., 2020). Hypercoagulability is a prothrombotic state exaggerated by tissue damage underlying vascular endothelial cells. The fibrin degradation product, D-dimer, correlates with SARS-CoV-2 severity. Serum D-dimer concentrations increased massively in patients with severe COVID-19 infection compared to those with mild or improved symptoms (Griffin, Jensen, Khan, Chin, Chin, Saad, et al., 2020). Macrophages produce the proinflammatory cytokine TNF-α during the inflammatory processes induced by SARS-CoV-2. This causes cell death through both necrotic and apoptotic pathways. TNF-α stimulates the activation of tissue factors and activation of the extrinsic pathway of coagulation, causing the production of cross-linked fibrin clots. This is followed by fibrinolysis mediated by tissue plasminogen activator. During acute inflammation caused by COVID-19, TNF-α increases while protein C level decreases, and this enhances the persistence of venous thromboembolism (Li, Zhao, Wei, Chen, Wang, Jia, et al., 2020b).

Step 7. COVID-19 mortality

Reported COVID-19 mortality rates are quite variable among countries and nations (ranging from 0.3 to 10%). The lowest rates of 2.5% and 4.0% in China and neighboring countries and increased to about 10% in Italy (which has the highest fatality rate) (Yuan, Li, Lv & Lu 2020), where the elderly (above 75 years) constituted a significant proportion of fatalities (about 85% of deaths due to the COVID-19 pandemic).

Gastrointestinal manifestations in the adult and pediatric population

Variable clinical presentations may be encountered in the course of SARS-CoV-2 infection. Gastrointestinal symptoms as nausea, abdominal pain, and diarrhea, are usually seen during COVID-19 pathogenesis and may contribute to

Figures legends

Figure 1. Pathophysiology of cytokine storm-induced death in COVID-19 patients: SARS-CoV-2 virus infects respiratory as gastrointestinal cells e.g. enterocytes and hepatocytes. SARS-CoV-2 also afflicts vascular endothelial cells. Routes of entry in all are ACE-2 receptors. Immunological responses include the activation of T helper lymphocytes (immunological orchestrator) that activate T cytotoxic, macrophages, neutrophils, and NK cells. Subsequent cytokines production participates in cell damage and hypercytokinemic-induced death. T cytotoxic cells produce perforins and granzymes that cause damage to virus-infected cells. NK cells cause lysis of virus-infected cells. Neutrophils degranulate causing the release of interleukin-6 causing fever and increased acute phase proteins. Both neutrophils and macrophages produce tumor necrosis factor-α that enhances vascular permeability, vascular thrombosis, edema, DIC, and septic shock. That collectively causes cellular damage to enterocytes (diarrhea and shock) and hepatocytes (raised serum liver enzymes, ALT, and AST). TaibUVID nutritional components (nigella sativa, natural honey, costus, senna, fennel, and chamomile) suppress inflammatory cytokines production and effects and were reported to effectively help cure COVID-19 patients.

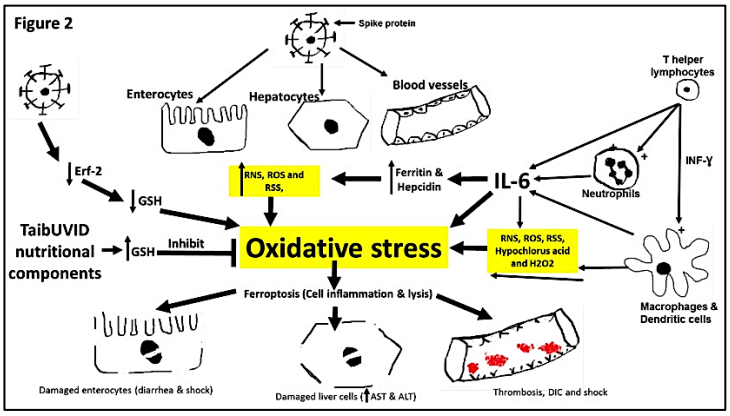

Figure 2. Pathophysiology of oxidative stress-induced death in COVID-19 patients:

Figure 2. Pathophysiology of oxidative stress-induced death in COVID-19 patients: Oxidative stress is a key player in cell damage and cell death in COVID-19 patients. Immunological responses include activation of T helper lymphocytes (immunological orchestrator) that activate T cytotoxic, macrophages and neutrophils. T helper lymphocytes, neutrophils, and macrophages produce interleukin-6 that enhances serum ferritin and hepcidin causing increased RNS, ROS, and RSS. Concomitantly, SARS-CoV-2 causes decreased Erf-2 which decreases serum GSH. All that increases oxidative stress vs. antioxidant power causing cell damage and apoptosis (ferroptosis). That collectively causes cellular damage to enterocytes (diarrhea and shock) and hepatocytes (raised serum liver enzymes, ALT, and AST). TaibUVID nutritional components (nigella sativa, natural honey, costus, senna, fennel, and chamomile) cause increased glutathione and decreased oxidative stress. Such effects effectively help cure COVID-19 patients. GSH reduced glutathione. Erf-2, erythroid releasing factor-2, RNS, reactive nitrogen species, ROS, reactive oxygen species, RSS, reactive sulfur species

Step 3: Either recovery or progression Recovery

As previously reported by the center for disease control, COVID-19 resolution involves recovery from the fever and respiratory symptoms with no

Paessler & Huang 2020). Hypercytokinemia causes acute respiratory distress syndrome and multiple organ damage. Immunological response against SARS-CoV-2 is related to race, gender, and age. Many therapeutic strategies investigate the cytokine storm in patients with severe COVID-19 (Rabaan, Al-Ahmed, Muhammad, Khan, Sule, Tirupathi, et al., 2021b).

Upon antigen presentation (e.g. due to SARS-CoV-2 infection), T helper lymphocytes (Th1 and Th2 subtypes) release inflammation-induced cytokines as IL-6, interferon-gamma (IFN-γ), IL-4, granulocyte-macrophage colony-stimulating factor, IL-2, and IL-10. IL-2 enhances the maturation of helper and cytotoxic T cells, while IL-4 enhances B cell growth and differentiation into plasma cells (to secrete antibodies) (figures 1-2) (Rabaan, Al-Ahmed, Garout, Al-Qaaneh, Sule, Tirupathi, et al., 2021a). IFN-γ enhances phagocytosis (exerted by macrophages and monocytes) and potentiates natural killer (NK) cells-induced lysis of virus-infected cells (Lang, Lee, Teijaro, Becher & Hamilton (2020). The granulocyte-macrophage colony-stimulating factor is a glycoprotein that induces maturation and then differentiation of neutrophils and CD14+/CD16+ monocytes, which produce massive amounts of IL-6 that are not seen in healthy subjects (Figure 1) (Boyette, Macedo, Hadi, Elinoff, Walters, Ramaswami, et al., 2017). Immune cells, e.g. activated lymphocytes, macrophages, and neutrophils produce different inflammatory cytokines such as IL-6 and TNF-α. IL-6 induces fever and increases the production of acute-phase proteins. TNF-α enhances leukocyte-induced development of disseminated intravascular coagulopathy and septic shock (Figure1) (Velazquez-Salinas, Verdugo-Rodriguez, Rodriguez & Borca 2019). Increased serum ferritin (> 400 ng/ml) was reported to be high in patients having severe COVID-19 disease upon hospitalization. Serum ferritin levels were 3 and 4 times higher in patients who died than those observed in patients who survived (Gómez-Pastora, Weigand, Kim, Wu, Strayer, Palmer, et al., 2020). High serum ferritin and IL-6 are both diagnostic and prognostic markers of COVID-19 deterioration, progression, and deterioration of the cytokines storm. Patients who recovered tended to have lower serum IL-6 and ferritin levels (Liu, Zhang, Yang, Ma, Li, Zhang, et al., 2020). The cytokine storm (with increased levels of IL-6) results in increased ferritin and hepcidin levels. This indirectly causes lethal oxidative stress via sequestering iron intracellularly with the resultant generation of reactive nitrogen species, reactive oxygen species, and reactive sulfur species. That collectively maximizes tissue damage in affected organs, e.g. the gastrointestinal tract, respiratory tract, and elsewhere (Cortese-Krott, Koning, Kuhnle, Nagy, Bianco, Pasch, et al., 2017). Sequestered iron may react with clotting factors in coagulation pathways, resulting in hypercoagulable conditions (Tang, Zhang, Fang, Han, Wang, Wang, et al., 2020c). Moreover, high levels of intracellular iron can enhance a recently reported cell death mechanism termed ferroptosis (Gao, Monian, Pan, Zhang, Xiang & Jiang 2016).

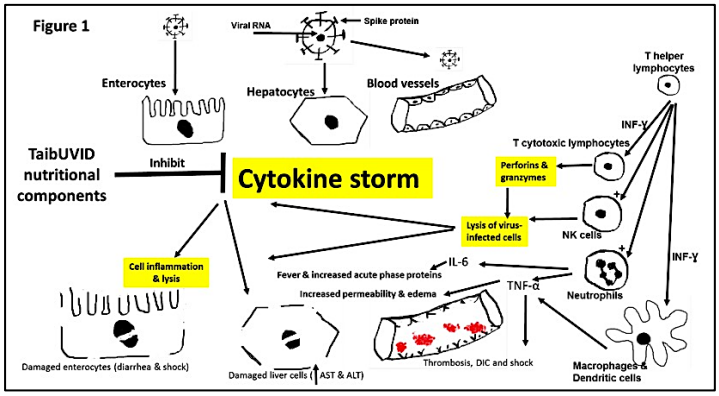

Figure 1. Pathophysiology of cytokine storm-induced death in COVID-19 patients

Step 1: SARS-COV-2 infects the upper respiratory tract

In the early stages of COVID-19, coronavirus infection starts with the inhalation of droplets containing SARS-CoV-2 virions that gain access to the nasal mucosa, causing cellular swelling and inflammation. Respiratory epithelial cells (having cilia) and mucus (a product of goblet cells of the respiratory tract) extrude the pathogen via mucociliary defense mechanisms. Co-morbidities such as diabetes, cardiovascular disease, or tobacco use impair pathogen excretion via this innate mechanism, which allows for virus colonization in the lower respiratory tract (Brodin 2021). Patients infected with COVID-19 are usually asymptomatic in cases where there is no colonization of the lower respiratory tract. Host barriers and defenses of the respiratory epithelial lining, e.g. immunoglobulin A, reduced glutathione, and beta-defensins tend to clear COVID-19 infection in its early stages, although patient nasopharyngeal PCR swabs are still positive (Cao and Li 2020). When SARS-CoV-2 arrives at the lower respiratory tract, it attaches to ACE2 on type II alveolar pneumocytes (which produce surfactant and regenerate type I alveolar pneumocytes that facilitate gas exchange) via the viral S protein. Subsequently, SARS-CoV-2 enters target cells, releases its single-stranded RNA genome, and utilizes the host enzyme machinery for viral replication. Consequently, damaged type II pneumocytes result in decreased surfactant levels, and suppressed type I pneumocytes functions impair gas exchange and minimize lung compliance, leading to lung edema and pneumonitis (Mason 2020). Intestinal epithelial cells have ACE2 receptors, allowing SARS-CoV-2 to infect intestinal cells (enterocytes), causing early gastrointestinal manifestations, e.g. diarrhea (Guan, Ni, Hu, Liang, Ou, He, et al., 2020). Based on that, COVID-19 patients may present with respiratory or gastrointestinal symptoms (Table 2).

Step 2: SARS-CoV-2 induces the oxidative stress-induced acute inflammatory process

Local immunological defenses in pulmonary tissues affect type II pneumocytes, alveolar macrophages, and dendritic cells. Macrophages and type II pneumocytes secrete IL-8 (a vital neutrophil chemotactic agent) (Costela-Ruiz, Illescas-Montes, Puerta-Puerta, Ruiz & Melguizo-Rodríguez 2020). Acute inflammation occurs with neutrophil and monocyte migration to lung alveoli (García 2020), with neutrophilic degranulation and release of acute phase reactants, e.g. IL-6 and TNF-α. Phagocytes use reduced nicotinamide adenine dinucleotide phosphate (NADPH) as a coenzyme for NADPH oxidase for generating cytotoxic reactive oxygen species, i.e. hypochlorite and hydrogen peroxide (Polonikov 2020). Acute inflammatory processes caused by a combination of ROS and pro-inflammatory cytokines participate in causing the severe parenchymal lung injury commonly encountered in COVID-19. Decreased levels of pro-inflammatory cytokines, reactive oxygen species, hypochlorite, and hydrogen peroxide are associated with rapid recovery and a mild course of COVID-19 illness (Polonikov 2020).

Both components of type I interferon (IFN-α and IFN-β) play a significant role in the innate response to viruses. Human embryonic kidney (HEK293) cells expressing structural proteins of SARS-CoV-2 maximally resisted the effects of IFN-β and NF-κβ (Li, Liao, Wang, Tan, Luo, Qiu et al., 2020a). Moreover, incubating Vero cells with recombinant human IFN-α caused decreased SARS-CoV-2 viral titers compared to non-incubated Vero cells (Tang et al. 2020a).

Cytotoxic T lymphocytes recognize viral antigens presented by antigen-presenting cells (e.g. dendritic cells and B cells) in association with major histocompatibility complex (MHC) Class I. Cytotoxic T lymphocytes degranulate, causing released cytotoxic perforins and granzyme-B. Perforin proteins cause perforations and increase the permeability of the membranes of virus-infected cells, while granzymes cause proteolytic activation of intracellular caspases, resulting in apoptosis (Tang et al. 2020a). Uncontrolled and dysregulated secretion of inflammatory and pro-inflammatory cytokines (as TNF-α, IL-1, and IL-6 causing cytokine storm) positively correlates with viral infection severity and high mortality rate via recruiting macrophages, T and B cells in the lung alveolar cells (Mantlo, Bukreyeva, Maruyama,

SARS-CoV-2 is vital for receptor specificity, tissue homing, and cellular binding. ACE2 expression is present in the oral mucosa and nasal epithelial cells of the upper respiratory system and explains the high transmission rates of the virus (Sungnak et al. 2020).

ACE2 receptors are found in type 2 alveolar cells and muscle cells of the pulmonary vasculature. This partially gives explanations about the severe respiratory symptomatology associated with these viruses (Tang et al. 2020a). Male patients suffer more from inflammatory disease than females. Hormones may play a role. Females may be more protected from respiratory viral pathogens of SARS-CoV-2, than males possibly due to the effects of estrogen and other sex hormones on both T and B lymphocytes (Vadakedath, Kandi, Mohapatra, Pinnelli, Yegurla, Shahapur, et al., 2021).

ACE2 receptors are also found in the epithelial cells all over the gastrointestinal tract, e.g. oral mucosa, cytoplasm of the gastric and intestinal epithelia and the ciliary lining of the digestive glands, colonic enterocytes, myocardial cells, vascular endothelium, proximal tubule, bladder urothelial cells, and cholangiocytes (Xiao, Tang, Zheng, Liu, Li & Shan 2020). In a recent study, the *ACE2* gene was found to exhibit single nucleotide polymorphisms with many different allele frequencies across the globe (Cao, Li, Feng, Wan, Huang, Sun, et al., 2020). SARS-CoV-2 may direct damage to the intestinal mucosa. This can lead to increased intestinal permeability to foreign pathogens by compromising intestinal barrier function, resulting in diarrhea and malabsorption (Gu, Han & Wang 2020).

The allele frequency of the host gene varies among males and females. In COVID-19 patients, many risk factors aggravate infection (Table 1). The presence of viral nucleocapsid protein was confirmed in the gastrointestinal lumen of many digestive organs, e.g. stomach, duodenum, and rectum glandular epithelial cells excluding the esophagus. The SARS-CoV-2 virus subverts cellular capabilities to serve the viral replication process. Viral RNA polymerase is quite necessary for viral replication (Xu, Chen, Wang, Feng, Zhou, Li, et al., 2020). The incubation period for SARS-CoV-2 may last 4-14 days. Within this period, symptomatology may appear and is mostly mild (80%). However, severe cases may be encountered (20%) when comorbidities and high viral load are present (Wang, Tang and Wei 2020c). Severe symptomatology encountered with novel SARS-CoV-2 results from the interaction of immune responses, cytokines effects, and defensive measures.

Cytokine storm

The cytokine storm takes place as a consequence of events in response to the pathogenesis of SARS-CoV-2 infection. This causes an increase in the volume of mucus and fluids inside the lung alveoli, with subsequent collapse of pulmonary function, up to respiratory failure (Corman, Landt, Kaiser, Molenkamp, Meijer, Chu, et al., 2020).

Table 1 : Risk factors aggravating novel SARS-CoV-2 infection (Zhou, Yu, Du, Fan, Liu, Liu, et al., 2020; Lippi, Wong & Henry 2020; Baud, Qi & Nielsen-Saines 2020; Verma and Shakya 2021)

- **Age:** older than 60 years of age
- **Co-morbidities** (particularly chronic diseases): diabetes mellitus, diabetic complications, chronic renal disease, hypertension, hyperlipidemia, cardiovascular diseases, cancer
- **Differential expression of the ACE2 receptor**
- **Chronic obstructive pulmonary disease**
- **Malnutrition**
- **Immunocompromise**
- **Viral load**
- **Occupation** (physicians, physician's families, and hospital staff)
- **Virulence** of COVID-19 strains and genomic mutations

subsequent genomic recombination possibilities quite common (Kautz and Forrester 2018; Smith 2017). This may explain the evolution of SARS-CoV-2. In Wuhan, China, the L type of SARS-COV-2 was seen in about 70% of COVID-19 patients and was confirmed to be more pathogenic and infectious compared to the original S type (Tang et al. 2020b).

COVID-19 transmission

The SARS-CoV-2 virus remains contagious in air droplets for approximately 3 hours (median half-life of 1.1-1.2 hours). Moreover, SARS-CoV-2 remains on plastic surfaces and stainless steel objects for an average period of three days (72 hours) after virus contamination. Moreover, the SARS-CoV-2 virus has been found on copper or metal surfaces for 4 to 24 hours. Aerosol and fomite transmission is highly likely as the virus remains infectious in aerosols for three hours and on contaminated surfaces for more than 72 hours (Van Doremalen, Bushmaker, Morris, Holbrook, Gamble, Williamson, et al., 2020).

SARS-CoV-2 infection has a high mortality rate that increases with age. In the 55- to 74-year-old age group, the mortality rate is 1.4-4.9%; this increases to 4.3-10.5% in the age group 75-84 years. However, the highest fatality rate is 10.4-27.3% in the age group above 85 years (Uddin, Mustafa, Rizvi, Loney, Al Suwaidi, Al-Marzouqi, et al., 2020).

SARS-CoV-2 entry into target cells

SARS-CoV-2 synthesizes many non-structural proteins that negatively impair the host's immune system and host cell physiological functions by enhancing virus virulence factors. A close interaction occurs between the SARS-CoV-2 virus and host cell receptors to mediate virus entry. In many people, the COVID-19 pandemic remains symptomless, while in other patients the pandemic may present with severe complications, e.g. pneumonia, respiratory distress, and respiratory failure (Astuti 2020).

Enveloped viral species, e.g. Coronaviridae target angiotensin-converting enzyme (ACE) cellular receptors that mediate virus internalization via endocytosis resulting in endosome formation. That endosome is acidic and this acidity continuously and progressively increases. Protonation of the binding viral glycoproteins soon increases. Enzyme activities are enhanced, facilitating the binding of viral proteins to the virus membranes and other cellular membranes, with the final release of the viral RNA into the cytoplasm. Upon coronavirus attachment to cellular membranes, viral spike protein interacts with cellular receptors followed by acid-dependent proteolytic cleavage of the viral spike proteins using a protease enzyme (cathepsin). This is followed by the fusion of viral and cellular membranes to form endosomes. The acidic pH of endosomes accelerates the viral-cell fusion processes (Tang, Bidon, Jaimes, Whittaker & Daniel 2020a).

Remedies used to treat COVID-19 patients e.g. Remdesivir, Ivermectin, and hydroxychloroquine can bind the active position viral protease protein (Hoffmann, Kleine-Weber, Schroeder, Krüger, Herrler, Erichsen, et al., 2020). The emergence of a new UK variant B.1.1.7 of SARS-CoV2 virus had exaggerated COVID-2 suffering. SARS-CoV2 virus is mainly transmitted through coughs, sneezes, talks, or breaths and on different surfaces (Mohapatra, Das, Pintilie & Dhama 2021). With the emergence of the new variants of concern of SARS-CoV-2, the efficacy of vaccines requires consideration. Vaccines' lack of efficacy against variants of concern of SARS-CoV-2 may subject the vaccinated population to health threats. Students in countries with the highest rates of infection (e.g., India, the USA, and Brazil) are prone to infection. SARS-CoV-2 strain variant (UK variant B.1.1.7) had spread in various Indian states among students. This maximizes vaccination necessity (Hoffmann et al. 2020; Mohapatra et al., 2021; Sah, Khatiwada, Shrestha, Bhuvan, Tiwari, Mohapatra, et al., 2021; & Sungnak, Huang, Bécavin, Berg, Queen, Litvinukova, et al., 2020)).

Pathophysiology of COVID-19

SARS-CoV-2 is a single-stranded RNA virus containing four different viral proteins. The spike proteins attach SARS-CoV-2 to ACE2 and ease viral entry to target host cells. The spike protein of

1. INTRODUCTION

Antioxidants are still missing vital remedies in COVID-19 treatment that need more light to be shed on them for more effective therapeutic outcomes. Our previous publications confirm the merits of antioxidants in combating the COVID-19 pandemic, particularly at the early stages of disease pathophysiology. Oxidants are increased and antioxidants are decreased in COVID-19 patients which may affect its severity. This review investigates that and provides practical preventive and therapeutic solutions.

SARS-CoV-2 is the causative virus of the COVID-19 pandemic. This virus belongs to the beta-coronaviruses family that are also implicated in the pathogenesis of severe acute respiratory syndrome (SARS) and the subsequent Middle East respiratory syndrome (Patel, Patel, Vunnam, Hewlett, Jain, Jing & Vunnam (2020). The COVID-19 pandemic first emerged in December 2019 in the Far East where many patients presented with atypical pneumonia that was first observed in health centers in Wuhan, China. Oxidant/antioxidant status is impaired in COVID-19 patients due to depleted total antioxidant capacity that can be regarded as a predictive marker of COVID-19 severity (Wang, Horby, Hayden & Gao 2020b). On March 11, 2020, the WHO declared COVID-19 as a worldwide pandemic. Interestingly, the serum levels of reduced glutathione, total antioxidant capacity, and total oxidant status were estimated in COVID-19 patients. It was found that COVID-19 patients had elevated levels of oxidative stress and reduction of antioxidant indices that aggravated the severity of COVID-19 in hospitalized patients. Moreover, that strongly suggested antioxidants as adjuvant therapeutics to combat the pandemic (Mann, Sekhon & Sekhon 2021). Patients presented with vague pneumonia. Early health reports indicated that these cases had bird flu, swine flu, and influenza-like symptoms. SARS-CoV-2 is genetically similar to SARS-CoV-1 (by about 79-80%) and to MERS-CoV (by about 51.8%) and is also 96% similar to the whole genomic structure of coronavirus-affecting bats (Chen, Liu, & Guo 2020). This novel virus massively disseminated across the world within a relatively short period (a few months), resulting in an emerging pandemic that threatened millions of lives and constituted a real danger to human health worldwide. Later, the causative virus was delineated to be a novel SARS-CoV-2 that maximally and rapidly caused worldwide morbidity and mortality in a relatively short duration. Despite worldwide lockdown, SARS-CoV-2 caused a lethal pandemic threatening human health (Rothan and Byrareddy 2020). The current COVID-19 pandemic has caused 3.7 million victims and more deaths are expected in the coming months (Arias-Carrasco, Giddaluru, Cardozo, Martins, Maracaja-Coutinho & Nakaya 2021). Gastrointestinal presentation is a serious topic related to COVID-19 lethality. In this review article, the merits of antioxidants for treating COVID-19 are introduced and correlated to pandemic pathology and pathophysiology, and new vital therapeutic targets are discussed with a special emphasis on the gastrointestinal picture.

Genome of SARS-CoV-2

SARS-CoV-2 belongs to the coronaviruses, i.e. it is an enveloped virus having a single-stranded nucleic acid (positive-sense RNA) lacking genomic segmentation. The viral genome (~30 kb in size) carries genetic information for synthesizing about 16 non-structural proteins (which facilitate viral replication, entry, and pathogenesis). These structural proteins include the envelope protein (E), membrane protein (M), nucleocapsid protein (N), and spike glycoprotein (S) (Kim, Lee, Yang, Kim, Kim & Chang 2020). The genomic sequence of SARS-CoV-2 confirms that it is about 75-80% similar to the genomic structure of SARS-CoV (Andersen, Rambaut, Lipkin, Holmes & Garry 2020). There are two major subtypes of SARS-CoV-2 upon studying 103 SARS-CoV-2 genomes (referred to as L and S) using single nucleotide polymorphisms (Tang, Wu, Li, Song, Yao, Wu, Duan, Zhang, Wang & Qian 2020b).

Future mutagenesis of SARS-COV-2 viruses may occur as they have error-prone RNA-dependent RNA polymerases. This may increase the frequency of future genetic mutations, making

المملكة العربية السعودية
جامعة الحدود الشمالية (NBU)
مجلة الشمال للعلوم الأساسية والتطبيقية (JNBAS)
طباعة ردمد: 1658-7022/ إلكتروني – ردمد: 1658-7014
www.nbu.edu.sa
s.journal@nbu.edu.sa

بحث مرجعي

الآثار المحتملة لمضادات الأكسدة كمواد مساعدة للعلاجات الحالية لوباء COVID-19:دروس من الفسيولوجيا المرضية للأمراض

معتصم صالح أبوعنق

(قدم للنشر في 1444/9/6هـ؛ وقبل للنشر في 1445/2/14هـ)

مستخلص البحث: لا تزال جائحة COVID-19 تمثل تحديًا. و تعتبرمضادات الأكسدة من العلاجات الحيوية في علاج COVID-19. و تزداد المواد المؤكسدة بينما تنخفض مضادات الأكسدة لدى مرضى كوفيد -19 مما قد يؤثر على شدة المرض. تبحث هذه المراجعة في ذلك وتثبت الحلول الوقائية والعلاجية العملية. و تسهل بوليمرات الحمض النووي الريبي المعرضة للخطأ حدوث طفرات فيروس السارس-CoV-2 وظهور سلالات جديدة. و يبدأ التسبب في الإصابة بفيروس COVID-19 بربط بروتينات سبايك بمستقبلات الإنزيم -2 المحول للأنجيوتنسين على الخلايا المستهدفة في الجهاز التنفسي والجهاز الهضمي. و يساعد فيروس السارس- CoV-2 حدوث العمليات الالتهابية الحادة التي يسببها الإجهاد التأكسدي مثل المواد الالتهابية انترلوكين-6 (IL-6) وعامل تنكرز الأورام ألفا TNF-α. كما يعزز الإجهاد التأكسدي ومتلازمة الضائقة التنفسية الحادة التي تسببها عاصفة السيتوكينات من تلف الأنسجة متعدد الأنظمة، وفشل الجهاز التنفسي والصدمة الدموية. و تتفاوت معدلات وفيات COVID-19 على مستوى العالم ، حيث سجلت المملكة العربية السعودية أدنى معدلات الوفيات. كما أظهر مرضى COVID-19وباء كورونا نقصا في القدرة الكلية لمضادات الأكسدة الكاملة والتي يمكن اعتبارها علامة تنبؤية لشدة المرض. و لقد كان لدى مرضى COVID-19 مستويات مرتفعة من الإجهاد التأكسدي يصحبه نقص في علامات مضادات الأكسدة. و عادة ما تتفاقم أعراض الجهاز الهضمي لوباء COVID-19 مع تطور المرض وتشمل فقدان الشهية والإسهال وإصابة الكبد والغثيان وآلام البطن. كما أدى نقص مضادات الأكسدة (مثل الجلوتاثيون) إلى تفاقم عدوى السارس- CoV-2. و يؤدي انخفاض مستوى الجلوتاثيون في الدم إلى انخفاض نسبة الأكسجين إلى الدم وقصر فترة المرض. و يُقترح بشدة استخدام مضادات الأكسدة كعلاجات مساعدة لمكافحة الوباء. لقد أثبتنا سابقًا أن مضادات الأكسدة الواعدة TaibUVID ساعدت مرضى COVID-19 على التعافي. و يؤدي نقص مضادات الأكسدة (مثل الجلوتاثيون) إلى تضخيم عدوى السارس. كما أدت نتائج تناول الجلوتاثيون إلى تقليل أنواع الأكسجين التفاعلية و نقص مسار المرض مع تحسن الالتهاب الرئوي وعسر الهضم ونقص حاسة الشم فور العلاج بمضادات الأكسدة. و تعمل جميع مكونات TaibUVID على رفع مستويات الجلوتاثيون وتقوية المناعة ومكافحة الفيروسات و حماية الأنسجة كما نناقشه هنا.

كلمات مفتاحية: كوفيد-19 ، الفسيولوجيا المرضية، عاصفة السيتوكينز، مضادات الاكسدة، الجلوتاثيون، TaibUVID .

للمراسلة:
أستاذ مشارك. قسم: علم وظائف الأعضاء، جامعة طيبة، المدينة المنورة.

e-mail: aboonq@yahoo.co.uk

DOI: 10.12816/0061645

Journal of the North for Basic and Applied Sciences, Vol. (8), Issue (2), (November 2023/ Rabi' II 1445 H) 134-150

KINGDOM OF SAUDI ARABIA
Northern Border University (NBU)
Journal of the North for Basic & Applied Sciences(JNBAS)
p - ISSN : 1658 -7022 / **e-ISSN: 1658 - 7014**
www.nbu.edu.sa
s.journal@nbu.edu.sa

(A review article)

The potential effects of antioxidants as adjuvants to current therapeutics of COVID-19 pandemic: lessons from disease pathophysiology

Moutasem S Aboonq *

(Received 28/3/2023 ; accepted 30/8/2023)

Abstract: The COVID-19 pandemic is still challenging. Antioxidants are missing vital remedies in COVID-19 treatment. Oxidants are increased and antioxidants are decreased in COVID-19 patients which may affect the disease severity. This review investigates that and provides practical preventive and therapeutic solutions. Error-prone RNA polymerases explain SARS-CoV-2 mutagenesis and the emergence of novel strains. COVID-19 pathogenesis starts with the attachment of spike proteins to angiotensin-converting enzyme-2 receptors on target cells in the respiratory and digestive systems. SARS-CoV-2 induces oxidative stress-induced acute inflammatory processes. Neutrophilic degranulation releases IL-6 and TNF-α. This enhances oxidative stress and cytokine storm-induced acute respiratory distress syndrome with overwhelming proinflammatory hypercytokinemia, multisystem tissue damage, respiratory failure, and shock. COVID-19 mortality rates differ globally, with Saudi Arabia among the countries having the lowest fatalities. COVID-19 patients COVID-19 exhibited depleted total antioxidant capacity that can be regarded as a predictive marker of severity. COVID-19 patients had elevated levels of oxidative stress and reduction of antioxidant markers. Gastrointestinal symptoms of the COVID-19 pandemic usually worsen with disease progression and include anorexia, diarrhea, liver injury, nausea, and abdominal pain. Antioxidants (e.g. glutathione) deficiency aggravated SARS-CoV-2 infection. High serum-reduced glutathione causes decreased ROS and a shorter course of illness. Antioxidants are strongly suggested as adjuvant therapeutics to combat the pandemic. We previously reported promising TaibUVID antioxidants that help COVID-19 patients to recover. Antioxidant (e.g. glutathione) deficiency exaggerates SARS-CoV-2 infection. Glutathione intake results in decreased ROS and shortened illness course. Pneumonia, dysgeusia, and hyposmia improved immediately upon antioxidant treatment. All TaibUVID components raise glutathione levels, enhance immunity, combat viruses, and exert tissue protection. This review discusses this vital issue.

Keywords: COVID-19, pathophysiology, cytokine storm, antioxidants, glutathione, TaibUVID

DOI: 10.12816/0061645

* **Corresponding Author:**
Associate Professor, Dept.: Physiology, Faculty: Medicine, University: Taibah, City: Medina, Kingdom of Saudi Arabia.

e-mail: : aboonq@yahoo.co.uk

uncertainty: Two-stage stochastic model and application to a food supply chain. International Journal of Production Economics, 201:89–101.

Soares, J., Canizes, B., Ghazvini, M. A., Vale, Z., and Kumar, G., Venayagamoorthy, G. K., (2017). Two-stage stochastic model using benders' decomposition for large-scale energy resource management in smart grids. IEEE Transactions on Industry Applications, 53(6):5905–5914.

Shah, M., Rahmat, G., Shah, S. A., Shah, Z., Deebani, W., et al, (2022). Strong convergence of krasnoselskii–mann process for non- expansive evolution families. Mathematical Problems in Engineering.

Shah, M., Rahmat, R., Shah, S. A., et. Al., (2022). Convergence for a fixed point of evolution families in banach space via iterative process. Journal of Mathematics.

Wang, C., Mohammed, A. Q., and Ison, G. S., (2011). Predicting ac- cident frequency at their severity levels and its application in site ranking using a two-stage mixed multivariate model. Accident Analysis & Preven- tion, 43(6):1979–1990.

Wang, S., and Huang, H. G., (2015). A multi-level taguchi-factorial two-stage stochastic programming approach for characterization of parameter uncer-tainties and their interactions: An application to water resources manage- ment. European Journal of Operational Research, 240(2):572–581.

Yalcin, C., and Stott A. W., (2000). Dynamic programming to investigate financial impacts of mastitis control decisions in milk production systems. Journal of Dairy Research, 67:515–528.

Yang, T., (2010). A two-stage stochastic model for airline network design with uncertain demand. Transportmetrica, 6(3):187–213.

Zimmerman, J .F., and Carter, M. R., (2003). Asset smoothing, consumption smoothing and the reproduction of inequality under risk and subsistence constraints. Journal of Development Economics, 71:233–260.

from S_k by solving the minimization problem (15).

2. Replace first-stage problem by the following approximate problem:

$$\min_{\boldsymbol{x}} = c'\boldsymbol{x} + q_k(\boldsymbol{x}) \quad (17)$$
$$A\boldsymbol{x} \leq b$$
$$\boldsymbol{x} \geq 0$$

And the solution denoted by $\boldsymbol{x}_k$

3. If $\boldsymbol{x}_k$ is "optimal", then the solution found, otherwise generate a sample for ξ_k and calculate $q_k \sim Q(\boldsymbol{x}_k)$ and add it to the previous set that is, $S_{k+1} = S_k \cup \{\boldsymbol{x}_k, q_k\}$ by increasing the number f iteration $k := k + 1$ and go back to the second step.

6. Conclusion

Stochastic programming has gained a major of optimization for modeling uncertainties in mathematical optimization problems. Two-stage stochastic programming with random is dealing the problem under uncertainty in models, and use optimization concepts optimization along with statistics and probability. stochastic programming continues develop a huge of algorithm and theoretical by researchers and scientists. In this paper, we build the algorithm of two stage problem which we name it successive exponential regression approximations (SERA) to solve the two-stage stochastic programming for both one-dimension and multidimensional. The algorithm for solving a two-stage model with probabilistic constraint (successive exponential regression approximations (SERA)) was proposed based on replacing the expected recourse function, which is numerically hard to be solve by the regression function then solving this problem by this technique. So by this idea we can solve any two stage Stochastic programming. For future work we will use real application data to with successive exponential regression approximations (SERA).

References

Alreshidi, A., Mrad, M., Subasi, E., et. Al., (2020). Two-stage bond portfolio optimization and its application to saudi sukuk market. Annals of Operations Research, 288(1):1–43.

Aranguren, M., Castillo-Villar, K., and Ojeda, M., (2021). A two-stage stochastic model for co-firing biomass supply chain networks. Journal of Cleaner Production, 319: 12858.

Cote, G. and Laughton. M, (1982). Stochastic production costing in generation planning: a lagescale mixed integer model. Mathematical Programming Study.

Deak, I., (2021). Computer experiences with successive regression approximations for solving equations. In Optimization Theory, pages 65–80. Springer.

Deak, I., (2004). Solving stochastic programming problems by successive regression approximations: Numerical results. In Dynamic Stochastic Optimization, pages 209–224. Springer.

Deak, I., (2006). Two-stage stochastic problems with correlated normal variables: computational experiences. Annals of Operations Research, 142(1):79–97.

Deak, I., (2011). Testing successive regression approximations by large-scale two- stage problems. Annals of Operations Research, 186(1):83–99, 2011.

Hrabec, D., Popela, P., Roupec, J., Mazal, J., and Stodola, P., (2016). Two- stage stochastic programming for transportation network design problem. In International Conference on Soft Computing-MENDEL, pages 17–25. Springer.

Kim, K., and Mehrotra, S., (2015). A two-stage stochastic integer programming approach to integrated staffing and scheduling with application to nurse management. Operations Research, 63(6):1431–1451.

Kall, P., and Wallace, W. S., (1994). Stochastic Programming. New York, NY: Wiley.

Nawaz, R., Nasir, A. N., Zada, L., et. Al., (2020). Comparative analysis of natural transform decom-position method and new iterative method for fractional foam drainage problem and fractional order modified regularized long-wave equation. Fractals, 28(07):2050124.

Nawa,. R., Kumam, P., Farid, S., Shutayw, M., Shah, Z., and Deebani, W., (2020). Application of new iterative method to time fractional whitham–broer–kaup equations. Frontiers in Physics, 8:104.

Prekopa, A., (1995). Stochastic Programming. Kluwer Academic Publishers Group, Dordrecht.

Ruszczynski, A., and Shapiro, A., (2003). Stochastic Programming Handbook in Op- erations Research and Management Science. Amsterdam: Elsevier Science.

Shapiro, A., Dentcheva, D., and Ruszczynski, A., (2009). Lectures on stochastic programming: Modeling and theory. In MPS-SIAM Series in Optimization. Philadelphia.

Stefansdottir, B., and Grunow, M., (2018). Selecting new product designs and processing technologies under

4. SERA Algorithm for the Two-Stage Problem

The two-stage programming with recourse can be written as:

$$\min c^T \boldsymbol{x} + Q(\boldsymbol{x}) \text{ subject to } A\boldsymbol{x} = b,\ x \geq 0 \qquad (12)$$

where the expected recourse function Q(x) can be giving as $Q(\boldsymbol{x}) = E(q(\boldsymbol{x}, \xi) = E(min_y q^T y | W_y = \xi - T\boldsymbol{x}, y \geq 0)$ where q is a random variable and we assume that the matrices T and W are deterministic. The main difficult computationally is computing the value of the expected recourse when the being multidimensional integral is hard to calculate the expected value. It is easily computed for any x and $\xi_i$by unbiased estimate of it:

$$q_i = q(\boldsymbol{x}, \xi_i) = min\ q^T y \quad \text{s.t} \quad T\boldsymbol{x} + \boldsymbol{W}y = \xi_i, \quad y \geq 0 \qquad (13)$$

We can easily compute the expected recourse $E(q(\boldsymbol{x}, \xi)) =$ by given an unbiased estimate of it. Let $\xi_i$to be independent sample with the random variable ξ, for each $\boldsymbol{x}_i$ then $q_i = q(\boldsymbol{x}_i, \xi_i)$ and $q_i \sim Q(\boldsymbol{x}_i)$ for $i = 1, 2, \dots, k$. In this case:

$$q_k = \alpha_k e^{\boldsymbol{b'}_k x} \qquad (14)$$

To find the solution for the unknown α_k and b_k, by solving the following minimization problem, we can compute the L^2 minimum norm, that is

$$\min_{\gamma, b} \sum_{i=1}^{n} [q_i - q_k(\boldsymbol{x}_i)]^2 \qquad (15)$$

Since this is a minimization problem then the first order necessary conditions of the above problem give the solution of the unknown α_k and b_k:

$$\sum_{i=1}^{k} [q_i - (\gamma_k + \boldsymbol{b}' x_i] = 0,$$

$$\sum_{i=1}^{k} x_{ij} [q_i - (\gamma_k + \boldsymbol{b}' x_i] = 0,\ j = 1, 2, \dots, k.$$

where $\boldsymbol{x}_{ij}$ is the $j - th$ component of the vector $\boldsymbol{x}_i$ and $\gamma = ln\alpha$ for more details see previous section.

For starting our algorithm we need to generate random k points of $\boldsymbol{x}_i$ and calculate q_i for these points. Thus giving the set $S_k = \{\boldsymbol{x}_i, q_i\}_{i=1}^{k}$

0. [start] let the iteration being with the number k of points in S_k.
1. Then, compute the following coefficient b_k and α_k of exponential regression function

$$q_k(\boldsymbol{x}) = \alpha_k e^{\boldsymbol{b'}_k x} \qquad (16)$$

respectively, and putting the derivatives equal to zero. Then we have

$$\sum_{i=1}^{n}[f_i - (\gamma + \beta x_i] = 0$$

$$\sum_{i=1}^{n} x_i[f_i - (\gamma + \beta x_i] = 0$$

By solving the above system in the unknowns constants γ and β following the same technique as given by [4], consider

$$m_0 = \frac{1}{k}\sum_{i=1}^{k} f_i, \qquad m_1 = \frac{1}{k}\sum_{i=1}^{k} f_i\, x_i,$$

$$M_0 = \frac{1}{k}\sum_{i=1}^{k} x_i^0 = 1, \qquad M_1 = \frac{1}{k}\sum_{i=1}^{k} x_i, \qquad M_2 = \frac{1}{k}\sum_{i=1}^{k} x_i^2,$$

Then, we can rewrite the system (3–3) as follows $\beta M_2 + \gamma M_1 = m_1, \quad \beta M_1 + \gamma M_0 = m_0,$ that is

$$\begin{pmatrix} M_2 & M_1 \\ M_1 & M_0 \end{pmatrix}\begin{pmatrix} \beta \\ \gamma \end{pmatrix} = \begin{pmatrix} m_1 \\ m_0 \end{pmatrix}.$$

Thus, we obtain $\beta = \frac{-m_0 M_1 + m_1}{M_2 - M_1^2}$, and $\gamma = \frac{-m_0 M_2 - m_1 M_1}{M_2 - M_1^2}$.

Furthermore, the solution of the minimization problem (7) is given by

$$\beta = \frac{k\sum_{i=1}^{k} x_i lny_i - \sum_{i=1}^{k}\sum_{i=1}^{k} x_i lny_i}{k\sum_{i=1}^{k} x_i^2 - \left(\sum_{i=1}^{k} x_i\right)^2}, \text{ and}$$

$$\gamma = exp\left[\frac{-\sum_{i=1}^{k} x_i \sum_{i=1}^{k} x_i\, lny_i + \sum_{i=1}^{k} lny_i \sum_{i=1}^{k} x_i^2}{k\sum_{i=1}^{k} x_i^2 - \left(\sum_{i=1}^{k} x_i\right)^2}\right]$$

3. Multidimensional SERA

Co**nsid**er we have $\boldsymbol{k}$ distinct points $\boldsymbol{x_i}, \mathbf{b} \in \mathbf{R^n}$ for $i = 1, 2, \dots, k$. We need an interpolate these points such that satisfies the exponential function

$$y_i = \alpha e^{\boldsymbol{b'x}}, \text{ for } i = 1, 2, \dots, k \qquad (9)$$

where α and b are unknown constants. Similarly as for the previous simple case, by taking the logarithm for both sides of Eq. (9). Assume that $f_i = lny_i$ and $\gamma = ln\alpha$, then by solving the following minimization problem we can compute the L^2 minimum norm, that is

$$\min_{\gamma,\beta} \sum_{i=1}^{n}[\boldsymbol{f}_i - (\gamma + \boldsymbol{b'x}]^2 \qquad (10)$$

for the unknown constant γ and b. By differentiating (10) with respect to γ and b, respectively. Then we obtain $\sum_{i=1}^{n}[\boldsymbol{f}_i - (\gamma + \boldsymbol{b'x}] = 0$,

$\sum_{i=1}^{n} x_{ij}[\boldsymbol{f}_i - (\gamma + \boldsymbol{b'x}] = 0$, for $j = 1, 2, \dots, n$, where x_{ij} is the $j - th$ component of the vector x_i. Following [5], we consider the following notations,

$$\boldsymbol{M}\Lambda = \boldsymbol{m}, \qquad (11)$$

where Λ is the vector of the unknown constants, $\Lambda' = (b_1, \dots, b_n)$, and and the vector m and the matrix and $\boldsymbol{M}$ are defined by

$$\boldsymbol{m} = \left(m_{1,1}, \dots, m_{1,n}, m_0\right)$$

$$m_0 = \frac{1}{k}\sum_{i=1}^{k} \boldsymbol{f}_i, \qquad m_{1,j} = \frac{1}{k}\sum_{i=1}^{k} x_{ij}\boldsymbol{f}_i,$$

$$M_{0,j} = \frac{1}{k}\sum_{i=1}^{k} x_{ij}^0 = 1, \qquad M_{1,j} = \frac{1}{k}\sum_{i=1}^{k} x_{ij}, \text{ and}$$

$$M_{2,jl} = \frac{1}{k}\sum_{i=1}^{k} x_{ij}x_{il},$$

Furthermore we can rewrite the above system as follows

$$\boldsymbol{M} = \begin{pmatrix} M_{2,11} & \cdots & M_{2,1n} & M_{1,1} \\ \vdots & \ddots & \vdots & \vdots \\ M_{2,n1} & \cdots & M_{2,nn} & M_{1,n} \\ M_{1,1} & \cdots & M_{1,n} & M_0 \end{pmatrix}$$

obtain the solution of the minimization problem (10).

following approximate one:

$$\min_{\boldsymbol{x}} = c'\boldsymbol{x} + q_k(\boldsymbol{x}) \qquad (5)$$
$$A\boldsymbol{x} \le b$$
$$x \ge 0$$

and denote its optimal solution by $\boldsymbol{x}_k$.

3. If $\boldsymbol{x}_k$ is "good enough" then STOP, otherwise compute $q_k \sim Q(\boldsymbol{x}_k)$, let $S_{k+1} = S_k \cup \{\boldsymbol{x}_k, q_k\}$ increase$k := k + 1$ and go back to Step 1" (Deak , 2004), the above algorithm was described and approved theoretically by (Deak, 2004).

The most recent development in the solution of two-stage model with probabilistic constraint is a heuristic approach (successive regression approximations (SRA) proposed by (Deak, 2003) for medium-size problems, which is extended for large scale problem with one hundred decision variables in the and first-stage with 120 dimensional normally distributed ξ in the second stage problem (Deak, 2011), where he claims that the computational test indicates that the method is working. However, no theoretical proof of the SRA method exists but the performance has been efficient for more details see (Deak, 2002; Deak, 2003; Deak, 2006). $Q(\boldsymbol{x}) = E(q(x,\xi) = E(min_y q^T y | W_y = \xi - Tx, y \ge 0)$ where q is a random variable and we assume that the matrices T and W are deterministic. The main difficult computationally is computing the value of the expected recourse when the being multidimensional integral is hard to calculate the expected value. It is easily computed for any x and ξ_i by unbiased estimate of it:

2. Computing a Least Squares-Regression for Exponential Approximation

Assume that we have k distinct points, for instance$(x_1, y_{1)}, \dots (x_k, y_{k)})$ and we need to interpolate a function $g_i = g(x_i)$ such that $g_i = y_i$ for all $i = 1, \dots, k$ Consider we need to an interpolation for these points that satisfy the exponential function, i.e.,

$$y_i = \alpha\, e^{\beta x_i}, \text{ for } \; i = 1, 2, \dots, k \qquad (6)$$

where α and β are unknown constants. In order to give the best approximation for the function g_i we shall solve the least square problem (L^2 minimum norm), that is,

$$\min_{\alpha,\beta} \sum_{i=1}^{n} [g_i - y_i]^2 \qquad (7)$$

Apply the natural logarithm for both sides of Eq. (6) then we obtain

$$lny_i = \ln\left(\alpha\, e^{\beta x_i}\right) = ln\alpha + \beta x_i$$

Let $f_i = lny_i$ and $\gamma = ln\alpha$, then the least square problem (7) can be transformed into

$$\min_{\alpha,\beta} \sum_{i=1}^{n} [f_i - (\gamma + \beta x_i]^2 \qquad (8)$$

Hence, we will solve the minimization problem (8) that is associated to the pints (x_i, f_i) for $i = 1, \dots, k$, then, we will obtain the solution of the minimization problem (7) by using $\alpha = \exp(\gamma)$. By differentiating (8) with respect to γ and β,

problem has a finite optimal solution, which means $\forall x$ x, ξ the $q(x,\xi)$ is less than ∞. The difficult part is to compute the expected recourse function because of the multidimensional integral but it is easy to give an unbiased estimate of it. Let $\xi_1, \xi_2, \dots, \xi_k$ to be independent samples from distribution of the random ξ that is for each point $\boldsymbol{x_i}$ then

$q_i = \frac{1}{k}\sum_{i=1}^{k} q(\boldsymbol{x}_i, \xi_i)$ is an unbiased estimate of the expected recourse function $Q(\boldsymbol{x})$ and ξ are independent samples. The SRA algorithm computes this estimated function value and constructs a quadratic approximation based on q_i.

To start the SRA algorithm, we need to make random initial points x_i and compute for each point of x_i an unbiased estimate q_i of $Q(\boldsymbol{x}_i)$which is linear programming problems that is $q_i \sim Q(x_i)$. Then, we have the set $S_k = \{x_i, q_i\}_{i=1}^{k}$ and the quadratic regression function of this form:

$$q_k(\boldsymbol{x}) = \boldsymbol{x}' D_k \boldsymbol{x} + b'_k + c_k$$

is replaced instead the expected recourse function $Q(\boldsymbol{x})$ which is hard to evaluate numerically, Where $\boldsymbol{D}_k$ is a assumed to be symmetric matrices and $\boldsymbol{D}_k$, $\boldsymbol{b}_k$, c_k are unknown parameters can be computed from the optimization problem:

$$\min_{\boldsymbol{D}_k, \boldsymbol{b}_k, c_k} = \sum_{i=1}^{k}[q_i - (x'_i \boldsymbol{D}_k \boldsymbol{x}_i + \boldsymbol{b}'_k \boldsymbol{x}_i + c_k)]^2 \qquad (2)$$

by the first order necessary conditions of (2), the solutions for the unknown parameters are giving by:

$$\sum_{i=1}^{k}[q_i - (\boldsymbol{x}'_i \boldsymbol{D}_k \boldsymbol{x}_i + \boldsymbol{b}'_k x_i + c_k)] = 0$$

$$\sum_{i=1}^{k}[q_i - (\boldsymbol{x}'_i \boldsymbol{D}_k \boldsymbol{x}_i + \boldsymbol{b}'_k x_i + c_k)]\boldsymbol{x}_{im} = 0,\ m = 1, \dots, n.$$

$$\sum_{i=1}^{k}[q_i - (\boldsymbol{x}'_i \boldsymbol{D}_k \boldsymbol{x}_i + \boldsymbol{b}'_k x_i + c_k)]\boldsymbol{x}_{im}\boldsymbol{x}_{il} = 0, l = 1, \dots, n,$$

where x_{im} is the mth component of the vector x_i. Furthermore, we can rewrite the system (2-2)

$$\boldsymbol{M}\Lambda = \boldsymbol{m}, \quad \Lambda = \boldsymbol{M}^{-1}\boldsymbol{m}, \qquad (3)$$

Where $\Lambda' =$

$(d_{11}, d_{12}, \dots, d_{1n}, d_{22}, \dots, d_{2n}, d_{33}, \dots, d_{nn},$

$d_1, \dots, d_n,\ c)$ and the

$\mathbf{m}' =$

$(m_{2,11}, m_{2,12}, \dots, m_{2,1n}, m_{2,12}, m_{2,22}, \dots, m_{2,nn}, m_{1,1}, m_{1,2}, \dots, m_{1,n},$

$m_0)$ and the component of $\mathbf{m}$ are:

$m_0 = \frac{1}{k}\sum_{i=1}^{k} q_i$, $m_{1,m} = \frac{1}{k}\sum_{i=1}^{k} q_i\, x_{im}$, $m_{2,ml} = \frac{1}{k}\sum_{i=1}^{k} q_i\, x_{im}x_{il}$,

And the elements of the matrix M are defined as:

$M_{0,m} = \frac{1}{k}\sum_{i=1}^{k} x_{im}^0 = 1$, $M_{1,m} = \frac{1}{k}\sum_{i=1}^{k} x_{im}$,

$M_{2,ml} = \frac{1}{k}\sum_{i=1}^{k} x_{im}x_{il}$,

$M_{3,mlr} = \frac{1}{k}\sum_{i=1}^{k} x_{im}x_{il}x_{ir}$ and $M_{4,mlrs} = \frac{1}{k}\sum_{i=1}^{k} x_{im}x_{il}x_{ir}x_{is}$

"These notations used to describe the matrix **M** and by solving the system (3), so the solution of problem (2) will obtain.

The SRA algorithm for two-stage problem which introduced by (Deak, 2004) is giving as following:

$$q_k(x) = \boldsymbol{x}'\boldsymbol{D}_k x + \boldsymbol{b}'_k + c_k \qquad (4)$$

from S_k by solving the minimization problem (2).

0. [Initialization.] Set the iteration counter to the number k of points and compute $q_i \sim Q(\boldsymbol{x}_i)$ and $S_k = \{\boldsymbol{x}_i, q_i\}_{i=1}^{k}$.
1. Compute the coefficients of $\boldsymbol{D}_k$, $\boldsymbol{b}_k$ and c_k of the quadratic regression function
2. Replace the original first stage problem with the

1. Introduction

Stochastic programming, or called optimization under uncertainty, is an optimization problem formulated mathematically with stochastic systems, where random variable parameters appear in objective functions or in the constraints. Uncertainty is dealt with random parameters in objective or constraints, or in both. (Prekopa,1995) shows a numerical example of a large-scale size of uncertainty problem.

Dynamic Stochastic programming models or static models are decision making problems where the equations are stochastics, (Prekopa, 1995) use a model where some or all of the parameters are random by considering of joint distribution function, for further details see (Prekopa, 1995; Deak, 2001; Deak, 2004; Deak, 2006; Deak, 2011; Shapiro, Dentcheva and Ruszczynski, 2009). Two stage stochastic problem see (Nasser Alreshidi et al., 2020; Rashid Nawaz et al., 2020) they show decomposition method which give quickly convergent and and encouraging results. Convergence of Krasnoselskii–Mann for more details see (Shah, 2022; Nawaz, 2020).

There are many real applications of two-stage models that done in many fields of DM such as Accident prediction models (Chao Wanget et al., 2011). Transportation problem (Hrabec et al., 2015). Outages of power plants (Cot´e and Laughton, 1982). Food supply chain (Bryndis Stefansdottir and Mar- tin Grunow 2018). Portfolio optimization (Nasser Alreshidi et al., 2020). Energy models (Jo˜ao Soares et al., 2017). Airline network (Yang T.H., 2010). Staffing and Scheduling (Kibaek Kim and Sanjay Mehrotra., 2015). Biomass supply chain networks (Maria Aranguren et al., 2021). Water resources problems (Wang and Huang., 2015). Milk production problems (Yalcin and Stott., 2000). Risk (Zimmerman and Carter., 2003). Two-stage stochastic programming with recourse is the most important and most used model in stochastic programming (Prekopa, 1995; Bryndis Stefansdottir and Martin Grunow, 2018). Recently Deak developed a heuristic algorithm, this procedure called successive regression approximations or SRA that is for solving the two-stage and probabilistic stochastic programming problems. The expected recourse function of the second stage problem (A. Ruszczynski and A. Shapiro, 2003), frequently cannot be evaluated accurately but some Monte Carlo techniques can compute them. The algorithm is based on replacing the expected recourse function, which is numerically hard to be solve by the regression function then solving this problem by this heuristic technique, see (Deak, 2001; Deak, 2004; Deak, 2006; Deak, 2011). Deak describes the SRA algorithm for tow stage stochastic programming problem as following. Two-stage stochastic programming with expected recourse:

$$\min c^T \boldsymbol{x} + Q(\boldsymbol{x}) \text{ subject to } A\boldsymbol{x} = b,\ x \geq 0 \qquad (1)$$

Where $Q(\boldsymbol{x}) = E(q(\boldsymbol{x}, \xi) = E(min_y q^T y | W_y = \xi - T\boldsymbol{x}, y \geq 0)$ and the vector $\boldsymbol{x} \in R^{n_1}$ and $y \in R^{n_2}$ are denoted for first-stage decisions and the second-stage decision variable, respectively. All the matrices here are deterministic A, T, W and the dimensions are $m_1 \times n_1$, $m_2 \times n_1$, $m_1 \times n_2$ respectively, for the other vectors are deterministic $b \in R^{m_1}$ and $q \in R^{n_2}$ except $\xi \in R^{m_1}$ the righthand side vector is random. In the SRA algorithm, he assumed [5], that ξ is uncertain with normal distribution and the problem has complete recourse to guarantee that the second stage problem is feasible which, means that for any x and any ξ there exists y feasible solution and the second stage linear programming

المملكة العربية السعودية
جامعة الحدود الشمالية (NBU)
مجلة الشمال للعلوم الأساسية والتطبيقية (JNBAS)
طباعة ردمد: 1658-7022/ إلكتروني – ردمد: 1658-7014
www.nbu.edu.sa
http://jnbas.nbu.edu.sa

حل مشاكل البرمجة العشوائية ذات المرحلتين باستخدام تقديرات الانحدار الأسي المتتالي

ناصر بن عائض الرشيدي

(قدم للنشر في 1443/8/8هـ؛ وقبل للنشر في 1444/7/4هـ)

مستخلص البحث: توجد مجموعة متنوعة من التقنيات لحل مسائل البرمجة العشوائية ذات المرحلتين.مؤخرًا يتم حل مشكلة البرمجة العشوائية ذات المرحلتين من خلال تقريب الانحدار التربيعي المتتالي. هنا قمنا بحل المسائل العشوائية ذات المرحلتين باستخدام الانحدار الأسي بدلاً من الانحدار التربيعي، ثم قمنا ببناء خوارزمية تقريب الانحدار الأسي المتتالي (SERA). تم تحسين إجراء تقريب الانحدار الأسي المتتالي (SERA) لحل المشكلات العشوائية ذات المرحلتين باستخدام نفس تقنية تقريب الانحدار التربيعي المتتالي حيث نستبدل دالة الانحدار الأسي بدلاً من دالة الانحدار التربيعية التي يتم فيها استبدال دالة الرجوع المتوقعة لـ مشكلة المرحلة الثانية والتي يصعب تقييمها عدديا، ثم نقوم بحساب الانحدار الأسي. لذلك يتم استخدام الخوارزمية لحل مشاكل واسعة النطاق متعددة المراحل. كما تقوم الخوارزمية الجديدة بحل مسألة ذات مرحلتين باستخدام تقريب الانحدار الأسي المتقارب.

كلمات مفتاحية: مشكلة العشوائية ذات المرحلتين، تقريب الانحدارالأسي ، تقريب الانحدار التربيعي.

للمراسلة:
قسم الرياضيات، كلية العلوم، جامعة الحدود الشمالية، عرعر 73222، المملكة العربية السعودية. .

e-mail: Nasser.alreshidi@nbu.edu.sa

DOI: 10.12816/0061643

Journal of the North for Basic and Applied Sciences, Vol. (8), Issue (2), (November 2023/ Rabi' II 1445 H) 125-133

KINGDOM OF SAUDI ARABIA
Northern Border University (NBU)
Journal of the North for Basic & Applied Sciences(JNBAS)
p - ISSN : 1658 -7022 / **e-ISSN: 1658 - 7014**
www.nbu.edu.sa
s.journal@nbu.edu.sa

Solving Two-Stage Stochastic Programming Problems by Successive Exponential Regression Approximations

Nasser Aedh Alreshidi*

(Received 11/3/2022 ; accepted 26/1/2023)

Abstract : There is a variety of technics for solving Two-Stage Stochastic Programming Problems. Recently the two-stage stochastic problem has been solved by the successive quadratic regression approximations. Here, we solve the two-stage stochastic problems by using the exponential regression instead of the quadratic one, then we build the algorithm of successive exponential regression approximations (SERA). Successive exponential regression approximations (SERA) procedure has been improved to solve two-stage stochastic problems by using the same technic of successive quadratic regression approximations where we replace the exponential regression function instead the quadratic regression function in which is replaced instead the expected recourse function of second stage problem which is hard to evaluate numerically, then we compute exponential regression. So the algorithm is used to solve large-scale of multi-stage problems. Also, the new algorithm is solving two-stage problem by using exponential regression approximations which is convergent.

Key Words: Two-stage stochastic problem, exponential regression approximations, quadratic regression approximations.

DOI: 10.12816/0061643

* **Corresponding Author:**
Department of Mathematics College of Science, Northern Border University, Arar, 73222, Saudi Arabia.

e-mail: Nasser.alreshidi@nbu.edu.sa

Zimmerman, R. D., Murillo-Sanchez, C. E., & Thomas, R. J. (n.d.). Feb 2011. MATPOWER: Steady-State Operations, Planning, and Analysis Tools for Power Systems Research and Education, 26(1), 12–19.

Generation, Transmission & Distribution, *5*(10), 989. https://doi.org/10.1049/iet-gtd.2011.0055

Niknam, T., Narimani, M. rasoul, Jabbari, M., & Malekpour, A. R. (2011). A modified shuffle frog leaping algorithm for multi-objective optimal power flow. *Energy*, *36*(11), 6420–6432. https://doi.org/10.1016/j.energy.2011.09.027

Ongsakul, W., & Tantimaporn, T. (2006). Optimal Power Flow by Improved Evolutionary Programming. *Electric Power Components and Systems*, *34*(1), 79–95. https://doi.org/10.1080/15325000691001458

Ouafa, H., Linda, S., & Tarek, B. (2017). Multi-objective optimal power flow considering the fuel cost, emission, voltage deviation and power losses using Multi-Objective Dragonfly algorithm. *Proceedings of the International Conference on Recent Advances in Electrical Systems, Tunusia*.

Panda, A., Tripathy, M., Barisal, A. K., & Prakash, T. (2017). A modified bacteria foraging based optimal power flow framework for Hydro-Thermal-Wind generation system in the presence of STATCOM. *Energy*, *124*, 720–740. https://doi.org/10.1016/j.energy.2017.02.090

Pulluri, H., Naresh, R., & Sharma, V. (2018). A solution network based on stud krill herd algorithm for optimal power flow problems. *Soft Computing*, *22*(1), 159–176. https://doi.org/10.1007/s00500-016-2319-3

Radosavljević, J., Klimenta, D., Jevtić, M., & Arsić, N. (2015). Optimal Power Flow Using a Hybrid Optimization Algorithm of Particle Swarm Optimization and Gravitational Search Algorithm. *Electric Power Components and Systems*, *43*(17), 1958–1970. https://doi.org/10.1080/15325008.2015.1061620

Rajabioun, R. (2011). Cuckoo optimization algorithm. *Applied Soft Computing*, *11*(8), 5508–5518.

Ramesh Kumar, A., & Premalatha, L. (2015). Optimal power flow for a deregulated power system using adaptive real coded biogeography-based optimization. *International Journal of Electrical Power & Energy Systems*, *73*, 393–399. https://doi.org/10.1016/j.ijepes.2015.05.011

Riaz, M., Hanif, A., Hussain, S. J., Memon, M. I., Ali, M. U., & Zafar, A. (2021). An optimization-based strategy for solving optimal power flow problems in a power system integrated with stochastic solar and wind power energy. *Applied Sciences*, *11*(15), 6883.

Roy, R., & Jadhav, H. T. (2015). Optimal power flow solution of power system incorporating stochastic wind power using Gbest guided artificial bee colony algorithm. *International Journal of Electrical Power & Energy Systems*, *64*, 562–578. https://doi.org/10.1016/j.ijepes.2014.07.010

Saha, A., Bhattacharya, A., Das, P., & Chakraborty, A. K. (2019). A novel approach towards uncertainty modeling in multiobjective optimal power flow with renewable integration. *International Transactions on Electrical Energy Systems*, *29*(12), e12136. https://doi.org/10.1002/2050-7038.12136

Sarda, J., Pandya, K., & Lee, K. Y. (2021). Hybrid cross entropy—Cuckoo search algorithm for solving optimal power flow with renewable generators and controllable loads. *Optimal Control Applications and Methods*.

Sarhan, S., El-Sehiemy, R., Abaza, A., & Gafar, M. (2022). Turbulent Flow of Water-Based Optimization for Solving Multi-Objective Technical and Economic Aspects of Optimal Power Flow Problems. *Mathematics*, *10*(12), 2106.

Sayah, S., & Zehar, K. (2008). Modified differential evolution algorithm for optimal power flow with non-smooth cost functions. *Energy Conversion and Management*, *49*(11), 3036–3042. https://doi.org/10.1016/j.enconman.2008.06.014

Shaheen, A. M., El-Sehiemy, R. A., Elattar, E. E., & Abd-Elrazek, A. S. (2021). A modified crow search optimizer for solving non-linear OPF problem with emissions. *IEEE Access*, *9*, 43107–43120.

Shi, L., Wang, C., Yao, L., Ni, Y., & Bazargan, M. (2011). Optimal power flow solution incorporating wind power. *IEEE Systems Journal*, *6*(2), 233–241.

Shilaja, C., & Ravi, K. (2017). Optimal power flow using hybrid DA-APSO algorithm in renewable energy resources. *Energy Procedia*, *117*, 1085–1092.

SOOD, Y. (2007). Evolutionary programming based optimal power flow and its validation for deregulated power system analysis. *International Journal of Electrical Power & Energy Systems*, *29*(1), 65–75. https://doi.org/10.1016/j.ijepes.2006.03.024

Ullah, Z., Wang, S., Radosavljević, J., & Lai, J. (2019). A solution to the optimal power flow problem considering WT and PV generation. *IEEE Access*, *7*, 46763–46772.

Venkateswara Rao, B., & Nagesh Kumar, G. V. (2015). Optimal power flow by BAT search algorithm for generation reallocation with unified power flow controller. *International Journal of Electrical Power & Energy Systems*, *68*, 81–88. https://doi.org/10.1016/j.ijepes.2014.12.057

Warid, W., Hizam, H., Mariun, N., & Abdul Wahab, N. I. (2018). A novel quasi-oppositional modified Jaya algorithm for multi-objective optimal power flow solution. *Applied Soft Computing*, *65*, 360–373. https://doi.org/10.1016/j.asoc.2018.01.039

Warid, W., Hizam, H., Mariun, N., & Abdul-Wahab, N. (2016). Optimal Power Flow Using the Jaya Algorithm. *Energies*, *9*(9), 678. https://doi.org/10.3390/en9090678

Xiao, L., Shao, W., Yu, M., Ma, J., & Jin, C. (2017). Research and application of a hybrid wavelet neural network model with the improved cuckoo search algorithm for electrical power system forecasting. *Applied Energy*, *198*, 203–222.

Yuan, X., Zhang, B., Wang, P., Liang, J., Yuan, Y., Huang, Y., & Lei, X. (2017). Multi-objective optimal power flow based on improved strength Pareto evolutionary algorithm. *Energy*, *122*, 70–82. https://doi.org/10.1016/j.energy.2017.01.071

Zeynal, H., Hui, L. X., Jiazhen, Y., Eidiani, M., & Azzopardi, B. (2014). Improving lagrangian relaxation unit commitment with cuckoo search algorithm. *2014 IEEE International Conference on Power and Energy (PECon)*, 77–82.

Zhang, J., Wang, S., Tang, Q., Zhou, Y., & Zeng, T. (2019). An improved NSGA-III integrating adaptive elimination strategy to solution of many-objective optimal power flow problems. *Energy*, *172*, 945–957.

Minimizations and Performance Enhancements of Power Systems Using Spherical Prune Differential Evolution Algorithm Including Modal Analysis. *Sustainability*, *13*(14), 8113.

Gupta, S., Kumar, N., Srivastava, L., Malik, H., Pliego Marugán, A., & Garc\'\ia Márquez, F. P. (2021). A Hybrid Jaya—Powell's Pattern Search Algorithm for Multi-Objective Optimal Power Flow Incorporating Distributed Generation. *Energies*, *14*(10), 2831.

Guvenc, U., Bakir, H., Duman, S., & Ozkaya, B. (2020). Optimal Power Flow Using Manta Ray Foraging Optimization. *The International Conference on Artificial Intelligence and Applied Mathematics in Engineering*, 136–149.

Hassan, M. H., Elsayed, S. K., Kamel, S., Rahmann, C., & Taha, I. B. M. (n.d.). Developing chaotic Bonobo optimizer for optimal power flow analysis considering stochastic renewable energy resources. *International Journal of Energy Research*.

Hassan, M. H., Kamel, S., Selim, A., Khurshaid, T., & Domínguez-García, J. L. (2021). A modified Rao-2 algorithm for optimal power flow incorporating renewable energy sources. *Mathematics*, *9*(13), 1532.

Hazra, J., & Sinha, A. K. (2011). A multi-objective optimal power flow using particle swarm optimization. *European Transactions on Electrical Power*, *21*(1), 1028–1045. https://doi.org/10.1002/etep.494

Herbadji, O., Slimani, L., & Bouktir, T. (2019). Optimal power flow with four conflicting objective functions using multiobjective ant lion algorithm: A case study of the algerian electrical network. *Iranian Journal of Electrical and Electronic Engineering*, *15*(1), 94–113. https://doi.org/10.22068/IJEEE.15.1.94

Islam, M. Z., Wahab, N. I. A., Veerasamy, V., Hizam, H., Mailah, N. F., Guerrero, J. M., & Mohd Nasir, M. N. (2020). A Harris Hawks optimization based single- and multi-objective optimal power flow considering environmental emission. *Sustainability*, *12*(13), 5248.

Jebaraj, L., & Sakthivel, S. (2022). A new swarm intelligence optimization approach to solve power flow optimization problem incorporating conflicting and fuel cost based objective functions. *E-Prime-Advances in Electrical Engineering, Electronics and Energy*, *2*, 100031.

Kahraman, H. T., Akbel, M., & Duman, S. (2022). Optimization of optimal power flow problem using multi-objective manta ray foraging optimizer. *Applied Soft Computing*, *116*, 108334.

Kamel, S., Ebeed, M., & Jurado, F. (2021). An improved version of salp swarm algorithm for solving optimal power flow problem. *Soft Computing*, *25*(5), 4027–4052.

Khamees, A. K., Abdelaziz, A. Y., Eskaros, M. R., El-Shahat, A., & Attia, M. A. (2021). Optimal Power Flow Solution of Wind-Integrated Power System Using Novel Metaheuristic Method. *Energies*, *14*(19), 6117.

Khan, I. U., Javaid, N., Gamage, K. A. A., Taylor, C. J., Baig, S., & Ma, X. (2020). Heuristic algorithm based optimal power flow model incorporating stochastic renewable energy sources. *IEEE Access*, *8*, 148622–148643.

Khorsandi, A., Hosseinian, S. H., & Ghazanfari, A. (2013). Modified artificial bee colony algorithm based on fuzzy multi-objective technique for optimal power flow problem. *Electric Power Systems Research*, *95*, 206–213. https://doi.org/10.1016/j.epsr.2012.09.002

Kumari, B. A., & Vaisakh, K. (2022). Integration of solar and flexible resources into expected security cost with dynamic optimal power flow problem using a Novel DE algorithm. *Renewable Energy Focus*.

Kyomugisha, R., Muriithi, C. M., & Nyakoe, G. N. (2022). Performance of Various Voltage Stability Indices in a Stochastic Multiobjective Optimal Power Flow Using Mayfly Algorithm. *Journal of Electrical and Computer Engineering*, *2022*.

Li, S., Gong, W., Wang, L., Yan, X., & Hu, C. (2020). Optimal power flow by means of improved adaptive differential evolution. *Energy*, *198*, 117314. https://doi.org/10.1016/j.energy.2020.117314

Ma, R., Li, X., Luo, Y., Wu, X., & Jiang, F. (2019). Multi-objective dynamic optimal power flow of wind integrated power systems considering demand response. *CSEE Journal of Power and Energy Systems*, *5*(4), 466–473.

Maheshwari, A., Sood, Y. R., Jaiswal, S., Sharma, S., & Kaur, J. (2021). Ant Lion Optimization Based OPF Solution Incorporating Wind Turbines and Carbon Emissions. *2021 Innovations in Power and Advanced Computing Technologies (i-PACT)*, 1–6.

Meng, A., Zeng, C., Wang, P., Chen, D., Zhou, T., Zheng, X., & Yin, H. (2021). A high-performance crisscross search based grey wolf optimizer for solving optimal power flow problem. *Energy*, *225*, 120211.

Mohamed, A.-A. A., Mohamed, Y. S., El-Gaafary, A. A. M., & Hemeida, A. M. (2017). Optimal power flow using moth swarm algorithm. *Electric Power Systems Research*, *142*, 190–206. https://doi.org/10.1016/j.epsr.2016.09.025

Mohapatra, P., Chakravarty, S., & Dash, P. K. (2015). An improved cuckoo search based extreme learning machine for medical data classification. *Swarm and Evolutionary Computation*, *24*, 25–49.

Nadimi-Shahraki, M. H., Taghian, S., Mirjalili, S., Abualigah, L., Abd Elaziz, M., & Oliva, D. (2021). EWOA-OPF: Effective Whale Optimization Algorithm to Solve Optimal Power Flow Problem. *Electronics*, *10*(23), 2975.

Narimani, M. R., Azizipanah-Abarghooee, R., Zoghdar-Moghadam-Shahrekohne, B., & Gholami, K. (2013). A novel approach to multi-objective optimal power flow by a new hybrid optimization algorithm considering generator constraints and multi-fuel type. *Energy*, *49*, 119–136. https://doi.org/10.1016/j.energy.2012.09.031

Nguyen, T. T. (2019). A high performance social spider optimization algorithm for optimal power flow solution with single objective optimization. *Energy*, *171*, 218–240. https://doi.org/10.1016/j.energy.2019.01.021

Niknam, T., Narimani, M. R., Aghaei, J., Tabatabaei, S., & Nayeripour, M. (2011). Modified Honey Bee Mating Optimisation to solve dynamic optimal power flow considering generator constraints. *IET*

orthogonal learning for optimal power flow problem. *Control Engineering Practice*, *61*, 163–172.

Bentouati, B., Khelifi, A., Shaheen, A. M., & El-Sehiemy, R. A. (2020). An enhanced moth-swarm algorithm for efficient energy management based multi dimensions OPF problem. *Journal of Ambient Intelligence and Humanized Computing*, 1–21. https://doi.org/10.1007/s12652-020-02692-7

Biswas, P. P., Suganthan, P. N., Mallipeddi, R., & Amaratunga, G. A. J. (2018). Optimal power flow solutions using differential evolution algorithm integrated with effective constraint handling techniques. *Engineering Applications of Artificial Intelligence*, *68*, 81–100. https://doi.org/10.1016/j.engappai.2017.10.019

Bouchekara, H. R. E. H., Chaib, A. E., Abido, M. A., & El-Sehiemy, R. A. (2016). Optimal power flow using an Improved Colliding Bodies Optimization algorithm. *Applied Soft Computing*, *42*, 119–131. https://doi.org/10.1016/j.asoc.2016.01.041

Chen, G., Qian, J., Zhang, Z., & Sun, Z. (2019). Multi-objective optimal power flow based on hybrid firefly-bat algorithm and constraints-prior object-fuzzy sorting strategy. *IEEE Access*, *7*, 139726–139745.

Dalali, M., & Kazemi Karegar, H. (2016). Optimal PMU placement for full observability of the power network with maximum redundancy using modified binary cuckoo optimisation algorithm. *IET Generation, Transmission \& Distribution*, *10*(11), 2817–2824.

Daryani, N., Hagh, M. T., & Teimourzadeh, S. (2016). Adaptive group search optimization algorithm for multi-objective optimal power flow problem. *Applied Soft Computing*, *38*, 1012–1024. https://doi.org/10.1016/j.asoc.2015.10.057

Dasgupta, K., Roy, P. K., & Mukherjee, V. (2020). Power flow based hydro-thermal-wind scheduling of hybrid power system using sine cosine algorithm. *Electric Power Systems Research*, *178*, 106018.

Dehghanpour, E., Karegar, H. K., Kheirollahi, R., & Soleymani, T. (2016). Optimal coordination of directional overcurrent relays in microgrids by using cuckoo-linear optimization algorithm and fault current limiter. *IEEE Transactions on Smart Grid*, *9*(2), 1365–1375.

Duman, S., Akbel, M., & Kahraman, H. T. (2021). Development of the multi-objective adaptive guided differential evolution and optimization of the MO-ACOPF for wind/PV/tidal energy sources. *Applied Soft Computing*, *112*, 107814.

Duman, S., Li, J., Wu, L., & Guvenc, U. (2020). Optimal power flow with stochastic wind power and FACTS devices: A modified hybrid PSOGSA with chaotic maps approach. *Neural Computing and Applications*, *32*(12), 8463–8492. https://doi.org/10.1007/s00521-019-04338-y

Duman, S., Rivera, S., Li, J., & Wu, L. (2020). Optimal power flow of power systems with controllable wind-photovoltaic energy systems via differential evolutionary particle swarm optimization. *International Transactions on Electrical Energy Systems*, *30*(4), e12270. https://doi.org/10.1002/2050-7038.12270

El Sehiemy, R. A., Selim, F., Bentouati, B., & Abido, M. A. (2020). A novel multi-objective hybrid particle swarm and salp optimization algorithm for technical-economical-environmental operation in power systems. *Energy*, *193*, 116817.

Elattar, E. E. (2019). Optimal power flow of a power system incorporating stochastic wind power based on modified moth swarm algorithm. *IEEE Access*, *7*, 89581–89593.

Elattar, E. E., & ElSayed, S. K. (2019). Modified JAYA algorithm for optimal power flow incorporating renewable energy sources considering the cost, emission, power loss and voltage profile improvement. *Energy*, *178*, 598–609. https://doi.org/10.1016/j.energy.2019.04.159

El-Fergany, A. A., & Hasanien, H. M. (2015). Single and Multi-objective Optimal Power Flow Using Grey Wolf Optimizer and Differential Evolution Algorithms. *Electric Power Components and Systems*, *43*(13), 1548–1559. https://doi.org/10.1080/15325008.2015.1041625

El-Sehiemy, R. A. (2022). A novel single/multi-objective frameworks for techno-economic operation in power systems using tunicate swarm optimization technique. *Journal of Ambient Intelligence and Humanized Computing*, 1–19.

Ghasemi, M., Ghavidel, S., Akbari, E., & Vahed, A. A. (2014). Solving non-linear, non-smooth and non-convex optimal power flow problems using chaotic invasive weed optimization algorithms based on chaos. *Energy*, *73*, 340–353. https://doi.org/10.1016/j.energy.2014.06.026

Ghasemi, M., Ghavidel, S., Ghanbarian, M. M., Gharibzadeh, M., & Azizi Vahed, A. (2014). Multi-objective optimal power flow considering the cost, emission, voltage deviation and power losses using multi-objective modified imperialist competitive algorithm. *Energy*, *78*, 276–289. https://doi.org/10.1016/j.energy.2014.10.007

Ghasemi, M., Ghavidel, S., Ghanbarian, M. M., & Gitizadeh, M. (2015). Multi-objective optimal electric power planning in the power system using Gaussian bare-bones imperialist competitive algorithm. *Information Sciences*, *294*. https://doi.org/10.1016/j.ins.2014.09.051

Ghasemi, M., Ghavidel, S., Gitizadeh, M., & Akbari, E. (2015). An improved teaching–learning-based optimization algorithm using Lévy mutation strategy for non-smooth optimal power flow. *International Journal of Electrical Power & Energy Systems*, *65*, 375–384. https://doi.org/10.1016/j.ijepes.2014.10.027

Ghasemi, M., Ghavidel, S., Rahmani, S., Roosta, A., & Falah, H. (2014). A novel hybrid algorithm of imperialist competitive algorithm and teaching learning algorithm for optimal power flow problem with non-smooth cost functions. *Engineering Applications of Artificial Intelligence*, *29*, 54–69. https://doi.org/10.1016/j.engappai.2013.11.003

Ghasemi, M., Rahimnejad, A., Hemmati, R., Akbari, E., & Gadsden, S. A. (2021). Wild Geese Algorithm: A novel algorithm for large scale optimization based on the natural life and death of wild geese. *Array*, *11*, 100074.

Ghoneim, S. S. M., Kotb, M. F., Hasanien, H. M., Alharthi, M. M., & El-Fergany, A. A. (2021). Cost

MSA (Duman, Rivera, et al., 2020)	107695.0619	111205.0554	116303.6361	1857.2167	-
DEEPSO (Duman, Rivera, et al., 2020)	103407.6296	103889.1446	104507.4884	292.8782	-

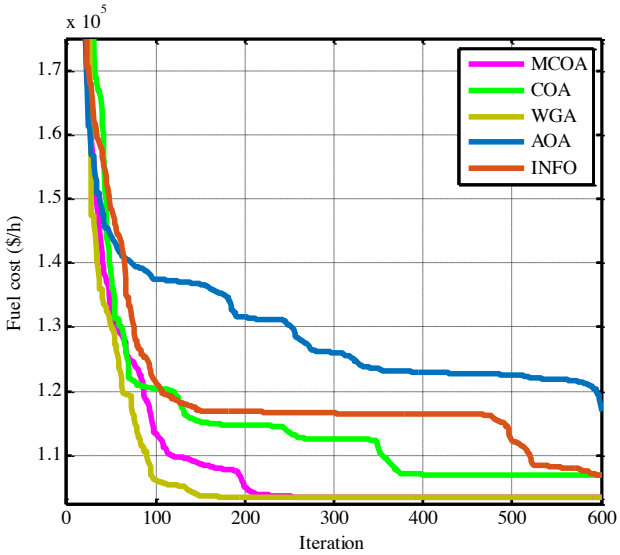

Figure 11: Convergence for case 2.

6 . Conclusion

The OPF problem, among various goals, is quickly becoming one of the most in-demand optimization problems in today's modern power networks. This article investigates multiple multiobjective OPF challenges, including renewable energy. A wide range of possible scenarios are considered considering power systems' complexities and constraints. These concerns include power loss, fuel expense, environmental effects, and voltage deviation values. In addition, a modified version of the Cuckoo optimization algorithm (COA) (MCOA) is built. A variety of algorithms have been developed for optimal multiobjective OPF under a variety of circumstances. Studies have demonstrated the efficiency and reliability of the MCOA algorithm in solving OPF problems in the presence of renewable DG resources.

References

Abaci, K., & Yamacli, V. (2016). Differential search algorithm for solving multi-objective optimal power flow problem. *International Journal of Electrical Power & Energy Systems*, *79*, 1–10. https://doi.org/10.1016/j.ijepes.2015.12.021

Abido, M. A. (2002). Optimal Power Flow Using Tabu Search Algorithm. *Electric Power Components and Systems*, *30*(5), 469–483. https://doi.org/10.1080/15325000252888425

Abualigah, L., Diabat, A., Mirjalili, S., Abd Elaziz, M., & Gandomi, A. H. (2021). The arithmetic optimization algorithm. *Computer Methods in Applied Mechanics and Engineering*, *376*, 113609.

Ahmad, M., Javaid, N., Niaz, I. A., Almogren, A., & Radwan, A. (2021). A Bio-Inspired Heuristic Algorithm for Solving Optimal Power Flow Problem in Hybrid Power System. *IEEE Access*, *9*, 159809–159826.

Ahmadianfar, I., Heidari, A. A., Noshadian, S., Chen, H., & Gandomi, A. H. (2022). INFO: An efficient optimization algorithm based on weighted mean of vectors. *Expert Systems with Applications*, *195*, 116516. https://doi.org/10.1016/j.eswa.2022.116516

Alsac, O., & Stott, B. (1974). Optimal load flow with steady-state security. *IEEE Transactions on Power Apparatus and Systems*, *3*, 745–751.

Attia, A.-F., El Sehiemy, R. A., & Hasanien, H. M. (2018). Optimal power flow solution in power systems using a novel Sine-Cosine algorithm. *International Journal of Electrical Power & Energy Systems*, *99*, 331–343. https://doi.org/10.1016/j.ijepes.2018.01.024

Bai, W., Eke, I., & Lee, K. Y. (2017). An improved artificial bee colony optimization algorithm based on

PG46~ PG54	42.000	145.000	30.000	30.009	120.000	401.000	30.001	30.050	30.001
Voltage magnitude of generators									
VG1~ VG9	0.9498	0.980	0.970	0.983	0.998	0.971	0.959	0.959	0.961
VG10~ VG18	0.974	0.974	0.983	0.974	0.958	0.972	0.961	0.953	0.946
VG19~ VG27	0.949	0.981	0.981	0.951	0.951	0.951	0.963	0.963	0.963
VG28~ VG36	0.970	1.025	1.025	0.975	0.987	0.987	0.955	0.955	0.979
VG3~ VG45	1.01	0.949	0.958	0.968	0.953	0.971	0.972	0.995	0.982
VG46~ VG54	0.980	0.948	0.960	0.9560	0.961	0.947	0.961	0.961	0.970
Transformers' tap									
T1~ T9	0.962	1.033	1.000	1.000	0.995	0.995	0.987	0.9890	0.941
VAR compensating units									
QC1~QC9	12.714	11.2903	0.250	4.171	18.000	0.010	11.000	13.886	11.002
QC10~QC 14	6.557	13.001	23.357	1.106	5.999	Cost ($/h)	103395.78	PLoss	55.119

Table 14: Optimal results for case 2.

Optimizer	Min	Mean	Max	Std.	Time (s)
MCOA	103395.78	103406.94	103415.67	10.42	781
COA	107008.21	109639.71	112617.55	818.2	759
WGA	103405.36	103412.05	103419.40	25.94	810
AOA	116994.05	120201.73	124011.65	1095.3	1240
INFO	106849.00	109114.19	113867.14	504.6	1405
DS (Duman, Rivera, et al., 2020)	110992.4249	112680.2902	114787.7786	953.6529	-
BSA (Duman, Rivera, et al., 2020)	117149.9833	120443.2982	123385.1256	1638.0949	-

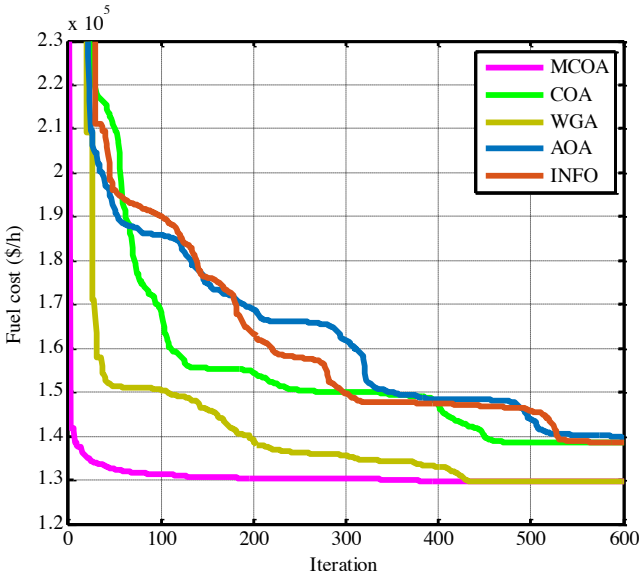

Figure 10: Convergence for case 1.

5.2. Case 2: OPF problem with quadratic cost function for traditional generators including the solar and wind energy sources.

Similar to the previous case system, wind energy sources are located in buses 18, 32, 36, 55, 104, and 110. Also, solar energy generation units are in nodes 6, 15 and 34. The best solution for this case is obtained by the proposed MCOA algorithm, as shown in Table 13. In addition, Table 14 represents a comparative study between the results of the algorithms studied in this article and the solutions obtained in the reference (Duman, Rivera, et al., 2020). From these results, the MCOA is a very powerful algorithm for optimizing and distributing optimization in large and real power systems. The characteristic of the convergence of the algorithms studied in this case is shown in Figure 11, demonstrating the good convergence performance of the proposed optimization algorithm.

In the case of the 118-bus system, OPF's superiority over MCOA is demonstrated as the system dimensions increase.

Table 13: Optimal decision variables settings for case 2.

Actual power output of generators									
PG1~ PG9	33.000	30.500	79.910 0	30.102	169.52 6	59.401	100.000	150.00 00	30.095
PG10~ PG18	30.505	96.011	144.98 2	30.000	32.103	120.00 0	149.655	120.00 0	30.082
PG19~ PG27	30.000 0	35.696	121.49 8	45.000	150.00 0	34.167	102.935	102.29 9	30.0
PG28~ PG36	202.17 7	205.48 9	273.78 0	30.200	30.200	30.200	30.000	30.100	30.100
PG3~ PG45	262.00 0	30.0	31.189	292.27 5	30.081	30.000	30.000	30.393	112.70 1

QC10~QC14	29.9984	9.006	29.996	1.000	11.010	Cost ($/h)	129517.37	PLoss	76. 360

Table 12: Optimal results for case 1.

Optimizer	Min	Mean	Max	Std.	Time (s)
MCOA	129537.37	129549.25	129555.14	6.37	726
COA	138685.15	142950.74	144007.34	699.4	730
WGA	129540.44	129552.81	129558.95	8.93	703
AOA	139569.56	143175.14	145509.84	801.2	1134
INFO	138672.82	142884.29	143578.68	445.7	1378
CS-GWO (Meng et al., 2021)	129544.0	129558.9	129568.8	10.7	4252.5
PSOGSA (Mohamed et al., 2017)	129733.6	-	-	-	-
FPA (Mohamed et al., 2017)	129688.7	-	-	-	-
MFO (Mohamed et al., 2017)	129708.1	-	-	-	-
Rao-1 (Hassan et al., 2021)	131817.9	-	-	-	808.0
Rao-3 (Hassan et al., 2021)	131793.1	-	-	-	806.7
Rao-2 (Hassan et al., 2021)	131490.7	-	-	-	804.6
MRao-2 (Hassan et al., 2021)	131457.8	-	-	-	1160.3
EWOA (Nadimi-Shahraki et al., 2021)	140175.8	-	-	-	-
MCSA (Shaheen et al., 2021)	129873.6	-	-	-	-
ICBO (Bouchekara et al., 2016)	135121.6	-	-	-	-
MSA (Mohamed et al., 2017)	129640.7	-	-	-	-
SSO (Hassan et al., 2021)	132080.4	-	-	-	-
GWO (El-Fergany & Hasanien, 2015)	139948.1	142989.3	145484.6	797.8	1766.2
IABC (Bai et al., 2017)	129862.0	129895.0	-	40.8	4157.8

available reactive powers ranging from 0 to 30 MVAR (Duman, Rivera, et al., 2020).

5.1. Case 1: OPF problem with quadratic cost function for traditional generators without the solar and wind energy sources

In Tables 11 and 12, the result is compared to the results of other algorithms under investigation and some other techniques reported in the literature, including CS-GWO (Meng et al., 2021); MSA (Mohamed et al., 2017), FPA (Mohamed et al., 2017), MFO (Mohamed et al., 2017), PSOGSA (Mohamed et al., 2017), IABC (Bai et al., 2017), MCSA (Shaheen et al., 2021), MRao-2 and Rao algorithms (Hassan et al., 2021), SSO (Hassan et al., 2021), ICBO (Bouchekara et al., 2016), GWO (El-Fergany & Hasanien, 2015), and EWOA (Nadimi-Shahraki et al., 2021). According to this table, the MCOA outperforms various optimization techniques used to solve the large-scale OPF. According to the obtained simulation data, the minimum cost obtained from MCOA is 129517.37 $/h, which is less comparing to result of other algorithms. Also, Figure 10 depicts, after that, the convergence characteristic of the studied algorithms used in this case.

Table 11: Optimal decision variables settings for case 1.

Actual power output of generators									
PG1~ PG9	24.195	0.028	0.012	0.030	403.000	85.600	20.000	11.000	20.200
PG10~ PG18	0.015	195.982	281.021	10.918	7.149	15.998	0.183	5.000	48.300
PG19~ PG27	41.898	19.000	194.017	49.210	31.000	32.522	149.991	148.403	0.000
PG28~ PG36	354.500	350.903	458.220	0.000	0.000	0.000	15.822	19.620	0.000
PG3~ PG45	432.000	0.000	3.601	506.989	0.000	0.000	0.000	0.000	233.375
PG46~ PG54	37.885	0.220	3.998	29.041	6.000	35.000	36.500	0.011	0.000
Voltage magnitude of generators									
VG1~ VG9	1.020	1.038	1.040	1.075	1.100	1.029	1.036	1.042	1.028
VG10~ VG18	1.065	1.093	1.100	1.052	1.048	1.048	1.048	1.032	1.025
VG19~ VG27	1.021	1.049	1.060	1.031	1.027	1.029	1.049	1.068	1.055
VG28~ VG36	1.071	1.071	1.079	1.061	1.061	1.048	1.048	1.030	1.058
VG3~ VG45	1.069	1.080	1.078	1.092	1.068	1.075	1.076	1.600	1.061
VG46~ VG54	1.050	1.041	1.030	1.028	1.029	1.042	1.020	1.050	1.060
Transformers' tap									
T1~ T9	1.047	1.047	0.965	0.963	1.000	1.008	0.982	0.980	0.971
VAR compensating units									
QC1~QC9	30.000	0.000	0.000	2.000	20.000	8.000	8.000	28.235	28.748

AOA	815.5255	28.1	817.6217	816.8410	1.01
INFO	814.3942	33.4	816.5601	815.5889	1.26
WGA	813.5269	23.8	814.2247	813.7112	0.604
COA	814.7277	22.5	816.2242	815.5209	1.25
MCOA	813.1276	22.5	813.7012	813.3723	0.429
Method	Min	Time (s)	Max	Mean	Std.
			Case 6		
AOA	968.4278	25.5	971.2885	970.2347	2.61
INFO	965.0305	29.0	970.4143	968.1889	2.43
WGA	964.8344	23.6	965.4578	965.6549	0.738
COA	968.0184	22.5	968.1634	967.0625	1.68
MCOA	964.2521	22.5	965.0307	964.5846	0.814
Method	Min	Time (s)	Max	Mean	Std.
			Case 7		
AOA	783.5939	27.6	785.2641	784.9991	0.977
INFO	782.4830	29.7	784.9170	783.3454	0.868
WGA	782.2985	25.4	782.9775	782.7531	0.852
COA	782.5129	26.4	783.9485	783.2901	1.34
MCOA	782.1910	26.4	782.7316	782.4721	0.663
Method	Min	Time (s)	Max	Mean	Std.
			Case 8		
AOA	812.7563	30.1	815.1569	814.3313	3.92
INFO	811.6345	32.3	814.2818	812.8100	2.84
WGA	810.6845	27.3	811.4569	811.1184	0.923
COA	811.6948	26.5	813.5013	812.1716	2.04
MCOA	810.5542	26.6	811.1652	810.8203	0.698

5. OPF in the IEEE 118-Bus large-scale test System

In this part, the IEEE 118-bus test system (Meng et al., 2021) is used to evaluate the efficiency of the proposed MCOA in solving a larger power system. This test system has 54 generators, 186 branches, 9 transformers, 2 reactors, and 12 capacitors. It has 129 control variables considered for 54 generator active powers and bus voltages, 9 transformer tap settings, and 12 shunt capacitor reactive power injections. All buses have voltage limitations between 0.94 and 1.06 p.u. Within the range of 0.90–1.10 p.u., the transformer tap settings are evaluated. Shunt capacitors have

Table 10: Statistical results of MCOA and COA.

Method	Min	Time (s)	Max	Mean	Std.
			Case 1		
AOA	802.6318	28.7	804.9570	803.7042	1.78
INFO	801.8834	30.4	804.3152	802.8556	2.93
WGA	800.9701	21.9	801.6926	801.2999	0.842
COA	801.7449	22.4	802.8623	802.0724	2.81
MCOA	800.4791	22.4	800.7816	800.5629	0.283
Method	Min	Time (s)	Max	Mean	Std.
			Case 2		
AOA	649.2593	26.9	651.5815	650.3662	2.46
INFO	647.7004	23.0	650.0457	648.9654	1.43
WGA	646.9731	21.1	647.3950	647.8821	0.749
COA	649.8857	22.5	651.1421	650.2790	1.94
MCOA	646.4890	22.5	646.9002	646.6874	0.375
Method	Min	Time (s)	Max	Mean	Std.
			Case 3		
AOA	833.7423	22.9	834.6465	835.9325	2.34
INFO	832.8083	29.7	834.3280	833.4100	1.12
WGA	832.4601	25.1	833.1994	832.7543	0.554
COA	832.8498	22.5	833.9849	833.3615	1.75
MCOA	832.2134	22.4	832.7816	832.5022	0.341
Method	Min	Time (s)	Max	Mean	Std.
			Case 4		
AOA	1041.5309	26.0	1042.8252	1042.0067	1.20
INFO	1040.9591	30.2	1042.3516	1041.8404	1.74
WGA	1040.3394	20.9	1040.9139	1040.6612	0.916
COA	1040.6773	22.4	1042.4279	1041.6434	1.96
MCOA	1040.0674	22.5	1040.6715	1040.3200	0.507
Method	Min	Time (s)	Max	Mean	Std.
			Case 5		

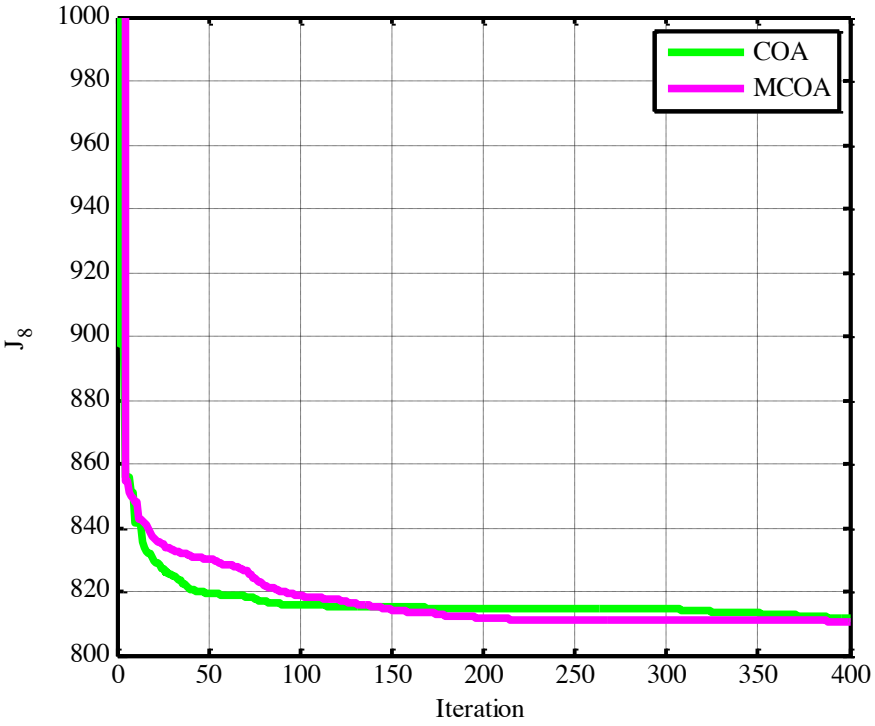

Figure 9: Convergence for case 8.

4.8 Discussions on the IEEE 30-bus network

In this section, we comprehensively compare between the suggested MCOA and the basic COA, and also, three modern powerful recent algorithms, arithmetic optimization algorithm (AOA) (Abualigah et al., 2021), weighted mean of vectors (INFO) (Ahmadianfar et al., 2022) and wild geese algorithm (WGA) (Ghasemi et al., 2021), over all of the scenarios covered in this article on the IEEE 30-bus network. Best, average, and worst results from 30 runs, as well as standard deviation and average running time, are shown in Table 10. An in-depth examination of this table demonstrates that the suggested MCOA method has triumphed over the original COA algorithm and three modern powerful recent algorithms, AOA, INFO and WGA in every situation tested and that it has done so without increasing the time it takes to execute the original algorithm or the complexity of the computations it conducts.

It is, therefore, evident that the suggested MCOA performs statistically differently from its competitors. According to these quantitative and qualitative findings, the proposed MCOA can produce challenging and competitive results at faster convergence speeds. Adopting a revolutionary hybrid optimization approach for the MCOA algorithm is proposed. This enhances its global search capability while balancing exploration and exploitation to achieve high-quality solutions. The algorithm can achieve better search efficiency by leveraging this approach and avoiding local optima. As part of the evaluation of the performance of the MCOA algorithm, it has been compared with the AOA, the INFO, the WGA, and the basic COA algorithms. As a result of the results, the suggested MCOA is superior and effective. The proposed algorithm has the advantage of fast convergence to global optima, making it suitable for solving complex real-world power system problems. We expect that as time progresses, the OPF problem will include emergency events, large-scale testing systems, and the penetration of electric vehicles.

Table 9: The optimal variables value for case 8.

Variables	COA	MCOA
PG1 (MW)	123.98540	123.23593
PG2 (MW)	34.3509	32.2800
Pws1 (MW)	46.6899	45.6210
PG3 (MW)	10.0000	10.0000
Pws2 (MW)	39.2993	38.4229
Pss (MW)	34.3579	39.1160
VG1 (p.u.)	1.0704	1.0704
VG2 (p.u.)	1.0569	1.0569
VG5 (p.u.)	1.0359	1.0357
VG8 (p.u.)	1.1000	1.0403
VG11 (p.u.)	1.0983	1.0998
VG13 (p.u.)	1.0498	1.0566
QG1 (MVAR)	-2.97776	-2.74168
QG2 (MVAR)	11.05753	12.23749
Qws1 (MVAR)	22.23269	22.97597
QG3(MVAR)	40.00000	35.18169
Qws2 (MVAR)	30.00000	30.00000
Qss (MVAR)	15.37773	18.01536
Fuelvlvcost ($/h)	435.0921	426.2147
Wind gen cost ($/h)	264.8905	257.9513
Solar gen cost ($/h)	93.4094	108.8521
Total Cost ($/h)	793.3920	793.0180
Emission (t/h)	0.91514	0.87681
J8	811.6948	810.5542
Power losses (MW)	5.2833	5.2758
V.D. (p.u.)	0.45900	0.47042
Carbon tax ($/h)	18.3028	17.5362

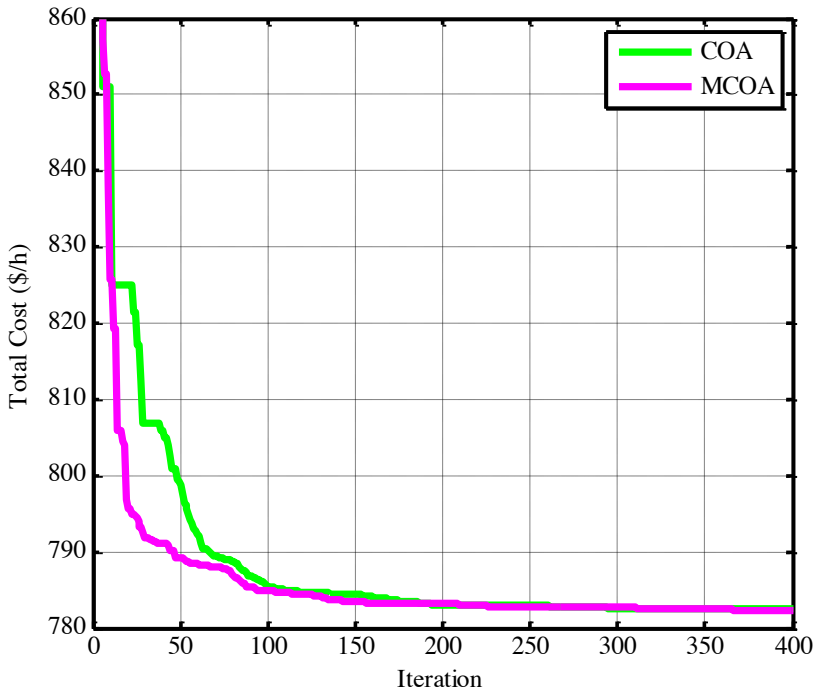

Figure 8: Convergence for case 7.

4.7.2 Case 8: Minimizing generating costs while accounting for the cost of carbon and the variable output of renewable sources

The threat of climate change has led some nations to raise their demands that the whole energy sector cut carbon emissions. *Ctax*, or carbon taxes, are charged on emissions of greenhouse gases.

This tax is intended to encourage financial investments in renewable energy sources like wind and solar power. The following is a breakdown, in USD per hour, of the cost of publishing (Biswas et al., 2018):

$$\text{Emission cost: } C_E = C_{tax}E \tag{50}$$

$$J_8 = J_7 + C_{tax}E \tag{51}$$

As a way of reducing the total costs associated with the generation of electrical power, the concluding case study of this article suggests imposing a financial penalty in the form of a carbon tax on the emissions of greenhouse gases by traditional thermal energy producers. The anticipated total cost of Equation (51) is what needs to be maintained at the lowest feasible level. It is anticipated that the rate of the carbon tax will be twenty dollars per ton.

Table 9 presents the results of a simulation conducted using these two methods to determine the ideal load distribution. The result produced by the proposed adjusted version of the algorithm is superior to that produced by the original method. More specifically, the pace of development of energy production programs based on renewable energy production will be decided by the volume of emissions and the degree of pricing and taxes on carbon. The convergent behavior of the two algorithms is shown in Figure 9 for case 8 of the research.

Table 8 displays the best possible answers obtained from each algorithm tested in this research after 30 iterations. P_{ws1} shows the expected output from W_{G1}, and so on, for each successive wind generator. According to this table, the proposed MCOA algorithm has successfully located optimal solutions that are both of a higher quality and perform much better than the original COA approach. The convergent behavior of the two algorithms is shown in Figure 8 for case 7 of the research.

Table 8: The optimal variables for case 7.

Variables	COA	MCOA
PG1 (MW)	134.90794	134.90791
PG2 (MW)	27.5907	27.7283
Pws1 (MW)	43.1839	43.3109
PG3 (MW)	10.0001	10
Pws2 (MW)	36.2407	36.5707
Pss (MW)	37.2677	36.6646
VG1 (p.u.)	1.0717	1.0721
VG2 (p.u.)	1.0567	1.0571
VG5 (p.u.)	1.0346	1.035
VG8 (p.u.)	1.0396	1.0397
VG11 (p.u.)	1.0992	1.0983
VG13 (p.u.)	1.0587	1.0551
QG1 (MVAR)	-2.12274	-1.95067
QG2 (MVAR)	12.4535	13.2051
Qws1 (MVAR)	23.1089	23.2034
QG3(MVAR)	34.7495	35.0095
Qws2 (MVAR)	30	30
Qss (MVAR)	18.8345	17.5462
Fuelvlvcost ($/h)	437.5577	438.0114
Wind gen cost ($/h)	241.8954	243.4495
Solar gen cost ($/h)	103.0597	100.7301
Total Cost ($/h)	782.5129	782.1910
Emission (t/h)	1.76231	1.76227
Power losses (MW)	5.7911	5.7823
V.D. (p.u.)	0.47399	0.46413

$$C_S^T = \sum_{k=1}^{N_S}\left[C_{s,j}\left(P_{ss,k}\right)+C_{Rs,k}\left(P_{ss,k}-P_{sav,k}\right)+C_{Ps,k}\left(P_{sav,k}-P_{ss,k}\right)\right] \quad (38)$$

wind/solar integrated OPF constraints and variables

To incorporate the variables associated with the wind and solar power generations into the conventional OPF problem, some modifications and additional constraints should be considered. So, the equality constraints (6) and (7) are expressed as given in (39) and (40).

$$P_{Gi}+P_{ws,i}+P_{ss,i}-P_{Di}-V_i\sum_{j=1}^{NB}V_j\left[B_{ij}\sin\left(\delta_i-\delta_j\right)+G_{ij}\cos\left(\delta_i-\delta_j\right)\right]=0 \quad (39)$$

$$Q_{Gi}+Q_{ws,i}+Q_{ss,i}-Q_{Di}-V_i\sum_{j=1}^{NB}V_j\left[G_{ij}\sin\left(\delta_i-\delta_j\right)-B_{ij}\cos\left(\delta_i-\delta_j\right)\right]=0 \quad (40)$$

Also, the voltage magnitude, active and reactive power generations at the installed locations of the wind and solar power generation units are restricted using the constraints (41) to (46).

$$V_{ws,i}^{min}\le V_{ws,i}\le V_{ws,i}^{max} \quad (41)$$

$$P_{ws,i}^{min}\le P_{ws,i}\le P_{ws,i}^{max} \quad (42)$$

$$Q_{ws,i}^{min}\le Q_{ws,i}\le Q_{ws,i}^{max} \quad (43)$$

$$V_{ss,i}^{min}\le V_{ss,i}\le V_{ss,i}^{max} \quad (44)$$

$$P_{ss,i}^{min}\le P_{ss,i}\le P_{ss,i}^{max} \quad (45)$$

$$Q_{ss,i}^{min}\le Q_{ss,i}\le Q_{ss,i}^{max} \quad (46)$$

In the wind/solar integrated OPF problem, the control variables, u is defined as follows:

$$\begin{aligned}
u &= [Q, V_G, V_w, V_s, P_w, P_s, P_G, T],\\
Q &= [Q_{C_1}, \dots, Q_{C_{NC}}],\\
V_G &= [V_{G_1}, \dots, V_{G_{NG}}],\\
V_w &= [V_{ws,1}, \dots, V_{ws,_{Nw}}],\\
V_s &= [V_{ss,_1}, \dots, V_{ss,_{Ns}}],\\
P_w &= [P_{ws,1}, \dots, P_{ws,_{Nw}}],
\end{aligned} \quad (47)$$

$$\begin{aligned}
P_s &= [P_{ss,_1}, \dots, P_{ss,_{Ns}}],\\
P_G &= [P_{G_2}, \dots, P_{G_{NG}}],\\
T &= [T_1, \dots, T_{NT}].
\end{aligned}$$

Besides, the state variables, x is represented as follows:

$$\begin{aligned}
x &= [S, Q_w, Q_s, Q_G, V_l, P_{G_1}],\\
S &= [S_{l_1}, \dots, S_{l_{NTL}}],\\
Q_w &= [Q_{ws,1}, \dots, Q_{ws,_{Nw}}],\\
Q_s &= [Q_{ss,_1}, \dots, Q_{ss,_{Ns}}],\\
Q_G &= [Q_{G_1}, \dots, Q_{G_{NG}}],\\
V_l &= [P_{ws,1}, \dots, P_{ws,_{Nw}}].
\end{aligned} \quad (48)$$

4.7.1 Case 7: Minimizing generation costs considering the variable nature of renewable sources

According to (39), case 7 minimizes and maximizes the overall cost of generating electricity by thermal and renewable energy sources (Biswas et al., 2018). The PDF parameters are outlined in (Biswas et al., 2018), and the cost coefficients are unchanged from case 1.

$$\begin{aligned}
J_7 = J_1 &+ \sum_{k=1}^{N_S}\left[C_{s,j}\left(P_{ss,k}\right)+C_{Ps,k}\left(P_{sav,k}-P_{ss,k}\right)+C_{Rs,k}\left(P_{ss,k}-P_{sav,k}\right)\right]\\
&+\sum_{j=1}^{N_W}\left[C_{w,j}\left(P_{ws,j}\right)+C_{Pw,j}\left(P_{wav,j}-P_{ws,j}\right)+C_{Rw,j}\left(P_{ws,j}-P_{wav,j}\right)\right]
\end{aligned} \quad (49)$$

4.7 OPF solutions, including stochastic solar and wind power.

Wind Power

In order to construct a work optimization strategy to deal with OPF challenges, a future wind energy profile prediction is required. These forecasts are calculated with the use of the Weibull probability distribution function. The first stage in finding a solution to a problem is to estimate how much energy can be generated from the wind, which may be done independently. Wind speed is a common input into models of wind power generation. Here, the Weibull probability distribution function is used to create and simulate the wind speed $f_v(v)$, where k and c are dimensionless form factors and step sizes, respectively, in the following equations (Biswas et al., 2018):

$$f_v(v) = \frac{k}{c}\left(\frac{v}{c}\right)^{k-1} \times e^{-\left(\frac{v}{c}\right)^k} \qquad (31)$$

According to formula (33), [22] the average of the Weibull probability distribution (M_{wbl}) is mainly determined by $\Gamma(x)$ (32) (Biswas et al., 2018):

$$M_{wbl} = c * \Gamma(1 + K^{-1}) \qquad (32)$$

$$\Gamma(x) = \int_0^{\infty} e^{-t} t^{x-1} dt \qquad (33)$$

A wind turbine is a device that generates electricity from the kinetic and potential energy of the wind. The relation between wind velocity and the electrical power generated by a wind turbine is given by equation (34) (Biswas et al., 2018).

$$P_w(v) = \begin{cases} 0;\ v \le v_{in} \text{and} v > v_{out} \\ P_{wr}\left(\frac{v - v_{in}}{v_r - v_{in}}\right);\ v_{in} < v \le v_r \\ P_{wr};\ v_r < v \le v_{out} \end{cases} \qquad (34)$$

where P_{wr} is the wind turbine's rated power, wind turbine's cut-in wind rate is v_{in}, and v_{out} is the cut-out wind rate and v_r is the valued wind speed.

Equation (43) describes the total cost of wind power generation in (USD/h), which includes three main items: direct wind turbine, storage, and penalty costs (Biswas et al., 2018).

$$C_W^T = \sum_{j=1}^{N_W} \left[C_{w,j}\left(P_{ws,j}\right) + C_{Pw,j}\left(P_{wav,j} - P_{ws,j}\right) + C_{Rw,j}\left(P_{ws,j} - P_{wav,j}\right)\right] \qquad (35)$$

Suppose the power production from the wind turbine is less than the value anticipated. In that case, a storage charge will be levied to compensate for the forecasted value. A fine is imposed on the company if the actual consumption of wind energy is higher than the predicted figure. Because of this, having a system that provides an accurate assessment of the wind power profile is of the utmost importance. The costs are broken down into USD per hour using the methodology outlined in (Biswas et al., 2018).

Solar power units

It is difficult to forecast how much energy can be harvested from the sun because of atmospheric variables like clouds and solar radiation. Since solar radiation is a known quantity, it may be used to calculate the maximum power generated by solar systems (G).

In this section, the lognormal probability distribution function $f_G(G)$(Biswas et al., 2018):

$$f_G(G) = \frac{k}{G\sigma\sqrt{2\pi}} \times e^{-\left(\frac{(\ln x - \mu)}{2\sigma^2}\right)} \text{ for G>0} \qquad (36)$$

The conversion of solar energy into usable power is the final goal of a solar energy system.

In equation (36), the estimated solar radiation is utilized to describe the output power of this system, which is denoted by the function $P_s(G)$ as a function (Biswas et al., 2018):

$$P_s(G) = \begin{cases} P_{sr}\frac{G^2}{G_{std}R_c};\ 0 < G < R_c \\ P_{sr}\frac{G}{G_{std_c}};\ G \ge R_c \end{cases} \qquad (37)$$

The cost of producing energy from solar sources is broken down into three distinct categories, much as the cost of producing electricity from wind sources, to mitigate the effects of the inherent uncertainty in the cost estimate.

Equation (38) determine the following sum of all components in terms of their respective (USD/h) values (Biswas et al., 2018):

Table 7: The optimal solutions for case 6.

Algorithm	Fuel cost ($/h)	Emission (t/h)	Power losses (MW)	V.D. (p.u.)	J_6
MSA (Mohamed et al., 2017)	830.639	0.25258	5.6219	0.29385	965.2907
SSO (El Sehiemy et al., 2020)	829.978	0.25	5.426	0.516	964.9360
PSO (El Sehiemy et al., 2020)	828.2904	0.261	5.644	0.55	968.9674
J-PPS3 (Gupta et al., 2021)	830.3088	0.2363	5.6377	0.2949	965.0228
J-PPS2 (Gupta et al., 2021)	830.8672	0.2357	5.6175	0.2948	965.1201
J-PPS1 (Gupta et al., 2021)	830.9938	0.2355	5.6120	0.2990	965.2159
MNSGA-II (Ghasemi, Ghavidel, Ghanbarian, et al., 2014)	834.5616	0.2527	5.6606	0.4308	972.9429
MFO (Mohamed et al., 2017)	830.9135	0.25231	5.5971	0.33164	965.8080
MOALO (Herbadji et al., 2019)	826.2676	0.2730	7.2073	0.7160	1005.0512
MODA (Ouafa et al., 2017)	828.49	0.265	5.912	0.585	975.8740
I-NSGA-III (Zhang et al., 2019)	881.9395	0.2209	4.7449	0.1754	994.2078
BB-MOPSO (Ghasemi, Ghavidel, Ghanbarian, et al., 2014)	833.0345	0.2479	5.6504	0.3945	970.3379
COA	830.2933	0.2558	5.7225	0.3319	968.0184
MCOA	830.2798	0.2529	5.5876	0.2971	964.2521

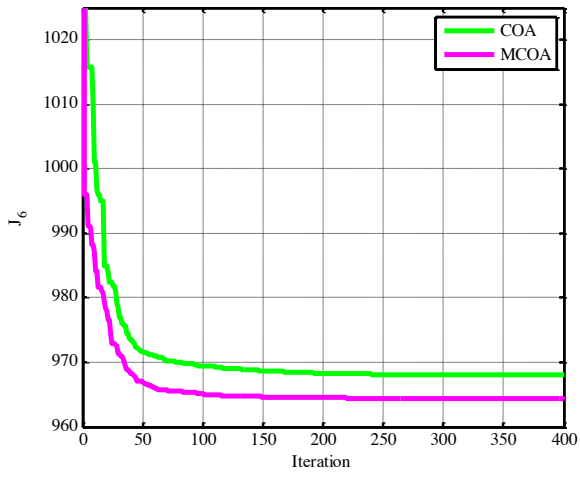

Figure 7: Convergence for case 6.

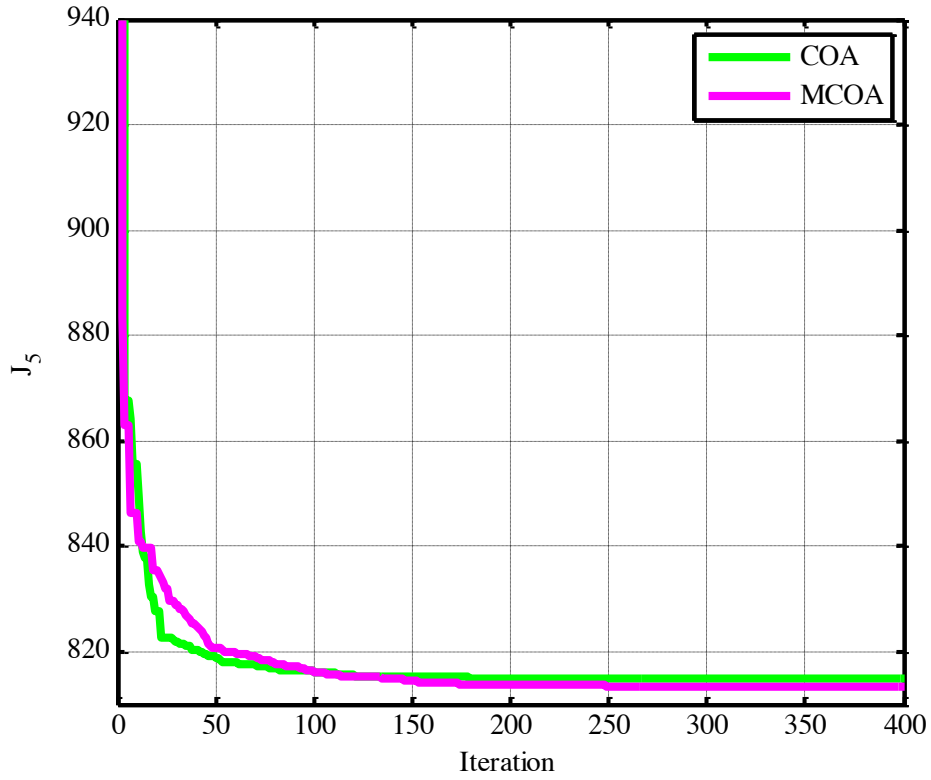

Figure 6: Convergence for case 5.

4.6 Case 6: Minimizing the fuel cost, voltage deviation, emissions, and losses

This function models fuel cost, voltage deviation, active power loss and emission with λv = 21, λp = 22 and λe = 19 (Biswas et al., 2018):

$$J_6 = J_1 + \lambda v * \sum_{i=1}^{NPQ} |V_i - 1.0| + \lambda e * \sum_{i=1}^{NG} F_{Ei}(P_{Gi}) + \lambda p * P_{Loss} \quad (29)$$

$\sum_{i=1}^{NG} F_{Ei}(P_{Gi})$ is expressed as follows:

$$F_E = \sum_{i=1}^{NG} \left(\alpha_i + \xi_i \, exp(\lambda_i P_{Gi}) + \beta_i P_{Gi} + \gamma_i P_{Gi}^2\right) \quad (30)$$

where F_{Ei} signifies the emission,γ_i,β_i, ξ_i and λ_i show the emission coefficients of *i*th generator.

Table 7 summarizes the findings of the algorithms investigated in this study compared to the most successful results of more recent papers. This table makes it abundantly evident that the MCOA optimization technique is the superior choice among these other optimization approaches for the sixth ideal load distribution scenario. Figure 7 depicts, after that, the convergence characteristic of the COA and MCOA algorithms used in this example.

$$J_5 = \lambda v * \sum_{i=1}^{NPQ} |V_i - 1.0| + J_1 \qquad (28)$$

where the value of the component λv is set to 100 (Biswas et al., 2018).

Table 6 presents the best results that could be achieved for case 5 using the techniques discussed in this article, as well as findings from more recent investigations. MCOA has produced the lowest and best values for this objective function in comparison to other approaches shown in Table 6. Figure 6 presents the characteristic convergence curves of the various methods.

Table 6: The optimal solutions for case 5.

Optimizer	Fuel cost ($/h)	Emission (t/h)	Power losses (MW)	V.D. (p.u.)	J_5
BB-MOPSO (Ghasemi, Ghavidel, Ghanbarian, et al., 2014)	804.9639	-	-	0.1021	815.1739
DA-APSO (Shilaja & Ravi, 2017)	802.63	-	-	0.1164	814.2700
SpDEA (Ghoneim et al., 2021)	803.0290	-	9.0949	0.2799	831.0190
MNSGA-II (Ghasemi, Ghavidel, Ghanbarian, et al., 2014)	805.0076	-	-	0.0989	814.8976
PSO-SSO (El Sehiemy et al., 2020)	803.9899	0.367	9.961	0.0940	813.3899
SSO (El Sehiemy et al., 2020)	803.73	0.365	9.841	0.1044	814.1700
PSO (El Sehiemy et al., 2020)	804.477	0.368	10.129	0.126	817.0770
MFO (Mohamed et al., 2017)	803.7911	0.36355	9.8685	0.10563	814.3541
EMSA (Bentouati et al., 2020)	803.4286	0.3643	9.7894	0.1073	814.1586
TFWO (Sarhan et al., 2022)	803.416	0.365	9.795	0.101	813.5160
ECHT-DE (Biswas et al., 2018)	803.7198	0.36384	9.8414	0.09454	813.1738
MOMICA (Ghasemi, Ghavidel, Ghanbarian, et al., 2014)	804.9611	0.3552	9.8212	0.0952	814.4811
MPSO (Mohamed et al., 2017)	803.9787	0.3636	9.9242	0.1202	815.9987
COA	804.0138	0.3673	10.0020	0.1071	814.7277
MCOA	803.7176	0.3614	9.7753	0.0941	813.1276

Table 5: The optimal solutions for case 4.

Optimizer	Fuel cost ($/h)	Emission (t/h)	Power losses (MW)	V.D. (p.u.)	J_4
SF-DE (Biswas et al., 2018)	859.1458	0.2289	4.5245	0.92731	1040.1258
MJaya (Warid et al., 2018)	827.9124	-	5.7960	-	1059.7524
QOMJaya (Warid et al., 2018)	826.9651	-	5.7596	-	1402.9251
EMSA (Bentouati et al., 2020)	859.9514	0.2278	4.6071	0.7758	1044.2354
MOALO (Herbadji et al., 2019)	826.4556	0.2642	5.7727	1.2560	1057.3636
SpDEA (Ghoneim et al., 2021)	837.8510	-	5.6093	0.8106	1062.223
MSA (Mohamed et al., 2017)	859.1915	0.2289	4.5404	0.92852	1040.8075
COA	859.2413	0.2291	4.5359	0.9113	1040.6773
MCOA	859.0154	0.2289	4.5263	0.9298	1040.0674

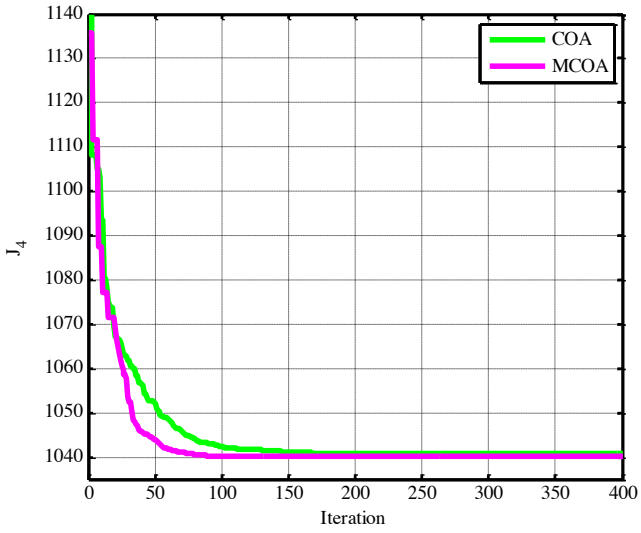

Figure 5: Convergence for case 4.

4.5 Case 5: Minimizing the fuel cost and voltage deviation.

The voltage specification is the most important of all the factors considered when determining a network's dependability. This may be modified by reducing the voltage gap between the load and the bus to a value closer to unity. An acceptable solution is found when the cost alone is used as the target function; however, the voltage variations associated with this solution are undesirable. Therefore, the objective function of the optimum load distribution in scenario 5 of this article is described below to minimize both voltage deviations (V.D.) and fuel costs.

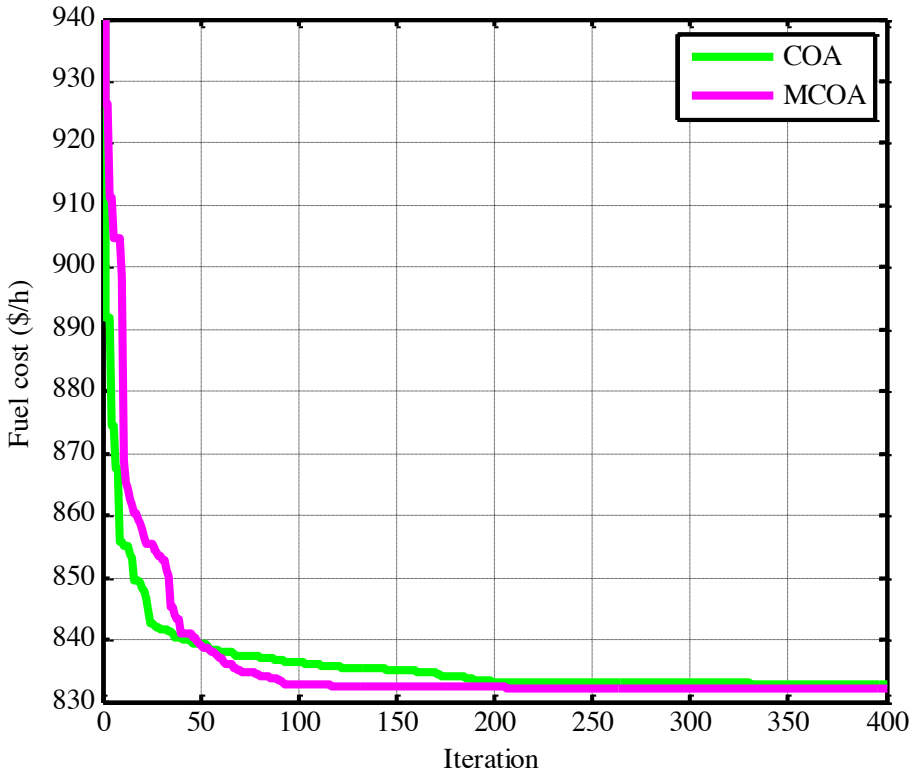

Figure 4: Convergence for case 3.

4.4 Case 4: Minimizing the fuel cost and real power loss

Engineers strive to minimize energy loss in the transmission of electricity. Therefore, we want to lessen network fuel and losses in this case. The correct form of the objective function is as follows:

$$J_4 = \lambda p * P_{Loss} + J_1 \quad (26)$$

The value of factor λp has been chosen as equal to 40 (Biswas et al., 2018).

Network loss (P_{Loss}) can be modeled as the following average (Biswas et al., 2018):

$$P_{Loss} = \sum_{\substack{k=1 \\ k=(i,j)}}^{NTL} g_k(V_i^2 + V_j^2 - 2\,V_i V_j \cos\delta_{ij}) \quad (27)$$

As seen above, the conductance of the kth branch is denoted by the symbol g_k.

In Table 5, we provide the optimal answers to this instance, as determined by the algorithms explored in this research and the techniques analyzed in the relevant prior literature. The results show that the approach put forth in this MCOA paper is the best option. Figure 5 below displays the convergence characteristics of the examined methods for the top 30 run-average solutions.

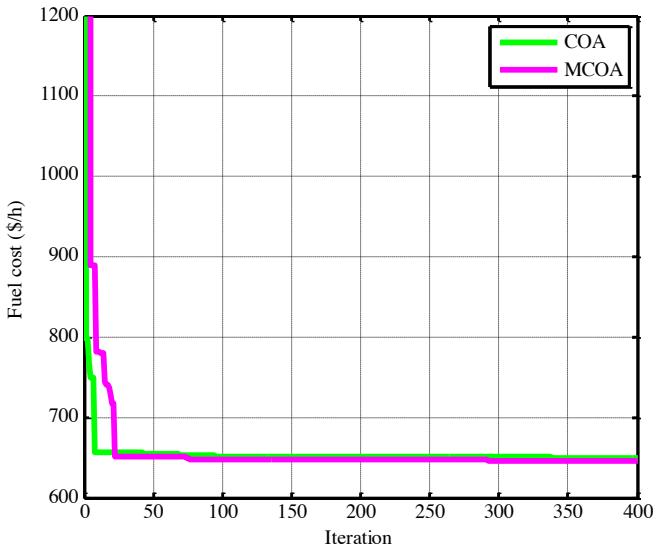

Figure 3: Convergence for case 2.

4.3 Case 3: Considering valve point effects (VPEs)

The quadratic cost function achieves a higher degree of accuracy and realism as a direct result of the influence of tap point loading. When steam is introduced, the valves on thermal generating units open, which results in rapid increases in losses and causes ripples in the cost function curve. This causes VPEs. The effect of this is that the cost function may be expressed as follows (Biswas et al., 2018):

$$J_3 = \sum_{i=1}^{NG} \left| d_i \sin\left(e_i \left(P_{Gi}^{\min} - P_{Gi}\right)\right)\right| + \sum_{i=1}^{NG} \alpha_i + b_i P_{Gi} + c_i P_{Gi}^2 \quad (25)$$

where d_i and e_i are the ith generator's price and efficiency factors (Biswas et al., 2018).

Results from SP-DE (Biswas et al., 2018), PSO (Bouchekara et al., 2016), COA, and MCOA algorithms are shown in Table 4. It is clear from the data presented in this table that the MCOA is an algorithm that is well-suited to the complex OPF. It is also clear from the algorithm convergence graph in Figure 4 that the MCOA can achieve good and acceptable optimal solutions.

Table 4: The optimal solutions for case 3.

Optimizer	Fuel cost ($/h)	Emission (t/h)	Power losses (MW)	V.D. (p.u.)
COA	832.8498	0.4390	10.9273	0.7216
MCOA	832.2134	0.4379	10.7009	0.8323
SP-DE (Biswas et al., 2018)	832.4813	0.43651	10.6762	0.75042
PSO (Bouchekara et al., 2016)	832.6871	-	-	-

Table 3: The optimal solutions for case 2.

Optimizer	Fuel cost ($/h)	Emission (t/h)	Power losses (MW)	V.D. (p.u.)
MDE (Sayah & Zehar, 2008)	647.846	-	7.095	-
MPSO-SFLA (Narimani et al., 2013)	647.55	-	-	-
MSA (Mohamed et al., 2017)	646.8364	0.28352	6.8001	0.84479
IEP (Ongsakul & Tantimaporn, 2006)	649.312	-	-	-
SSA (Jebaraj & Sakthivel, 2022)	646.7796	0.2836	6.5599	0.5320
SSO (Nguyen, 2019)	663.3518	-	-	-
GABC (Roy & Jadhav, 2015)	647.03	-	6.8160	0.8010
FPA (Mohamed et al., 2017)	651.3768	0.28083	7.2355	0.31259
MICA-TLA (Ghasemi, Ghavidel, Rahmani, et al., 2014)	647.1002	-	6.8945	-
MFO (Mohamed et al., 2017)	649.2727	0.28336	7.2293	0.47024
LTLBO (Ghasemi, Ghavidel, Gitizadeh, et al., 2015)	647.4315	0.2835	6.9347	0.8896
COA	649.8857	0.2824	7.4359	0.6474
MCOA	646.4890	0.2835	6.7217	0.9277

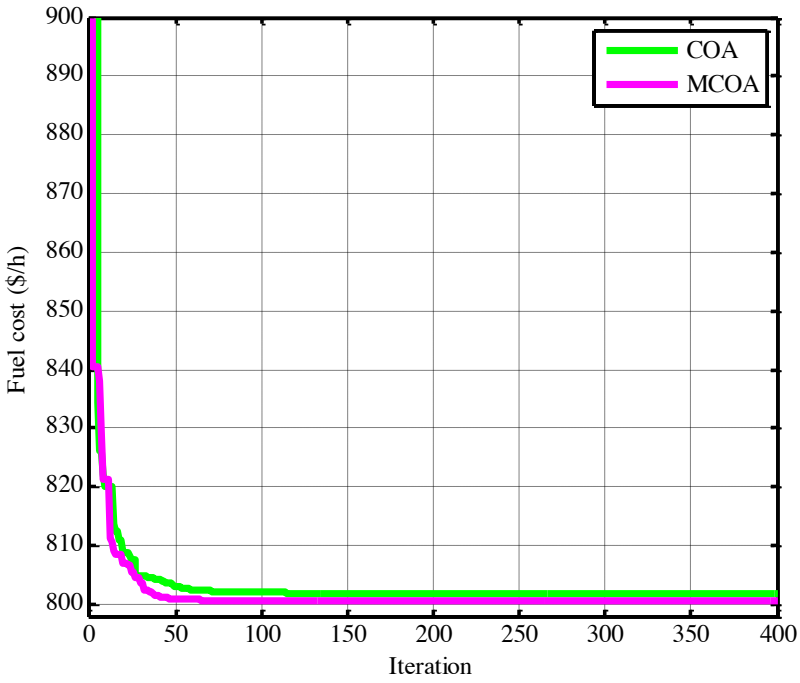

Figure 2: Convergence for case 1.

4.2 Case 2: Minimizing piecewise quadratic fuel cost functions.

Thermal generators can operate on a wide range of fuels depending on the requirements of the network. Consequently, we may consider the theoretical analysis of the F curve for these units (1 and 2) to be a collection of constraints.

$$F(P_{Gi}) = \begin{cases} \alpha_{i1} + c_{i1}P_{Gi}^2 + b_{i1}P_{Gi} & P_{Gi}^{\min} \le P_{Gi} \le P_{Gi1} \\ \dots & \\ \alpha_{ik} + c_{ik}P_{Gi}^2 + b_{ik}P_{Gi} & P_{Gik-1} \le P_{Gi} \le P_{Gi}^{\max} \end{cases} \quad (23)$$

For the kth kind of fuel, the cost coefficients of generator i are indicated by the notation a_{ik}, b_{ik}, and $c_{ik,}$ respectively.

As a direct consequence of this, the goal function for modeling the features of fuel costs may be shown as follows:

$$J_2 = \left(\sum_{i=1}^{NG} \alpha_{ik} + c_{ik}P_{Gi}^2 + b_{ik}P_{Gi} \right) \quad (24)$$

Table 3 compares these results to the outcomes that have been reported in the most recent research, such as MDE (Sayah & Zehar, 2008), MPSO-SFLA (Narimani et al., 2013), MSA (Mohamed et al., 2017), IEP (Ongsakul & Tantimaporn, 2006), SSA (Jebaraj & Sakthivel, 2022), SSO (Nguyen, 2019), GABC (Roy & Jadhav, 2015), FPA (Mohamed et al., 2017), MICA-TLA (Ghasemi, Ghavidel, Rahmani, et al., 2014), MFO (Mohamed et al., 2017), and LTLBO (Ghasemi, Ghavidel, Gitizadeh, et al., 2015). The fuel that costs the least per hour ($/h), produces the fewest emissions ($/ton), wastes the least amount of power (MW), and has the lowest *V.D.* (p.u.) is the one that wins. This table demonstrates that the MCOA approach described here performs better than the other algorithms that were taken into consideration. Figure 3 illustrates the convergence characteristic curve of the two algorithms that were investigated for this work to find the optimum solution.

GWO (Niknam, Narimani, Aghaei, et al., 2011)	801.41	-	9.30	-
FPA (Mohamed et al., 2017)	802.7983	0.35959	9.5406	0.36788
ARCBBO (Ramesh Kumar & Premalatha, 2015)	800.5159	0.3663	9.0255	0.8867
JAYA (Warid et al., 2016)	800.4794	-	9.06481	0.1273
MICA-TLA (Ghasemi, Ghavidel, Rahmani, et al., 2014)	801.0488	-	9.1895	-
PPSOGSA (Ullah et al., 2019)	800.528	-	9.02665	0.91136
DE (Sayah & Zehar, 2008)	802.39	-	9.466	-
MHBMO (El-Fergany & Hasanien, 2015)	801.985	-	9.49	-
MFO (Mohamed et al., 2017)	800.6863	0.36849	9.1492	0.75768
TS (Abido, 2002)	802.29	-	-	-
AGSO (Hazra & Sinha, 2011)	801.75	0.3703	-	-
SFLA-SA (Niknam, Narimani, Jabbari, et al., 2011)	801.79	-	-	-
SKH (Pulluri et al., 2018)	800.5141	0.3662	9.0282	-
ABC (Abaci & Yamacli, 2016)	800.660	0.365141	9.0328	0.9209
AO (Khamees et al., 2021)	801.83	-	-	-
COA	801.7449	0.3739	9.4432	0.5715
MCOA	800.4791	0.3663	9.0212	0.9091

4.1 Case 1: Minimizing the fuel cost

Several aspects of the objective function were considered while working on the OPF issue for this research. The first component of this goal function of minimizing fuel costs is resources, which is the same as the conventional cost function in that it has the same meaning.

$$J_1 = \sum_{i=1}^{NG} (\alpha_i + b_i P_{Gi} + c_i P_{Gi}^2) \qquad (22)$$

where the coefficients a_i, bi, and c_i (Mohamed et al., 2017) show the costs associated with the ith unit.

Table 2 compares testified findings from recent works such as MSA (Mohamed et al., 2017), MGBICA (Ghasemi, Ghavidel, Ghanbarian, et al., 2015), MRFO (Guvenc et al., 2020), MPSO-SFLA (Narimani et al., 2013), EP (SOOD, 2007), IEP (Ongsakul & Tantimaporn, 2006), PSOGSA (Radosavljević et al., 2015), GWO (Niknam, Narimani, Aghaei, et al., 2011), FPA (Mohamed et al., 2017), ARCBBO (Ramesh Kumar & Premalatha, 2015), JAYA (Warid et al., 2016), MICA-TLA (Ghasemi, Ghavidel, Rahmani, et al., 2014), PPSOGSA (Ullah et al., 2019), DE (Sayah & Zehar, 2008), MHBMO (El-Fergany & Hasanien, 2015), MFO (Mohamed et al., 2017), TS (Abido, 2002), AGSO (Hazra & Sinha, 2011), SFLA-SA (Niknam, Narimani, Jabbari, et al., 2011), SKH (Pulluri et al., 2018), ABC (Abaci & Yamacli, 2016), and AO (Khamees et al., 2021) on the OPF of COA and MCOA algorithms.

According to Table 2, the provided algorithm outperformed the others in attaining the lowest potential fuel cost. The convergence properties of the COA and MCOA algorithms are shown in Figure 2. From this diagram, it is easy to see that in case 1, the algorithms reach a correct final solution at the right moment.

Table 2: The optimal solutions for case 1.

Optimizer	Fuel cost ($/h)	Emission (t/h)	Power losses (MW)	V.D. (p.u.)
MSA (Mohamed et al., 2017)	800.5099	0.36645	9.0345	0.90357
MGBICA (Ghasemi, Ghavidel, Ghanbarian, et al., 2015)	801.1409	0.3296	-	-
MRFO (Guvenc et al., 2020)	800.7680	-	9.1150	-
MPSO-SFLA (Narimani et al., 2013)	801.75	-	9.54	-
EP (SOOD, 2007)	803.57	-	-	-
IEP (Ongsakul & Tantimaporn, 2006)	802.46	-	-	-
PSOGSA (Radosavljević et al., 2015)	800.49859	-	9.0339	0.12674

Table 1:The ideal values for the variables that MCOA found for OPF without using stochastic renewable energy.

Var.	Cases					
	1	2	3	4	5	6
PG1 (MW)	177.1373	140.0000	198.7757	102.6071	175.5192	122.1789
PG2	48.7211	55.0000	44.7459	55.5533	48.4117	52.5609
PG5	21.3808	24.1481	18.5791	38.1102	21.2771	31.4833
PG8	21.2481	34.9526	10.0000	35.0000	23.1580	35.0000
PG11	11.9338	19.2642	10.0002	30.0000	12.8093	26.7244
PG13	12.0001	16.7568	12.0000	26.6587	12.0000	21.0401
VG1 (p.u.)	1.0836	1.0757	1.0807	1.0698	1.0429	1.0732
VG2	1.0605	1.0581	1.0573	1.0576	1.0225	1.0574
VG5	1.0339	1.0324	1.0296	1.0359	1.0152	1.0325
VG8	1.0382	1.0410	1.0360	1.0438	1.0041	1.0407
VG11	1.0999	1.0810	1.0969	1.0834	1.0723	1.0401
VG13	1.0511	1.0561	1.0710	1.0573	0.9902	1.0246
T6–9	1.0782	1.0229	1.0987	1.0744	1.0972	1.0997
T6–10	0.9057	0.9611	0.9002	0.9111	0.9017	0.9509
T4-12	0.9787	0.9917	1.0040	0.9901	0.9399	1.0331
T28–27	0.9729	0.9737	0.9772	0.9750	0.9693	1.0046
QC10 (MVAR)	1.1748	4.9159	5.0000	4.6868	4.5850	3.1626
QC12	2.3807	3.3019	0.0029	0.1790	0.0289	0.0401
QC15	4.2578	4.1233	4.9995	4.4675	4.7603	3.8335
QC17	4.9792	5.0000	4.9941	5.0000	0.2594	4.9998
QC20	4.2860	4.4169	0.0	4.2431	4.9959	4.9997
QC21	4.9980	4.9918	4.9999	5.0000	4.7559	5.0000
QC23	3.3965	3.6741	3.5363	3.2614	4.9780	4.2152
QC24	4.9973	4.9986	5.0000	5.0000	4.9766	5.0000
QC29	2.6408	2.6782	2.7027	2.5507	2.7285	2.6110
Cost ($/h)	800.4791	646.4890	832.2134	859.0154	803.7176	830.2798
Emission (t/h)	0.3663	0.2835	0.4379	0.2289	0.3614	0.2529
Power losses (MW)	9.0212	6.7217	10.7009	4.5263	9.7753	5.5876
V.D. (p.u.)	0.9091	0.9277	0.8323	0.9298	0.0941	0.2971

method, which reduces the technique's overall complexity. The migration operator formula may be represented as a relation when using the modified cuckoo optimization approach, which is as follows:

$$X_i^{new} = X_i + rand \times (X_{best} - X_i) - rand \times (X_{worst} - X_i) \quad (21)$$

Here, *rand* represents the random values are numbers between 0 and 1.

3.3. Time Complexity

It is worthwhile to remember that MCOA's computational complexity is determined by three processes: initialization, fitness evaluation, and updating of the algorithm population. Consequently, the computational complexity of the initialization process is $O(Npop)$. As a result, the computational complexity of the updating mechanism is $O(Itermax + Npop)+O(Itermax + Npop + D)$, in which the aim is to find the most optimal location and update the location vector of all populations. The maximum number of iterations *itermax* is determined by the dimension of the problem, and D is the maximum number of iterations. MCOA, like the original COA algorithm, has a computational complexity of $O(Npop\times(Itermax + Itermax \times D + 1))$.

4. MCOA for Solving the Various OPF Problems in the IEEE standard 30-bus system

In this section, the proposed MCOA algorithm is implemented in MATLAB 2014a. And for load distribution analysis, MATPOWER (Zimmerman et al., n.d.) software is used. All cases are executed on the IEEE standard 30-bus system (Mohamed et al., 2017), which is used in many articles, as shown in Figure 1. For all investigated cases, a population of 60 and a number of repetitions of 400 were used in both COA and MCOA algorithms. In order to make the proposed MCOA method effective and compare it with COA, eight OPF scenarios have been considered and simulated.

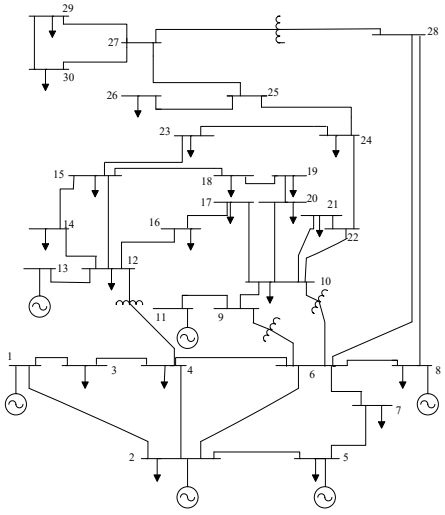

Figure 1: The layout of the IEEE 30-bus network.

In the supplemental material, Table 1 summarizes MCOA's conclusive findings for the 30-bus power system under six different OPF scenarios that do not use stochastic renewable energy.

work with. In the wild, a cuckoo will lay anywhere from 5 to 20 eggs in one location. Throughout several iterations, these values are utilized to determine the top and lower boundaries of the egg allotment given to each cuckoo.

The maximum laying range, also known as *ELR*, is a function of several factors, including the total number of eggs, the present number of cuckoo eggs, and the upper and lower bounds of the issue variables. In light of this, the *ELR* may be understood to refer to the following relationship:

$$ELR = \sigma \times \frac{\text{Number of current cuckoos eggs}}{\text{Tota l number of eggs } (Xmin_{max})} \quad (19)$$

σ The setting factor of the maximum radius is *ELR*.

Cuckoos have been seen to nest in the ELR of the host bird.

Then, after each round of egg-laying, the p% of eggs (often 10%) with the lowest objective function value or profit is destroyed.

Cuckoo habitats

K-means classification puts the cuckoos into groups, and k-values between 3 and 5 are generally enough. We can determine where a given community would be best served by averaging everyone's aims. Then the group whose average value of the goal function or profit is most significant is chosen as the target, and the other groups begin to move in that direction. Each cuckoo in this migration takes a detour φ from the best possible route, covering just δ% of the total distance between the origin and destination.

The cuckoo can better investigate its surroundings with these two variables. An angle φ between -π/6 and π/6, and δ a random value between 0 and 1, respectively. When all the cuckoos have arrived at their destination, and their new homes have been identified, they will each have a clutch of eggs. Each cuckoo is assigned an *ELR* based on its egg production, and laying starts afterward. The cuckoo optimization method uses a migration operator defined by the following formula:

$$X_i^{new} = X_i + F \times (X_{best} - X_i) \quad (20)$$

The parameter determines the level of divergence, denoted by F, and *Xbest* indicates the best solution the algorithm has produced to this point.

To keep the population from fluctuating too much, a maximum number of cuckoos, or algorithms, known as *Nmax*, has been established. If the cuckoo population surpasses this barrier, any birds found to be residing in areas where they are not welcome will be eradicated.

Convergent optimization with the use of COA

This method repeats itself until all cuckoo populations have the highest possible degree of egg likeness to their host birds and are situated such that they are close to the greatest number of food sources. This position will optimize revenues, or the function sought while lowering the number of eggs harmed.

3.2 The proposed method

The Cuckoo search algorithm has been updated to make local searches more effective in terms of their efficiency. In practice, the solutions in the COA move very quickly toward *Xbest* and a position equal to what they obtain with X_{best}. In other words, they become trapped in the optimal local solution, and the COA loses its ability to optimize, as shown by equation (20) and the simulations performed in this article. In addition, the COA loses its optimization power. Because of this, it is necessary to improve the algorithm's capability to do local searches. Because of this, we have suggested the usage of a new operator in the fundamental movement equation of the cuckoo optimization strategy. This operator is written as $-rand^*(X_{worst} - X_i)$. Whenever members of the population move very quickly to the X_{best} value and the value of $(X_{best} - X_i)$ tends to zero, the new operator $-rand^*(X_{worst} - X_i)$ tends to zero much more slowly due to the utilization of X_{worst}. This is the case regardless of whether the value of $(X_{best} - X_i)$ tends to zero. Therefore, members keep up their efforts to search and migrate around the country in the expectation that the outcomes of our simulation will illustrate the efficacy of the new search vector in the proper context. The F parameter of the modified COA (MCOA) is removed in favor of a random integer in this

$$T_i^{min} \le T_i \le T_i^{max} \quad (11)$$

$$Q_{Ci}^{min} \le Q_{Ci} \le Q_{Ci}^{max} \quad (12)$$

where T_i^{max} and T_i^{min} are the maximum and lowest taps of transformers for $i = 1, \ldots, NT$ that may be used to change the tap of the ith transformer. The range of VAR of the compensating compensators for $i = 1, \ldots, NC$ is denoted by Q_{Ci}^{min} and Q_{Ci}^{max}.

Finally, the following are some of the limitations of network security:

- The bus bar voltage constraints

As stated in (13), the voltage of system bus bars must be selected between the upper V_{Li}^{min} and lower V_{Li}^{max} limitations.

$$V_{Li}^{min} \le V_{Li} \le V_{Li}^{max}; i = 1, 2, \ldots, NPQ \quad (13)$$

- Power in transmission lines

The power in the network lines for $i = 1,2, \ldots, NTL$ should fulfill the relation (14):

$$S_{li} \le S_{li}^{max} \quad (14)$$

S_{li} and S_{li}^{max} signify the apparent power through ith transmission line and its higher range.

2.5 Control constraints

In order to consider the violation of the constraints of a penalty function, it is considered as follows (Ghasemi, Ghavidel, Gitizadeh, et al., 2015):

$$J = \sum_{i=1}^{NG} F_i(P_{Gi}) + \lambda_S \sum_{i=1}^{NTL} (S_{li} - S_{li}^{\lim})^2 + \lambda_V \sum_{i=1}^{NPQ} (V_{Li} - V_{Li}^{\lim})^2 + \lambda_Q \sum_{i=1}^{NG} (Q_{Gi} - Q_{Gi}^{\lim})^2 + \lambda_P (P_{G1} - P_{G1}^{\lim})^2 \quad (15)$$

where x^{lim} is a variable that is specified in the following equation as an auxiliary variable, where λ_S, λ_V, λ_Q, and λ_P are the punishment factors (Ghasemi, Ghavidel, Gitizadeh, et al., 2015):

$$x^{\lim} = \begin{cases} x & x^{\min} \le x \le x^{\max} \\ x^{\max}; & x > x^{\max} \\ x^{\min}; & x < x^{\min} \end{cases} \quad (16)$$

3 The Proposed Optimizer

3.1 COA overview

The key phases of the cuckoo bird optimization technique may be broken down (Rajabioun, 2011):

Stage 1: We'll randomly specify where the cuckoos are staying.

Stage 2: Distribute eggs among the cuckoos.

Stage 3: Calculate how far apart each cuckoo nest is.

Stage 4: The egg-laying by the cuckoo in the host bird's nest.

Stage 5: If host birds find eggs, they will be destroyed.

Stage 6: An incubator is used to grow eggs that have yet to be recognized.

Stage 7: Evaluate the cuckoos' new home.

Stage 8: After the maximum number of cuckoos for a specific area has been established, any cuckoos found in the wrong locations will be removed.

Stage 9: Cuckoos are sorted into groups using the k-means algorithm. The optimal cuckoo cluster is selected as the destination.

Stage 10: Transport the newly established cuckoo population to the designated area.

Stage 11: Verify the stop condition; if it has not been set, go to Step 2.

Production of cuckoo nesting areas (initial population solutions)

The habitat in this approach is an array whose elements are the values of the problem variables. The following is an example definition of a habitat for a *D*-dimensional optimization problem:

$$HabitatorX_i = [x_1, x_2, \ldots, x_D] \quad (17)$$

The degree of suitability (or amount of profit) in the current habitat is obtained by evaluating the profit function f in the habitat:

$$f(HabitatorX_i) = f([x_1, x_2, \ldots, x_D]) \quad (18)$$

It is sufficient to increase the cost function by a negative sign to use COA when finding solutions to minimization situations. Each of these environments is given a certain number of eggs to

following expression is used to create a typical OPF problem (Ghasemi, Ghavidel, Gitizadeh, et al., 2015):

$$MinF(u,x) \quad (1)$$
$$h(u,x) \leq 0 \quad (2)$$
$$g(u,x) = 0 \quad (3)$$

Within these associations, u and x represent, respectively, the independent and the control variables.

In addition, the objective function consists of a collection of equality requirements and a set of inequality constraints that pertain to the issue.

2.1 Control variables

The following are examples of control variables that are involved in OPF issue relationships (Ghasemi, Ghavidel, Gitizadeh, et al., 2015):

1. $P_{G_2},\ldots,P_{G_{NG}}$ The active power generated in the PV bus, except for the slack bus
2. $V_{G_1},\ldots,V_{G_{NG}}$ Voltage range in PV buses
3. $Q_{C_1},\ldots,Q_{C_{NC}}$ Compensation of parallel reactive amperes
4. $T_1,\ldots,T_{NT}$ Adjustment of tap transformers

According to the control variables, u is included:

$$u^T = \left[Q_{C_1},\ldots,Q_{C_{NC}},V_{G_1},\ldots,V_{G_{NG}},P_{G_2},\ldots,P_{G_{NG}},T_1,\ldots,T_{NT}\right] \quad (4)$$

Where *NG*, *NC* and *NT* show the number of generators, reactive power compensators and tap-changer transformers.

2.2 State variables

The set of state variables in OPF problem relationships include the following (Ghasemi, Ghavidel, Gitizadeh, et al., 2015):

1. P_{G_1} :Active production power in slack bass
2. $V_{L_1},\ldots,V_{L_{NPQ}}$ Voltage range in load buses
3. $Q_{G_1},\ldots,Q_{G_{NG}}$ Output reactive power of production units
4. $S_{l_1},\ldots,S_{l_{NTL}}$ Power loading in the lines

So, x is included:

$$x^T = \left[S_{l_1},\ldots,S_{l_{NTL}},Q_{G_1},\ldots,Q_{G_{NG}},V_{L_1},\ldots,V_{L_{NPQ}},P_{G_1}\right] \quad (5)$$

where the numbers represent the bus bars, network lines, and total lines (*NPQ*, *NTL*, and *NG*).

2.3 Equality constraints

The problem's insistence on equality places restrictions on how we may approach it, as discussed in this section. The technical status of the power network, as defined by OPF relations, is described by the parity constraints, also known as physical constraints, in OPF. This may convey these restrictions through the majority of the following links (Ghasemi, Ghavidel, Gitizadeh, et al., 2015):

$$P_{Gi} - P_{Di} - V_i \sum_{j=1}^{NB} V_j\left[B_{ij}\sin(\delta_i - \delta_j) + G_{ij}\cos(\delta_i - \delta_j)\right] = 0 \quad (6)$$

$$Q_{Gi} - Q_{Di} - V_i \sum_{j=1}^{NB} V_j\left[G_{ij}\sin(\delta_i - \delta_j) - B_{ij}\cos(\delta_i - \delta_j)\right] = 0 \quad (7)$$

Let's break this issue down into its component components to make things clearer:

"*i*" and "*j*" are bus number indices; "*Vi*" and "*Vj*" are voltage magnitudes; "*PGi*" and "*QGi*" are real and reactive power outputs from the generator; and "*QDi*" and "*PDi*" are real and reactive power demands from the load. Let's begin with "*i*" and "*j*" as these are the array indices. The following table details the susceptance *Bij* and conductance *Gij* of the branch connecting bus *i* and bus *j*, as well as the phase angle $(\delta_i - \delta_j)$ between the voltages of the buses and the total number of buses in the system.

2.4 Inequality constraints

The following are some technical limitations put on generators for *i*=1, 2, …, *NG* (Ghasemi, Ghavidel, Gitizadeh, et al., 2015):

$$V_{Gi}^{min} \leq V_{Gi} \leq V_{Gi}^{max} \quad (8)$$
$$P_{Gi}^{min} \leq P_{Gi} \leq P_{Gi}^{max} \quad (9)$$
$$Q_{Gi}^{min} \leq Q_{Gi} \leq Q_{Gi}^{max} \quad (10)$$

In this equation, V_{Gi}^{min} and V_{Gi}^{max} represent the minimum and maximum magnitudes of voltage for the *i*th unit, $P_{Gi}^{min}$and P_{Gi}^{max}represent the minimum and maximum values of real power for the *i*th unit, and $Q_{Gi}^{max}$and Q_{Gi}^{min}represent the maximum and minimum allowable values of reactive generation for the *i*th generator.

Furthermore, the following connections illuminate the technical limitations of transformers and parallel VAR compensators:

distance between the elite and their *k*-th closest neighbours. This keeps the population of the external archive accurate. Thirdly, the native search approach is included in the algorithmic program that makes up the strong Pareto organic process. The two-point estimation methodology (TPEM) (Saha et al., 2019), the social spider improvement algorithms (SSO) (Nguyen, 2019), and sine-cosine algorithm (SCA) (Attia et al., 2018; Dasgupta et al., 2020). The cuckoo optimization algorithm (COA) (Rajabioun, 2011) is a powerful and frequently used evolutionary optimization technique. It was invented by Ramin Rajabion in 2011 and is named after its namesake. This idea, which was first inspired by the cuckoo's habit of laying eggs and subsequently evolved to encompass the practice of stealing eggs from one's neighbours, has found application in a variety of industries like increasing lagrangian relaxation unit commitment (Zeynal et al., 2014), optimum coordination of directed overcurrent relays in microgrids (Dehghanpour et al., 2016), and electrical power system forecasting (Xiao et al., 2017), extreme learning machine for categorization of medical data (Mohapatra et al., 2015), etc.

It has been shown, however, that when used in complicated nonlinear circumstances, the technique risks being trapped in a local solution and losing the ability to optimize the solution (Dalali & Kazemi Karegar, 2016). The literature review shows that an efficient version of the COA has yet to be proposed for optimizing the various kinds of OPF problems. Also, some other optimization algorithms reviewed require improvements in robustness, finding better solutions, avoiding local optimal solutions, and improving convergence properties. Thus, this paper employs a new migration operator to balance the exploration-exploitation process strategically and improve the quality of optimal solutions through COA. The analysis of eight cases with different objectives on the IEEE 30-bus and IEEE 118-bus networks illustrated the cost-emission-effective scheduling of thermal power plants using renewable energies. Moreover, the simulation results demonstrate the MCOA's effectiveness and validity compared with other recently published algorithms for solving OPF problems. This study employs one of the effective strategies that has been applied in the past to maximize various load dispatch challenges in the two solar-and-wind-powered combined power systems.

Here are the main contributions of this paper:

1) Introducing a novel, efficient, and robust version of conventional cuckoo optimization algorithms, namely modified cuckoo optimization algorithms (MCOA), for optimizing optimal power flow (OPF) problems involving conventional thermal power plants and renewable energy sources, including solar photovoltaics and wind power distributed generation systems.
2) To address the uncertainties of renewable generations, in this work, the Weibull probability density function models the wind distribution, whereas the lognormal probability density function models the solar irradiation.
3) As part of the OPF problem, fuel costs, emissions, power losses, and voltage deviations are considered. These functions are constrained by economic, technical, and safety factors. Aside from the production cost of thermal power units, this study also considered reserve, direct, and penalty costs.
4) The amount of carbon tax is linked to the goal function to examine the potential effects of renewable energies on the optimal scheduling of thermal power plants in a cost-emission-effective manner.
5) Comparing the proposed MCOA and other recently published algorithms on the IEEE 30-bus and IEEE 118-bus networks to illustrate their effectiveness and validity.

This research continues in the following four sections: section 2, in which we discuss the formulation of OPF issues; section 3, in which we explain the concepts and structure of COA; and sections 4 and 5, in which we offer the proposed MCOA algorithm to solve OPF in the IEEE 30-bus and IEEE 118-bus networks, respectively. We will display and debate the simulation's results in the fourth part. In the concluding part, labelled "Conclusions," 6 will summarize the study's findings.

2 . OPF Problem Formulation

Solving the OPF problem involves determining and controlling a set of control variables to optimize the objectives in the operation of an electric network (while balancing all practical constraints). A primary goal is to minimize production costs while satisfying electrical demands.

A multiobjective OPF with different constraints is presented in this study as an alternative to other algorithms studied in the recent literature. The

1. Introduction

In today's engineering world, there is no standard and comprehensive way to address the problematic optimization issues of many sectors. Hence, hundreds of alternative strategies have been created recently, frequently proving their efficacy in handling specific optimization issues. One of the complicated challenges in engineering is optimal power flow (OPF), which is of significant significance in designing power systems (Ghasemi, Ghavidel, Gitizadeh, et al., 2015). The basic topic of OPF has been garnering the attention of researchers in the area of electrical engineering for more than 50 years. The first simplified issue is the OPF problem for vast networks (Ghasemi, Ghavidel, Gitizadeh, et al., 2015). In the past, researchers employed solution strategies based on mathematical methods such as nonlinear programming (NLP) (Alsac & Stott, 1974) to address these difficulties. Heuristic solutions were employed to address the OPF issue in the following. The difficulty of the actual OPF issue (owing to its nonlinear, non-convex and non-derivative character) has motivated academics to develop novel optimization approaches to address the problem in recent years.

Researchers have suggested the teaching-learning-based improvement (TLBO) algorithmic program increased with Lévy mutation (LTLBO) (Ghasemi, Ghavidel, Gitizadeh, et al., 2015), a modified lepidopteron swarm algorithm (MMSA) (Elattar, 2019) to account for indirect, overstated, and underestimated expenses connected with renewable energy systems. This endeavour aims to reduce the financial strain placed on businesses. Multiobjective accommodative guided differential evolution (DE) (Duman et al., 2021), a more effective method for multiobjective optimization of manta hunting (IMOMRFO) is presented in (Kahraman et al., 2022). Multiobjective mayfly algorithm (MOMA) (Kyomugisha et al., 2022), a particle swarm optimization (PSO) (Hazra & Sinha, 2011), Jaya algorithm (Warid et al., 2016), chaotic invasive weed optimization algorithms (CIWO) (Ghasemi, Ghavidel, Akbari, et al., 2014), and an algorithm for identifying new bacteria (MBFA) (Panda et al., 2017). At the level (Shi et al., 2011), a newly developed hybrid algorithmic program for the protection of OPF required the utilization of wind and heat generators. An new improved adaptive DE (Li et al., 2020), adaptive cluster search optimization (AGSO) (Daryani et al., 2016), ant lion algorithm (Maheshwari et al., 2021), the multiobjective First State algorithmic program (Elattar & ElSayed, 2019), the enhanced colliding bodies improvement (ICBO) (Bouchekara et al., 2016), BAT search algorithmic program (Venkateswara Rao & Nagesh Kumar, 2015), and the salp swarm algorithmic program (SSA) (Kamel et al., 2021). Improved artificial bee colonies (IABCs) (Khorsandi et al., 2013), multiobjective dynamic OPFs (Ma et al., 2019), the Harris hawks improvement (HHO) technique (Islam et al., 2020), a hybrid of phasor PSO (PPSO), and attraction search (PPSO-GSA) (Ullah et al., 2019) are also examples of recent developments in this field.

A novel hybrid firefly-bat algorithmic program with a constraints-priority object-fuzzy sorting approach has been developed and named gray wolf improvement (GWO) (Khan et al., 2020). This program is based on the firefly, and the bat (HFBA-COFS) (Chen et al., 2019), a hybrid PSO-GWO (Riaz et al., 2021) algorithmic program is created by combining the particle swarm optimization (PSO) method with the gray wolf optimization (GWO) algorithm. An anticipated security value dynamic OPF (ESCDOPF) with a hybrid system that makes use of both star resources and flexible resources (Kumari & Vaisakh, 2022), a bird swarm algorithmic program (BSA) (Ahmad et al., 2021), a chaotic Pan troglodytes optimizer (CBO) (Hassan et al., n.d.). Tunicate swarm algorithm (TSA) (El-Sehiemy, 2022), a modified flow of a water-based optimizer (TFWO) (Sarhan et al., 2022), and an improved hybrid PSO and GSA (PSOGSA) integrated with chaotic maps (CPSOGSA) for OPF with random alternative energy and FACTS devices (Duman, Li, et al., 2020). A new cross entropy-cuckoo search algorithm (CE-CSA) (Sarda et al., 2021), and a hybrid PSO and shuffle frog leap algorithmic program (SFLA) (Narimani et al., 2013).

Program with an improved algorithm for maximizing Pareto efficiency outlined in (Yuan et al., 2017) is three significant enhancements that have been made to the preliminary version of the algorithmic software for the Pareto organic process. To get things started, the population size of the external archive is just the number of persons who have a subordinate position in the choice operator of the surrounding environment. Second, the population of the external archive is maintained up to date by using the geometer

المملكة العربية السعودية
جامعة الحدود الشمالية (NBU)
مجلة الشمال للعلوم الأساسية والتطبيقية (JNBAS)
طباعة ردمد: 1658-7022/ إلكتروني – ردمد: 1658-7014
www.nbu.edu.sa
http://jnbas.nbu.edu.sa

التدفق الأمثل للطاقة مع مراعاة أنظمة الطاقة الشمسية وطاقة الرياح من خلال خوارزمية تحسين الوقواق المعدلة

عبدالعزيز فريح العنزي*

(قدم للنشر في 1444/9/11هـ؛ وقبل للنشر في 1445/2/21هـ)

مستخلص البحث: من خلال النظر في مجموعة متنوعة من الوظائف الموضوعية، أنشأت هذه المقالة طريقة تطورية فعالة وموثوقة لحل مشكلة تدفق الطاقة الأمثل متعدد القيود (OPF). حيث تقترح نموذج OPF متعدد الأهداف الذي يأخذ في الاعتبار مصادر الطاقة المتجددة في سيناريوهات عديدة. يعمل هذا النموذج على تحسين تكاليف الوقود والانبعاثات وفقدان الطاقة وتقلبات الجهد. تم أيضًا اقتراح خوارزمية تحسين الوقواق (MCOA) المعدلة للعثور على حلول تدفق الحمل الأمثل والمرضية. تم اختبار النموذج مقابل ثمانية سيناريوهات عبر شبكات IEEE 30-bus وIEEE 118-bus، مع الأخذ في الاعتبار وظائف موضوعية متعددة. توضح النتائج المثالية فعالية MCOA لـ OPF متعدد الأهداف مع قيود مختلفة مقارنة بالخوارزميات الأخرى التي تمت دراستها في الدراسات الحديثة.

كلمات مفتاحية: التدفق الأمثل للطاقة متعدد القيود، البحث المحلي، خوارزمية تحسين الوقواق، خوارزمية تحسين الوقواق المعدلة، وحدات الطاقة الشمسية وطاقة الرياح، وظائف التكلفة غير السلسة

*** للمراسلة:**
أستاذ مساعد، قسم الهندسة الكهربائية، كلية الهندسة، جامعة الحدود الشمالية ص ب: 1321 رمز بريدي: 91431 ، عرعر، المملكة العربية السعودية.

e-mail: af.alanazi@nbu.edu.sa

DOI: 10.12816/0061647

Journal of the North for Basic and Applied Sciences, Vol. (8), Issue (2), (November 2023/ Rabi' II 1445 H) 89-124

KINGDOM OF SAUDI ARABIA
Northern Border University (NBU)
Journal of the North for Basic & Applied Sciences(JNBAS)
p - ISSN : 1658 -7022 / **e-ISSN: 1658 - 7014**
www.nbu.edu.sa
s.journal@nbu.edu.sa

Optimal Power Flow Considering Solar and Wind Energy Systems Via Modified Cuckoo Optimization Algorithm

Abdulaziz Alanazi *

(Received 2/4/2023 ; accepted 6/9/2023)

Abstract: By considering a variety of objective functions, this paper has created an evolutionary method that is both effective and reliable for resolving the problem of multi-constraint optimal power flow (OPF). It proposes a multiobjective OPF model that considers renewable energy sources in numerous scenarios. This model optimizes fuel costs, emissions, power losses, and voltage fluctuations. The modified Cuckoo optimization algorithm (MCOA) is also suggested for finding optimized and satisfactory load flow solutions. The model is tested against eight scenarios over IEEE 30-bus and IEEE 118-bus networks, considering multiple objective functions. Optimal results demonstrate the effectiveness of MCOA for multiobjective OPF with various constraints compared to other algorithms studied in recent literature.

Keywords: Multi-constraint OPF, Local search, Cuckoo Optimization Algorithm, MCOA, Solar and wind energy units, Non-smooth cost functions

DOI: 10.12816/0061647

* **Corresponding Author:**
Assistant Professor, Electrical Engineering Dept., College of Engineering, Northern Border University, P.O. Box: 1321, Code: 91431, Arar, Kingdom of Saudi Arabia.

e-mail: af.alanazi@nbu.edu.sa

Wu, T. H., Pang, G. K. H., & Kwong, E. W. Y. (2014, December). Predicting systolic blood pressure using machine learning. In 7th international conference on information and automation for sustainability (pp. 1-6). IEEE.

Ye, C., Fu, T., Hao, S., Zhang, Y., Wang, O., Jin, B., ... & Ling, X. (2018). Prediction of incident hypertension within the next year: prospective study using statewide electronic health records and machine learning. Journal of medical Internet research, 20(1), e22.

Zhang, W. (2015). Identification of hypertension predictors and application to hypertension prediction in an urban Han Chinese population: A longitudinal study, 2005–2010. Preventing chronic disease, 12.

Farran, B., Channanath, A. M., Behbehani, K., & Thanaraj, T. A. (2013). Predictive models to assess risk of type 2 diabetes, hypertension and comorbidity: machine-learning algorithms and validation using national health data from Kuwait—a cohort study. BMJ open, 3(5), e002457.

Framingham, T., & Study, H. (2017). Article annals of internal medicine a risk score for predicting near-term incidence of hypertension. Annals of Internal Medicine, 148(2), 102–110. https://doi.org/10.7326/M16-1751.

Heo, B. M., & Ryu, K. H. (2018). Prediction of prehypertenison and hypertension based on anthropometry, blood parameters, and spirometry. International journal of environmental research and public health, 15(11), 2571.

Islam, S. M. S., & Maddison, R. (2021). Digital health approaches for cardiovascular diseases prevention and management: lessons from preliminary studies. Mhealth, 7.

Islam, S. M. S., & Tabassum, R. (2015). Implementation of information and communication technologies for health in Bangladesh. Bulletin of the World Health Organization, 93, 806-809.

Islam, S. M. S., Ahmed, S., Uddin, R., Siddiqui, M. U., Malekahmadi, M., Al Mamun, A., ... & Nahavandi, S. (2021). Cardiovascular diseases risk prediction in patients with diabetes: Posthoc analysis from a matched case-control study in Bangladesh. Journal of Diabetes & Metabolic Disorders, 20, 417-425.

Islam, S. M. S., Farmer, A. J., Bobrow, K., Maddison, R., Whittaker, R., Dale, L. A. P., ... & Chow, C. K. (2019). Mobile phone text-messaging interventions aimed to prevent cardiovascular diseases (Text2PreventCVD): systematic review and individual patient data meta-analysis. Open Heart, 6(2), e001017.

Islam, S. M. S., Peiffer, R., Chow, C. K., Maddison, R., Lechner, A., Holle, R., ... & Laxy, M. (2020). Cost-effectiveness of a mobile-phone text messaging intervention on type 2 diabetes—A randomized-controlled trial. Health Policy and Technology, 9(1), 79-85.

Kadomatsu, Y., Tsukamoto, M., Sasakabe, T., Kawai, S., Naito, M., Kubo, Y., ... & Wakai, K. (2019). A risk score predicting new incidence of hypertension in Japan. Journal of Human Hypertension, 33(10), 748-755.

Kanegae, H., Oikawa, T., Suzuki, K., Okawara, Y., & Kario, K. (2018). Developing and validating a new precise risk-prediction model for new-onset hypertension: The Jichi Genki hypertension prediction model (JG model). Journal of Clinical Hypertension, 20(5), 880–890.

Krittanawong, C., Zhang, H., Wang, Z., Aydar, M., & Kitai, T. (2017). Artificial intelligence in precision cardiovascular medicine. Journal of the American College of Cardiology, 69(21), 2657-2664.

Kshirsagar, A. V., Chiu, Y. L., Bomback, A. S., August, P. A., Viera, A. J., Colindres, R. E., & Bang, H. (2010). A hypertension risk score for middle-aged and older adults. The Journal of Clinical Hypertension, 12(10), 800-808.

Lim, N. K., Son, K. H., Lee, K. S., Park, H. Y., & Cho, M. C. (2013). Predicting the risk of incident hypertension in a Korean middle-aged population: Korean genome and epidemiology study. Journal of Clinical Hypertension, 15(5), 344–349.

Meinert, F., Thomopoulos, C., & Kreutz, R. (2023). Sex and gender in hypertension guidelines. Journal of Human Hypertension, 1-8.

Otsuka, T., Kachi, Y., Takada, H., Kato, K., Kodani, E., Ibuki, C., ... & Kawada, T. (2015). Development of a risk prediction model for incident hypertension in a working-age Japanese male population. Hypertension Research, 38(6), 419-425.

Paynter, N. P., Cook, N. R., Everett, B. M., Sesso, H. D., Buring, J. E., & Ridker, P. M. (2009). Prediction of incident hypertension risk in women with currently normal blood pressure. The American journal of medicine, 122(5), 464-471.

Pearson, T. A., LaCroix, A. Z., Mead, L. A., & Liang, K. Y. (1990). The prediction of midlife coronary heart disease and hypertension in young adults: The Johns Hopkins multiple risk equations. American Journal of Preventive Medicine, 6(2 SUPPL.), 23–28.

Ren, Z., Rao, B., Xie, S., Li, A., Wang, L., Cui, G., ... & Ding, S. (2020). A novel predicted model for hypertension based on a large cross-sectional study. Scientific Reports, 10(1), 1-9.

Sakr, S., Elshawi, R., Ahmed, A., Qureshi, W. T., Brawner, C., Keteyian, S., ... & Al-Mallah, M. H. (2018). Using machine learning on cardiorespiratory fitness data for predicting hypertension: The Henry Ford ExercIse Testing (FIT) Project. PLoS One, 13(4), e0195344.

Tayefi, M., Esmaeili, H., Karimian, M. S., Zadeh, A. A., Ebrahimi, M., Safarian, M., ... & Ghayour-Mobarhan, M. (2017). The application of a decision tree to establish the parameters associated with hypertension. Computer methods and programs in biomedicine, 139, 83-91.

Ture, M., Kurt, I., Kurum, A. T., & Ozdamar, K. (2005). Comparing classification techniques for predicting essential hypertension. Expert Systems with

Wang, B., Liu, Y., Sun, X., Yin, Z., Li, H., Ren, Y., ... & Hu, D. (2021). Prediction model and assessment of probability of incident hypertension: the Rural Chinese Cohort Study. Journal of Human Hypertension, 35(1), 74-84.

Weng, S. F., Reps, J., Kai, J., Garibaldi, J. M., & Qureshi, N. (2017). Can machine-learning improve cardiovascular risk prediction using routine clinical data?. PloS one, 12(4), e0174944.

Wu, T. H., Kwong, E. W. Y., & Pang, G. K. H. (2015, March). Bio-medical application on predicting systolic blood pressure using neural networks. In 2015 IEEE first international conference on big data computing service and applications (pp. 456-461). IEEE.

where age (Ren, Rao, Xie, Li, Wang, Cui, et al., 2020; Sakr, Elshawi, Ahmed, Qureshi, Brawner, Keteyian, et al., 2018; Kanegae et al., 2018), diabetes (Kshirsagar, Chiu, Bomback, August, Viera, Colindres, et al., 2010; Farran, Channanath, Behbehani, & Thanaraj, 2013; Sakr et al., 2018), cholesterol level (Tayefi, Esmaeili, Karimian, Zadeh, Ebrahimi, Safarian, et al., 2017; (Wu, Pang, & Kwong, 2014,& Wu, Kwong, & Pang, 2015) and BMI (Kshirsagar et al., 2010; Ren et al., 2020; Akdag, Fenkci, Degirmencioglu, Rota, Sermez, & Camdeviren, 2006). were identified as predictors of hypertension in various hypertension risk assessment models.

According to the findings of this study, general health was found to be a predictor of hypertension for the first time. This study showed that subjects who reported poor general health had a higher likelihood of developing hypertension. This study aimed to use non-invasive data to develop machine learning (ML) models to predict hypertension, utilizing the effectiveness and cost-effectiveness of mobile phones and digital technologies, which have been demonstrated in previous studies (Islam & Maddison, 2021; Islam, Peiffer, Chow, Maddison, Lechner, Holle, et al., 2020; Islam, Farmer, Bobrow, Maddison, Whittaker, Dale, et al., 2019; Islam & Tabassum, 2015; Krittanawong, Zhang, Wang, Aydar, & Kitai, 2017).

The results of this study should be interpreted with caution, taking into consideration several limitations. Firstly, only a limited number of variables were included in the models, and data on other risk factors such as family history, race, alcohol consumption, waist-hip ratio, physical activity levels, dietary intake, and biochemical parameters were unavailable, which might have affected the measurement precision. Secondly, the risk factors may have changed since some of the study data was from the 2016 survey. Thirdly, ML models have a weakness in claiming causation. Finally, the models were not externally validated using other data sources, so their results should be interpreted with caution.

Despite these limitations, the primary strength of this study is the use of large-scale nationally representative survey data using ML approaches to predict hypertension.

The findings of this study indicate that machine learning models can effectively predict hypertension using simple information such as age and diabetes, which were found to be among the most significant risk factors in our study population (Ye, Fu, Hao, Zhang, Wang, Jin, et al., 2018; Weng, Reps, Kai, Garibaldi, & Qureshi, 2017). However, future research is necessary to incorporate additional risk factors and biomarkers related to hypertension. These models could be made accessible online or through mobile phone applications, allowing individuals to check their hypertension risk at home by answering basic questions such as age, BMI, and sex. A two-step approach can also be implemented in clinical practice, where the ML model first identifies individuals at risk of hypertension and then a physician confirms the diagnosis and provides appropriate treatment (Ye et al., 2018).

Conclusion

This study highlights the superiority of ML models compared to traditional statistical techniques when it comes to dealing with complex relationships between variables that cannot be fully comprehended using standard statistics. This has significant implications for hypertension prevention, as these ML models can be applied to population-level data for hypertension screening.

References:

Akdag, B., Fenkci, S., Degirmencioglu, S., Rota, S., Sermez, Y., & Camdeviren, H. (2006). Determination of risk factors for hypertension through the classification tree method. Advances in therapy, 23, 885-892.

Bromfield S, Muntner P. High blood pressure: The leading global burden of disease risk factor and the need for worldwide prevention programs. Curr. Hypertens. Rep. 2013;15(3):134–136.

Chen, Y., Wang, C., Liu, Y., Yuan, Z., Zhang, W., Li, X., ... & Zhang, C. (2016). Incident hypertension and its prediction model in a prospective northern urban Han Chinese cohort study. Journal of human hypertension, 30(12), 794-800.

Chowdhury, M. Z., & Turin, T. C. (2020). Precision health through prediction modelling: factors to consider before implementing a prediction model in clinical practice. Journal of primary health care, 12(1), 3-9.

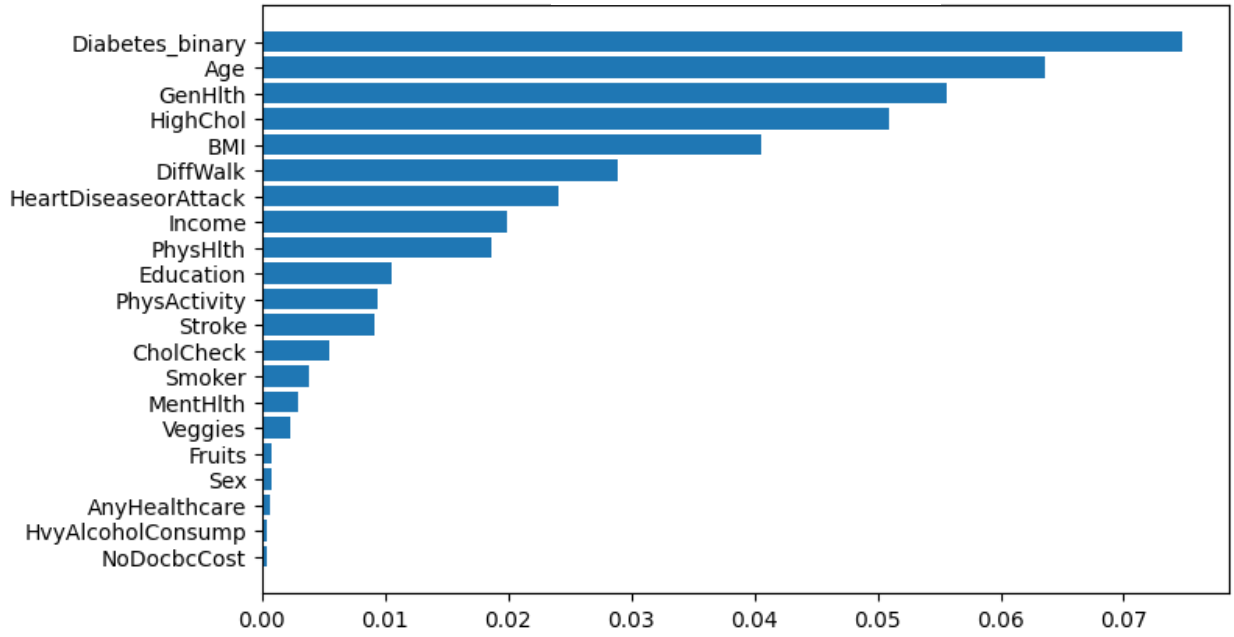

Figure 1: Mutual information scores of the selected variables.

In this study, predictive models for hypertension were built using various machine learning models instead of conventional methods. This study reports that Gradient Boosting Classifier, XGBoost, Adaboost, and MLP performed best with a ROC-AUC of 0.81 and accuracy of 0.74 on the test dataset followed by logistic regression. Among these, Gradient Boosting Classifier and XGBoost had slightly higher recall, while MLP had the highest precision followed by Adaboost. Both precision and recall are important when predicting hypertension, as they provide different but complementary measures of accuracy. Precision measures how many of the predicted labels are correct, while recall measures how many of the actual labels are correctly identified. In other words, precision measures how many true positives were identified, while recall measures how many false negatives were identified. Both measures are important when predicting hypertension, as accuracy is key when diagnosing and treating the condition. Therefore, building an ensemble model using these four models may deliver better accuracy.

Several studies have used mathematical techniques and machine learning models to predict risk in healthcare, including decision trees, statistical algorithms, and neural networks (Islam, Ahmed, Uddin, Siddiqui, Malekahmadi, Al Mamun, & Nahavandi, 2021). One study found that neural networks were the best predictor of hypertension, but its results were limited by missing data on obesity (Ture, Kurt, Kurum, & Ozdamar, 2005). Another study used decision trees, logistic regression, and Naive Bayes classifiers to predict hypertension using variables such as obesity, biomarkers, and spirometry indices, but was limited by a lack of data on other factors such as wealth index, education levels, smoking, alcohol use, and physical activity (Heo & Ryu, 2018).

The selected features in this study, including age, diabetes, high cholesterol, and general health, were found to have the strongest relationship with hypertension. This aligns with previous research,

The KNN model has a slightly higher test ROC-AUC and accuracy compared to the DT model, but still lower than the top models.
Overall, the top four models, Gradient Boosting Classifier, XGBBoost, Adaboost and, MLP are the best performance models in this case, with almost similar performance in terms of test ROC-AUC, accuracy, F1 Score, precision, and recall.

Table 2: Models metrics.

Model	Train ROC-AUC	Test ROC-AUC	Accuracy	F1 Score	Precision	Recall
Gradient Boosting Classifier	0.82	0.81	0.74	0.78	0.74	0.83
XGBBoost	0.82	0.81	0.74	0.78	0.74	0.83
Adaboost	0.81	0.81	0.74	0.78	0.75	0.81
MLP	0.81	0.81	0.74	0.77	0.76	0.79
Logistic Regression	0.80	0.80	0.73	0.77	0.74	0.81
Random Forest	1.00	0.78	0.73	0.77	0.74	0.81
XGBRFBoost	0.79	0.78	0.72	0.76	0.74	0.79
KNN	0.87	0.74	0.70	0.74	0.72	0.76
Decision Tree	1.00	0.64	0.64	0.67	0.69	0.66
mean	0.85	0.77	0.72	0.76	0.73	0.79
SD	0.08	0.05	0.03	0.03	0.02	0.05
Ensemble	0.96	0.80	0.74	0.77	0.76	0.79

To improve the accuracy of predictions in a model, it is important to identify the most important features. This can be done by analyzing the mutual information scores between various features and the dependent variable, hypertension, figure 1. A high mutual information score indicates a strong relationship between the feature and hypertension, while a low score indicates a weak relationship.
Diabetes_binary and Age have a high mutual information score of 0.09 and 0.07, respectively, signifying a strong relationship with hypertension. GenHlth and HighChol have a moderate relationship with hypertension. BMI has a lower relationship with hypertension compared to HighChol. DiffWalk, HeartDiseaseorAttack, Income, PhysHlth, Education, CholCheck, Stroke, PhysActivity, Veggies, AnyHealthcare, Smoker, Fruits, MentHlth, Sex have low scores, indicating a very weak relationship with hypertension. NoDocbcCost and HvyAlcoholConsump have a score of 0, indicating no relationship.

When deciding which features to include in a model, the mutual information scores should be taken into consideration. Typically, features with low scores are dropped as they do not provide significant information to the model. Thereore, droping BMI HighChol. DiffWalk, HeartDiseaseorAttack, Income, PhysHlth, Education, CholCheck, Stroke, PhysActivity, Veggies, AnyHealthcare, Smoker, Fruits, MentHlth, Sex will improve the perfomacne of the prediction models.

3. RESULTS AND DISCUSSION

The data analyzed in this study involves the examination of health-related variables of individuals, with all variables being categorical, table 1. There are 22 features, including Diabetes_binary, which indicates whether an individual has diabetes, with 0 being no diabetes, and 1 diabetes. The most common value is 0, appearing in 50% of the data. HighBP represents whether an individual has high blood pressure, with the most common value being 1 (indicating high blood pressure) appearing in 56% of the data. HighChol indicates high cholesterol levels, with 53% of individuals having high cholesterol. CholCheck represents whether an individual has had a cholesterol check in the past 5 years, with 98% of individuals having had a check. Smoker indicates whether an individual has smoked at least 100 cigarettes in their lifetime, with 52% of individuals reporting no. Stroke and Heart Disease or Attack represent if an individual has had a stroke or coronary heart disease, respectively, with 94% and 85% reporting no. PhysActivity and Fruits represent physical activity and daily fruit consumption, respectively, with 70% and 61% of individuals reporting positive. Veggies indicates daily vegetable consumption, with 79% of individuals reporting positive. HvyAlcoholConsump represents heavy alcohol consumption, with 96% of individuals reporting no. Other features include AnyHealthcare (95% have healthcare coverage), NoDocbcCost (91% have not been unable to see a doctor due to cost), GenHlth (33% rate their health as good), MentHlth (68% report no days of poor mental health), PhysHlth (56% report no days of physical illness), DiffWalk (75% have no difficulty walking) and Sex (54% female). The age distribution shows that the top group comprises 60-64 years old, accounting for 15% of the study population. The average BMI of the sample group is 29.86, signaling that the majority are classified as overweight. The distribution of the BMIs is well spread with a standard deviation of 7.11.

To evaluate the performance of the models used to predict hypertension, a variety of metrics were employed, including ROC-AUC, accuracy, F1 Score, precision, and recall. Table 2 shows the evaluation of all models used in this study. The given statistics in the table show the performance of the individual and ensemble models. For the individual models, the mean values ± standard deviation of Train ROC-AUC, Test ROC-AUC, Accuracy, F1 Score, Precision, and Recall are 0.85 ± 0.08, 0.77 ± 0.05, 0.72 ± 0.03, 0.76 ± 0.03, 0.73 ± 0.02, and 0.79 ± 0.05, respectively. These results indicate that the models have a good average performance, with Train ROC-AUC having the highest mean and accuracy having the lowest mean, but with relatively small standard deviations.

The Gradient Boosting Classifier, XGBBoost, Adaboost and MLP have the highest test ROC-AUC with a value of 0.81, followed by logistic with a value of 0.80. The accuracy of all four models is also the same with a value of 0.74 followed by logistic with a value of 0.73. The Gradient Boosting Classifier, XGBBoost, Adaboost have the highest F1 Score followed by MLP and logistic. Logistic have the highest precision followed by adaboost then both Gradient Boosting Classifier, XGBBoost. Gradient Boosting Classifier, XGBBoost have the highest recall followed by adaboost and logistic then MLP. XGBRFBoost model has slightly lower test ROC-AUC, accuracy, F1 Score and precision values compared to the top five models, but, similar recall as MLP.

The high difference between the Train ROC-AUC and Test ROC-AUC values for the RF and DT models suggests that these models are overfitting to the training data and not performing well on the test data. This means that these models are not generalizing well to new unseen data and therefore, they are not the best models for this task. This is a common issue with decision tree-based models, as they tend to memorize the training data and perform poorly on new unseen data. The Ensemble model which has high Train ROC-AUC value but it also has a large difference between the Train ROC-AUC and Test ROC-AUC values and low-test accuracy, F1 Score, Precision, and Recall values, indicating that it also suffers from the same overfitting issue. The DT model has the lowest test ROC-AUC and accuracy, with a value of 0.64, and it also has the lowest F1 Score, precision, and recall values.

Table 1: Variables descriptions.

Variable	Definition
Diabetes_binary	0 (No Diabetes), 1 (Diabetes)
HighBP	0 (No High Blood Pressure), 1 (High Blood Pressure)
HighChol	0 (No High Cholesterol), 1 (High Cholesterol)
CholCheck	0 (No Check), 1 (Cholesterol Check Done)
BMI	1: Underweight (BMI < 18.5 Kg/m^2), 2: Normal weight (BMI 18.5-24.9 Kg/m^2), 3: Overweight (BMI 25 - 29.9 Kg/m^2), 4: Obese (BMI ≥ 30 Kg/m^2)
Smoker	0 (No), 1 (Yes)
Stroke	0 (No), 1 (Yes)
HeartDiseaseorAttack	0 (No), 1 (Yes)
PhysActivity	0 (No), 1 (Yes)
Fruits	0 (No), 1 (Yes)
Veggies	0 (No), 1 (Yes)
HvyAlcoholConsump	0 (No), 1 (Yes)
AnyHealthcare	0 (No), 1 (Yes)
NoDocbcCost	0 (No), 1 (Yes)
GenHlth	Response to: you say that in general your health is: 1 (Excellent), 2 (Very Good), 3 (Good), 4 (Fair), 5 (Poor)
MentHlth	0 to 30 (number of days in the past 30 days that an individual reported poor mental health)
PhysHlth	0 to 30 (number of days in the past 30 days that an individual reported physical illness or injury)
DiffWalk	0 (No Difficulty), 1 (Serious Difficulty)
Sex	0 (Female), 1 (Male)
Age	13-level category (1: 18-24 y, 2: 25-29 y, 3: 30-34 y, 4: 35-39 y, 5: 40-44 y, 6: 45-49 y, 7: 50-54 y, 8: 55-59 y, 9: 60-64 y, 10: 65-69 y, 11: 70-74 y, 12: 75-79 y, 13: 80 y and above)
Education	6-level category (1-Never attended school or only attended kindergarten, 2, Grades 1 through 8 (Elementary), 3- Grades 9 through 11 (Some high school), 4- Grade 12 or GED (High school graduate), 5- College 1 year to 3 years (Some college or technical school), 6- College 4 years or more (College graduate)
Income	1: <$10 K, 2: $10–$15 K, 3: $15–$20 K, 4: $20–$25 K, 5: $25–$35 K, 6: $35–$50 K, 7: $50–$75 K, 8: >$75 K

1. INTRODUCTION

Hypertension is a critical public health challenge that affects a diverse range of demographic groups globally and is the leading risk factor for preventable cardiovascular morbidity and mortality (Bromfield & Muntner, 2013). Despite efforts to improve hypertension detection, treatment, and control, there has been little focus on primary prevention (Meinert & Thomopoulos, 2023).

Identifying individuals at an elevated risk of developing hypertension and target them for early prevention and treatment, health and clinical research initiatives aim to screen and predict hypertension risk. A prediction model can screen for high-risk individuals by estimating their probability of developing hypertension within a certain time frame (Chowdhury & Turin, 2020). While machine learning algorithms have proven successful in various fields, most hypertension prediction models still rely on conventional regression-based models (Chen, Wang, Liu, Yuan, Zhang, Li, et al., 2016; Framingham & Study, 2017; Kadomatsu, Tsukamoto, Sasakabe, Kawai, Naito, Kubo, et al., 2019; Kanegae, Oikawa, Suzuki, Okawara, & Kario, 2018; Lim, Son, Lee, Park, & Cho, 2013; Otsuka, Kachi, Takada, Kato, Kodani, Ibuki, et al., 2015; Paynter, Cook, Everett, Sesso, Buring, & Ridker, 2009; Pearson, LaCroix, Mead, & Liang, 1990; Wang, Liu, Sun, Yin, Li, Ren, et al., 2021; Zhang, 2015).

Hence, the purpose of this research is to construct a straightforward and feasible hypertension risk prediction model and validate it internally trying different machine learning models either as standalone models or in an ensemble fashion.

2. METHODS

Data source

This study conducted a cross-sectional analysis utilizing secondary data from the 2015 Behavioral Risk Factor Surveillance System (BRFSS) of the USA Centers for Disease Control and Prevention (CDC). The BRFSS is an open-access online database freely available to the public under the CC0 1.0 Universal (CC0 1.0) Public Domain Dedication license. The original data set consisted of 330 features and a total of 441,456 records.

Data analysis

The preprocessing of data for this study involved several steps including data cleaning, normalization, feature selection, and engineering. Data cleaning involved removing outliers and missing values, while data normalization scaled the data to a specific range. Feature selection involved selecting the most relevant features, and feature engineering combined existing features or created new ones. The final result was 70692 samples selected with 22 features, table 1. Out of the total records, 39,832 subjects were diagnosed with hypertension.

Multiple supervised machine learning algorithms have been evaluated for their ability to predict hypertension by using models either alone or in a combined manner. The models used for this purpose include Gradient Boosting Classifier, XGBoost, Adaboost, MLP, Logistic Regression, Random Forest (RF), XGBRFBoost, KNN, and Decision Trees(DT). These models were constructed using Google Colab and the Python programming language, with the aid of libraries such as numpy, pandas, matplotlib, seaborn, and sklearn. The code imports a dataset, performs data analysis and preprocessing, and separates the data into X and Y variables for machine learning model training and testing. The code evaluates various machine learning models metrics like ROC-AUC, accuracy, F1 score, precision, and recall. Additionally, the code uses an ensemble approach to combine the predictions of several models for a final prediction and calculates the ROC-AUC score. The code also determines the Mutual Information scores for the dataset's features.

المملكة العربية السعودية
جامعة الحدود الشمالية (NBU)
مجلة الشمال للعلوم الأساسية والتطبيقية (JNBAS)
طباعة ردمد: 1658-7022/ إلكتروني – ردمد: 1658-7014
www.nbu.edu.sa
http://jnbas.nbu.edu.sa

الوقاية من ارتفاع ضغط الدم من خلال التنبؤ بالمخاطر القائم على التعلم الآلي

سعيد عوض القحطاني

(قدم للنشر في 1444/7/14هـ؛ وقبل للنشر في 1445/3/4هـ)

مستخلص البحث: هدفت هذه الدراسة إلى التحقق من صحة نموذج توقع ارتفاع ضغط الدم باستخدام نماذج متعددة للتعلم الآلي ، بما في ذلك Gradient Boosting Classifier و XGBoost و Adaboost و MLP و Random Forest و XGBRFBoost و KNN و Decision Trees. تم استخدام البيانات من المركز الأمريكي (CDC) المتخصص في السيطرة على الأمراض والوقاية منها ، مع مجموعة البيانات المعالجة مسبقًا التي تتكون من 22 متغير و 70692 عينة. تم إجراء التقييم باستخدام عدد من أدوات التقييم ومنها ROC-AUC ، وأظهرت النتائج أفضل النماذج التي تتمتع بأداء عالٍ. وخلصت الدراسة إلى أن نماذج التعلم الآلي تتفوق في الأداء على الأساليب الإحصائية التقليدية للتنبؤ بمخاطر ارتفاع ضغط الدم المعقد ، مما يوفر فحصًا محسنًا للوقاية.

كلمات مفتاحية: نماذج التعلم الآلي ، ارتفاع ضغط الدم ، مقاييس التقييم.

للمراسلة:
أستاذ مشارك. قسم: علم وظائف الأعضاء ، جامعة طيبة، المدينة المنورة.

e-mail: dr_alqahtani@hotmail.com

DOI: 10.12816/0061646

Journal of the North for Basic and Applied Sciences, Vol. (8), Issue (2), (November 2023/ Rabi' II 1445 H) 79-88

KINGDOM OF SAUDI ARABIA
Northern Border University (NBU)
Journal of the North for Basic & Applied Sciences(JNBAS)
p - ISSN : 1658 -7022 / **e-ISSN: 1658 - 7014**
www.nbu.edu.sa
s.journal@nbu.edu.sa

Maximizing Hypertension Prevention through Machine Learning-Based Risk Prediction

Saeed Awad M. Alqahtani *

(Received 5/2/2023 ; accepted 19/9/2023)

Abstract: Background: Most current hypertension prediction models rely on conventional regression-based models, but this research aims to validate a straightforward and feasible model using various machine learning models such as Gradient Boosting Classifier, eXtreme Gradient Boosted (XGBoost), Adaptive Boosting (Adaboost), Multi-layer perceptron (MLP), Logistic Regression, Random Forest, eXtreme Gradient Boosted Random Forest (XGBRFBoost), K-Nearest Neighbors (KNN), and Decision Trees. Method: This study used data from the USA Centers for Disease Control and Prevention to predict hypertension using multiple machine learning algorithms. The preprocessed data set consists of 22 features and 70692 samples. Each individual and ensemble models were evaluated using ROC-AUC, accuracy, F1 score, precision, and recall. Results: The results show that the top 4 models that have high performance in terms of ROC-AUC, accuracy, F1 Score, precision, and recall are Gradient Boosting Classifier (Train ROC-AUC = 0.82, Test ROC-AUC = 0.81, Accuracy = 0.74, F1 Score = 0.78, Precision = 0.74, Recall = 0.83), XGBBoost (Train ROC-AUC = 0.82, Test ROC-AUC = 0.81, Accuracy = 0.74, F1 Score = 0.78, Precision = 0.74, Recall = 0.83), Adaboost (Train ROC-AUC = 0.81, Test ROC-AUC = 0.81, Accuracy = 0.74, F1 Score = 0.78, Precision = 0.75, Recall = 0.81) , MLP (Train ROC-AUC = 0.81, Test ROC-AUC = 0.81, Accuracy = 0.74, F1 Score = 0.77, Precision = 0.76, Recall = 0.79). Conclusion: This study shows Machine learning models outperform traditional statistical methods for complex hypertension risk prediction, offering improved screening for prevention.

Keywords: Machine learning Models, Hypertension, Evaluation metrics.

DOI: 10.12816/0061646

* **Corresponding Author:**
Associate Professor, Dept.: Physiology, Faculty: Medicine, University: Taibah, City: Medina, Kingdom of Saudi Arabia.

e-mail: dr_alqahtani@hotmail.com

Manuscripts in English Language

Journal of the North for Basic and Applied Sciences (JNBAS)
p-ISSN: 1658- 7022 e-ISSN: 1658- 7014

Vol. 8, Issue 2 November 2023 - Rabi' II 1445 H

CONTENTS

Manuscripts in Arabic Language

Manuscripts in English Language

Citation from a book of more than one author:

Timothy, N., Stepich, D., & James, R. (2014/1434 H) *Instructional technology for teaching and learning.* Riyadh, Kingdom of Suadi Arabia: University of King Saud Publications.

Citation from Periodicals:

Al Nafaa, A. H. (1427 H). Effect of driving off–road on wild vegetation parks: A study in environmental protection, in the center of the Kingdom of Saudi Arabia. *Saudi Journal of Life Sciences, 14*(1), 35-72.

Citation from M.A. or Ph.D. Thesis:

AlQadi, I. A. (1429 H). *Natural Plants in a Coastal Environment between Rassi Tanoura and Elmalouh in the Eastern Region: A Study in Botanical Geography and the Protection of Environment.* Unpublished Ph.D. Dissertation, College of Arts for Girls, Dammam, Kingdom of Suadi Arabia: King Faisal University.

Citation from Internet References:

Citing an online book:

Almazroui, M .R. & Madani, M. F. (2010). *Evaluation of performance in Higher Education Institutions.* Digital Object Identifier (doi:10.xxxx/xxxx-xxxxxxxx-x), or the Hypertext Transfer Protocol (http://www...), or the International Standard Book Number (ISBN: 000-0-00-000000-0) must be mentioned.

Citing an article in a periodical:

Almadani, M. F. (2014). The definition of debate in reaching consensus. *The British Journal of Educational Technology, 11*(6), 225-260. Digital Object Identifier (doi:10.xxxx/xxxx-xxxxxxxx-x) or the Hypertext Transfer Protocol (http://onlinelibrary.wiley.com/journal/10.1111), or the International Standard Serial Number of the journal (ISSN: 1467- 8535) must be mentioned.

15. It is the researcher's responsibility to translate into English the Arabic bibliography.

Example:

الجبر، سليمان. (1991م). تقويم طرق تدريس الجغرافيا ومـدى اختلافها باختلاف خبـرات المدرسين وجنسياتهم وتخصصاتهم في المرحلة المتوسطة بالمملكة العربية السعودية. ***مجلة جامعة الملك سعود- العلوم التربوية، 3***(1)، 143-170.

Al-Gabr, S. (1991). The evaluation of geography instruction and the variety of its teaching concerning the experience, nationality, and the field of study in intermediate schools in Kingdom of Saudi Arabia *(in Arabic). Journal of King Saud University- Educational Sciences, 3*(1), 143-170.

16. Numerals should be the original Arabic numbers (0, 1, 2, 3 ...) in the manuscript.

Required Documents

Researchers are required to submit the following:

1. An electronic copy of their submissions in two formats: Microsoft Word Document (WORD) and Portable Document Format (PDF), to be sent to the following email:

s.journal.nbu@gmail.com

&

s.journal@nbu.edu.sa

2. The researcher's CV, including his/her full name in Arabic and English, current work address, email, and academic rank.
3. The researcher must fill out and submit the application for publishing in the Journal of the North, along with the Pledge Statement that his/her submission has not been published before or has not been submitted for publishing elsewhere.

NB

1. The submissions received by the Journal of the North will not be returned whether they are published or not.
2. The published papers reflect only the author's points of view.
3. All accepted manuscripts devolve their property to *the Journal of the North for Basic and Applied Sciences (JNBAS)*.

PUBLICATION INSTRUCTIONS FOR AUTHORS

Submission Guidelines

1. Manuscript must not exceed 35 pages of plain paper (A4).
2. Manuscript must have a title and an abstract in both Arabic and English on one page; the abstract should not be more than 250 words. The manuscript should include, in both languages, keywords that indicate the field of specialization. The keywords are written below each summary and should not be more than six.
3. The author(s) name(s), affiliation(s) and address(es) must be written immediately below the title of the article, in Arabic and English.
4. The Arabic manuscript is typed in Simplified Arabic, in 14-font size for the main text, and 12-font size for notes.
5. The English manuscript is typed in Times New Roman, in 12- font size for the main text, and 9-font size for notes.
6. The manuscript is typed only on one side of the sheet, and line spacing should be single. Margins should be 2.5 cm (or 1.00 inches) on all four sides of the page.
7. The manuscript must have the following organization:

   Introduction: It should indicate the topic and aims of the research paper, and be consistent with its ideas, information and the established facts. The research problem(s) and importance of the literature review should also be introduced.

   Body: The manuscript body includes all necessary and basic details of research approach, tools and methods. All stated information should be arranged according to priority.

   Findings and Discussion: Research findings should be clear and brief, and the significance of these findings should be elucidated without repetition.

   Conclusion: It is a brief summary of the research topic, findings, recommendations and suggestions.
8. Figures, diagrams and illustrations should be included in the main text and consecutively numbered and given titles, with explanatory notes beneath them.
9. Tables should also be included in the main text, consecutively numbered and given titles at the top, with explanatory notes below.
10. Footnotes should be added at the bottom of each page, when necessary. They are to be indicated by numbers or asterisks, in 12-font size for Arabic and 9-font size for English.
11. The Journal of the North does not publish research and measurement tools (instruments). However, they must be included in the submission(s).
12. Citations must follow the American Psychological Association (APA) reference style in which both the author's name and year of publishing are mentioned in the main text, i.e. (name, year). Numbering the references inside the main text and adding footnotes are not allowed.

    Researchers' documentation must be as follows:

    - For single author, the author's family name, followed by a comma, and the publishing year, such as (Khayri, 1985). Page numbers are indicated in the main text in case of quotations, such as (Khayri, 1985, p. 33).
    - If a manuscript has two authors, they must both be cited as shown previously, e.g. (AL-Qahtani & AL-Adnani, 1426 H).
    - If there are multiple (more than two) authors, their family names must be mentioned the first time only, e.g. (Zahran, Al-Shihri, & Al-Dusari, 1995); if the researcher is quoting the same work several times, the family name of the first author followed by *"et al."*[for papers in English] and by "وآخرون" [for papers in Arabic] must be used, e.g. (Zahran *et al.*, 1995) / (زهران وآخرون، 1995) Full publishing data must be mentioned in the bibliography.
13. Hadith documentation must follow the following example: (Sahih Al-Bukhari, vol.1, p.5, hadith number 511).
14. The bibliography, list of all the sources used in the process of researching, must be added in alphabetical order using the author's last name according to the APA reference style (6th edition) in 12-font size for Arabic and 9-font size for English.

    The bibliography should be organized as follows:

    Citation from books:

    Citation from a one-authored book:

    Shotton, M. A. (1989). *Computer education? A study to computer dependency.* London, England: Taylor & Francis.

Journal of the North for Basic and Applied Sciences (JNBAS)

About the Journal

The Journal of the North is concerned with the publication of original, genuine scholarly studies and researches in Basic and Applied Sciences in Arabic and English. It publishes original papers, review papers, book reviews and translations, abstracts of dissertations, reports of conferences and academic symposia. It is a biannual publication (May and November).

Vision

The journal seeks to achieve leadership in the publication of refereed scientific papers and rank among the world's most renowned scientific periodicals.

Mission

The mission of the journal is to publish refereed scientific researches in the field of Basic & Applied Sciences according to well-defined international standards.

Objectives

1. Serve as a scholarly academic reference for researchers in the field of Basic & Applied Sciences.
2. Meet the needs of researchers, publish their scientific contributions and highlight their efforts at the local, regional and international levels.
3. Participate in building a knowledge community through the publication of research that contributes to the development of society.
4. Cover the refereed works of scientific conferences.

Terms of Submission

1. Originality, innovation, and soundness of both research methodology and orientation.
2. Sticking to the established research approaches, tools and methodologies in the respective discipline.
3. Accurate documentation.
4. Language accuracy.
5. The contribution must be unpublished or not submitted for publication elsewhere.
6. The research extracted from a thesis/dissertation must be unpublished or not submitted for publishing elsewhere and the researcher must indicate that the research submitted for publishing in the journal is extracted from a thesis/dissertation.

Correspondence

Editor-in-Chief
Journal of the North for Basic and Applied Sciences (JNBAS),
Northern Border University, P.O.Box 1321, Arar 91431,
Kingdom of Saudi Arabia.
Tel: +966(014)6615499
Fax: +966(014)6614439
email: *s.journal@nbu.edu.sa*
Website: *www.nbu.edu.sa*

Subscription & Exchange

Scientific Publishing Center,
Northern Border University,
P.O.Box. 1321, Arar 91431,
Kingdom of Saudi Arabia.

Journal of the North for Basic and Applied Sciences

(JNBAS)

Peer-Reviewed Scientific Journal

Published by

Scientific Publishing Center

Northern Border University

Vol. (8), Issue (2)

November 2023 – Rabi' II 1445 H

Website & Email

www.nbu.edu.sa

s.journal@nbu.edu.sa

p-ISSN: 1658- 7022 / e-ISSN: 1658- 7014

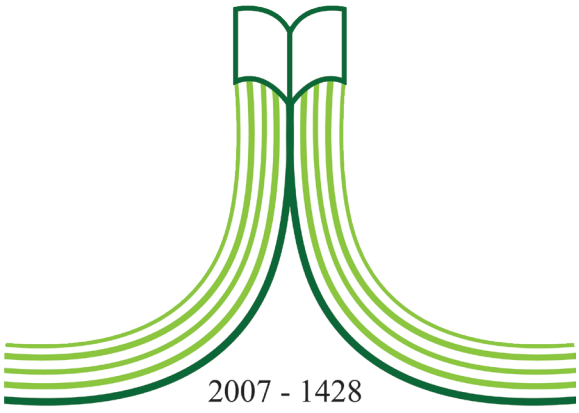

جامعة الحدود الشمالية

NORTHERN BORDER UNIVERSITY

Kingdom of Saudi Arabia

IN THE NAME OF ALLAH

THE MOST GRACIOUS, THE MOST MERCIFUL

Journal of the North for Basic and Applied Sciences (JNBAS)

Editorial Board

2007 - 1428
جامعة الحدود الشمالية
NORTHERN BORDER UNIVERSITY

Volume (8)
Issue (2)
November
2023
Rabi' II
1445 H

Journal of the North for Basic and Applied Sciences

Peer-Reviewed Scientific Journal

Northern Border University
www.nbu.edu.sa

p- ISSN: 1658 - 7022
e- ISSN: 1658 - 7014